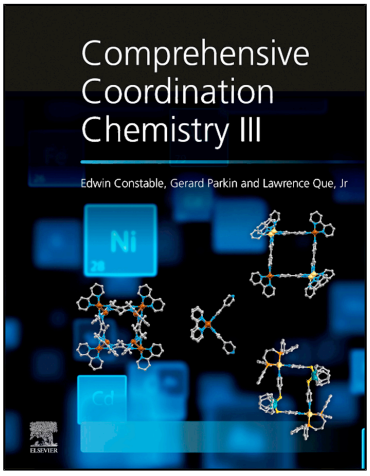

From Boudalis, A. K.; Kumar, K. S.; Ruben, M. Molecular Devices. In Comprehensive Coordination Chemistry III; Constable, E. C., Parkin, G., Que Jr, L., Eds., Vol. 7, Elsevier, 2021; pp 206–240.
https://dx.doi.org/10.1016/B978-0-08-102688-5.00061-1
ISBN: 9780081026885

7.07 Molecular Devices

Athanassios K. Boudalis, Institut de Physique et Chimie des Matériaux de Strasbourg (IPCMS), CNRS-Université de Strasbourg, Strasbourg, France
Kuppusamy Senthil Kumar, Institute of Nanotechnology, Karlsruhe Institute of Technology (KIT), Eggenstein-Leopoldshafen, Germany
Mario Ruben, Institute of Nanotechnology, Karlsruhe Institute of Technology (KIT), Eggenstein-Leopoldshafen, Germany; Institute for Quantum Materials and Technologies (IQMT), Karlsruhe Institute of Technology (KIT), Eggenstein-Leopoldshafen, Germany; and Université de Strasbourg (Unistra), Centre Européen de Sciences Quantiques (CESQ) within the Institute de Science et d'Ingénierie Supramoléculaire (ISIS), Strasbourg, France

Key Terms

Isotopologue coordination chemistry A branch of coordination chemistry in which isotopically enriched ligands (H versus D) and metals (151Eu versus 153Eu) are used to prepare coordination complexes with tailor made electronic, optical, and magnetic properties.
Spintronics Spin-based electronics, which uses both electronic charge and spin degree of freedoms.

Comprehensive Coordination Chemistry III, 2021, 206–240

Glossary

Coulomb blockade A resistance to charge flow observed in tunnel junctions at low bias conditions at low temperatures. The tunnel junctions typically involve a quantum dot (molecule, in the context of this chapter) placed in between two metallic electrodes.

Coulomb diamond The regions, in the source-drain current versus gate voltage diagram, where no current flow ($I = 0$) happens.

Grover's algorithm A quantum algorithm devised by Lov Grover in 1996 to perform function inversions, and which can be applied to speed up database searches by a factor of $N/\sqrt{N}$, where N is the database size.

Isotopologue coordination chemistry A branch of coordination chemistry in which isotopically enriched ligands (H vs D) and metals (^{151}Eu vs ^{153}Eu) are used to prepare coordination complexes with tailor made electronic, optical, and magnetic properties.

Light-induced excited spin-state trapping Photo-induced LS to HS switching and stabilization of the HS state at temperatures below 10 K. This phenomenon is typically observed in iron(II) SCO complexes and is a molecular phenomenon unlike the cooperative nature of the bulk SCO phenomenon.

Molecular junction A junction in which electrical transport characteristics of single or ensemble of molecules are probed.

QTM (Quantum tunneling of the magnetization) The presence of transverse terms in the spin Hamiltonian does not permit degeneracies between $+S_z$ and $-S_z$ (or $+J_z$ and $-J_z$) states at their level-crossing points of the magnetic field. These degeneracies are replaced by tunnelings at these field positions, leading to accelerated magnetic relaxation manifested as steps in the magnetic hysteresis curves. This behavior is referred to as QTM. Such transverse terms may be transverse magnetic fields, rhombic or quartic anisotropy terms, off-diagonal ligand field terms, hyperfine terms, or nuclear quadrupolar terms.

Quantum computing A method of computing, in which qubits are used to perform computing operations. Quantum computing relies on quantum mechanical properties of materials and an exponential increase in computing power is achieved.

Qubit Acronym of quantum bit, which is an analogue of classical bit. While a classical bit can take only the values of either 0 or 1, a qubit can be in a superposition of states $|0\rangle$ and $|1\rangle$, i.e. a linear combinations of 0 and 1.

Single molecule magnet An individual paramagnetic molecular entity that shows slow relaxation of magnetization caused by the presence of a spin reversal barrier. The magnetization of an SMM remains stable even in the absence of an external magnetic field. Unlike the bulk ferromagnetic materials no magnetic interaction between SMMs is needed for them to retain magnetization.

Spin valve A device in which electrons with a particular spin polarization—that is, spin-up or spin-down—is preferentially allowed. Molecular analogous of spin valves are called molecular spin valves.

Spin-crossover A phenomenon in which spin-state of transition metal ions with d^4-d^7 electronic configuration can be reversibly tuned between high spin and low spin states upon application of external stimuli, such as temperature, light, electric field, to name a few.

Spinterface Hybrid interfacial electronic/magnetic structure arising due to the strong interactions between a ferromagnetic substrate and a molecule. The strong interaction between a magnetic molecule and non-magnetic substrate also leads to the formation of spinterface.

Spintronics Spin-based electronics, which uses both electronic charge and spin degree of freedoms.

Tunneling A quantum mechanical phenomenon in which wave function propagates through an energy barrier instead of climbing the barrier. Such propagation leads to magnetization reversal in SMMs—termed as quantum tunneling of magnetization.

7.07.1 Introduction

The fascinating properties of metal complexes intrigued generations of chemists and spurred major technological developments. Their main features were first rationalized within Werner's seminal conception of coordination chemistry.[1,2] The vital points of his keen views are that a set of ligands is arranged about a metal center in a definite way, allowing coordination numbers up to 12. The Wernerian postulates provide a central pillar for metal chemistry to the present day.[3] Using all available metal ions—as there are main block, transition, lanthanide, and actinide ions—metal complexes can express a manifold of oxidation, magnetic, and optical states, which lay the base, depending on their specific constitution, for a multitude of physical functionalities, and chemical and biological activities.

To exploit the respective functionality of a metal complex, implementation and integration of the metal complex into a special configuration, called here a "device," will be of need. In a device, particles, mostly electrons, but depending on the geometry, also photons, phonons, spins, etc., will be used to unlock the physical property and to transduce it into an exploitable information bit, for example, within an electronic circuit (see Fig. 1). There, the metal complex can be considered as the active switching unit, which

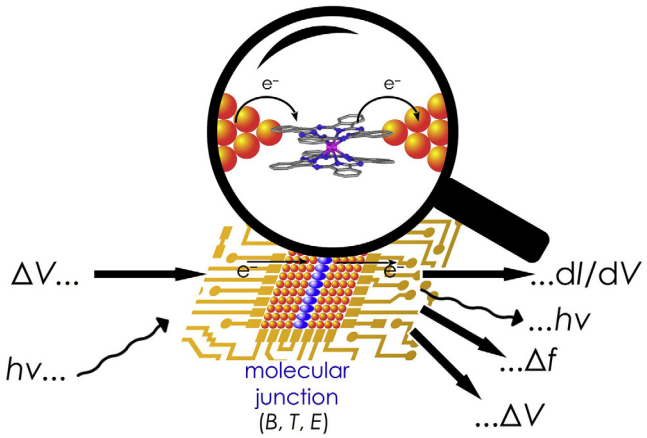

Fig. 1 Conceptual representation of the molecular devices. A molecular junction consisting of one or many molecules (blue) is subjected to an electric bias and a series of other stimuli (temperature, magnetic fields, electric fields, irradiation). The measurement of the device's conductance and the detection of additional emitted photons/phonons plays the analytical and/or functional role of the device.

upon a change of external field parameters follows to adapt its internal state and releases information. This process is comparable to spectroscopy, but takes place in a continuous and targeted way, illustrated best by the electric-field-driven controlled release of photons by emitting molecules in the touch screen device of a cellular phone. An argument for the use of molecular complexes in devices is that molecular objects can be produced by synthetic tools fine-tuning their properties and enabling integration by bottom-up self-assembly—a requirement for the production of reliably working devices. Importantly, molecular properties can be finely regulated by the concepts of coordination chemistry and molecular engineering, making possible the supply of molecular components based on demand.

During the last decade, the quest for devices able to unlock the quantum behavior of materials has become a major task. Here, the main advantage of the use of the metal complexes lies in that molecules are in general quantum objects that can be produced by synthetic tools in a large number of even atomically precise copies—a strong requirement for the scalable exploitation of the subtle quantum properties. Devices based on single, or small numbers of, molecules, could speed up information treatment or allow for processing schemes that have not been possible to date.

The electrical devices to read out the spin degree of freedom of magnetic metal complexes are defined as spintronic devices.[4] They rely on the scattering of the electron spin with the molecule spin and have to show a delicate trade-off between decoupling of the molecular quantum object for low decoherence from and connecting the metal complex to the electronic circuit to enable for the electrical read-out. On the metal complex side, the exact engineering required of the electronic and nuclear spin states can be achieved by the principles of isotopologue coordination chemistry,[5] in which the coordination chemistry pays special attention for the isotopic character of the central atom. This is a problem that coordination chemistry only has taken care so far with respect to radio-nuclide applications.

In the following, we will exemplarily show how two different classes of magnetic metal complexes can be integrated as active switching units in different spintronic devices, mainly supramolecular spin valves, molecular resonators and molecular spin transistors. After having introduced commercialized and non-commercialized molecular devices in general, we first discuss the spin-state dependent conductance switching and spin scattering characteristics of iron(II) spin crossover (SCO) complexes, arising due to their inherent non-magnetic low-spin (LS; $S = 0$) and the paramagnetic high-spin (HS; $S = 2$) states. By reading out this spin state difference, first indications of the quantum behavior of the switching process can be observed.[6] In the subsequent part we will discuss lanthanide single molecule magnets (SMMs) and addressing the quantum character of the lanthanide complexes via various molecular device interfaces. A series of recent studies has shown the utility of magnetic metal complexes as active quantum bits (qubits).[7] Thereby, it could be elucidated that the quantum information bearing nuclear spins implemented in metal ion complexes $TbPc_2$ ($Pc^{2-/\bullet-}$ = phthalocyaninate dianion or radical anion) are extremely well insulated from environmental perturbations, rendering the quantum information less prone to decoherence. This enables long enough spin coherence times (T_2), a key parameter that would allow $TbPc_2$ to function as a multi-level spin-qubit—qu*d*it—in quantum devices. Consequently, simple quantum algorithms, such as Grover's search algorithm, could finally be implemented in a single lanthanide metal ion.[8] In this context, molecular quantum complexes offer the advantage that the active quantum processing element comprises an atomic metal core surrounded by a shell of organic material; both parts can be modulated synthetically. At low experimental temperatures (typically tens of mK), the behavior of such molecular spin objects can be well described by simple few-level systems. Moreover, the molecule's spin degree of freedom can be sufficiently decoupled from environmental perturbations to attain long coherence times, thus making them the ideal candidates for the implementation of quantum computation schemes and beyond.

7.07.2 Scope and Organization

Among molecular devices, this review is situated in the domain of *molecular spintronics*, which encompasses phenomena and applications of *molecular electronics*, where the spin degree of freedom interacts with the electron charge. Thus, while molecular electronics

deals with the transport properties of molecules, molecular spintronics examines the interaction between molecular transport properties and the molecules' spin degree of freedom.

Among the multitude of materials and applications currently researched in this domain, our main focus will be on molecular spintronic devices based on *SCO* and *SMM molecular magnetic materials*. Both entail a magnetic degree of freedom, and are researched in the broader domain of Molecular Magnetism. However, to better present the perspectives of these devices in the broader context of molecular devices, we will give a brief overview of key technologies involving various types of molecular materials, including diamagnetic (i.e. non-magnetic) complexes, organometallic (i.e. not coordination) complexes, or purely organic materials.

Indicative of the interest in molecular devices is the 2016 Nobel Prize in Chemistry (to J.-P. Sauvage, F. Stoddart, and B. Feringa), which was awarded for the design and synthesis of molecular machines, and their respective studies on catenanes,[9] rotaxane-based molecular shuttles,[10] and the construction of a synthetic molecular motor.[11] Although these are not within the scope of the current review, they do illustrate the distance between conception and use. Almost four decades into this domain, and with it having generated beautiful chemistry and a lively research interest (see e.g. the chemically fueled motors reported by David Leigh[12,13] and a recent special issue of *Chemical Reviews*[14]), the realm of application still seems distant. As Bernard Feringa stated: "I'm less interested in making another motor than actually using it."[15]

Another note should be made regarding molecular wires (not to be confused with nanowires), a fundamental concept and component of molecular electronics. Literature prior to the 2000s has been criticized for a recurring misdefinition of molecules as "molecular wires," simply by virtue of an elongated or polymeric structure, neglecting the requirement of long-range conductivity. To address this, a 2005 definition considers a molecular wire as "a molecule or an assembly of molecules able to strongly electronically couple the terminal sites in order to mediate energy and charge transport over long distance";[16] we also refer to the terminological discussion in that volume.[17,18] Subsequent literature has gradually been influenced by the rise of (mono)molecular junctions since the first one was described in 2000 incorporating a C_{60} molecule.[19] Accordingly, alternate definitions have been proposed, for example, considering molecular wires as "molecules that can transfer carriers through the MMM junctions" (MMM = metal-electrode/molecule/metal-electrode). Such a definition removes the stress from the shape of the molecule and long-range conductivity and places it on the single-molecule character of the wire and junction.

To avoid such potentially conflicting definitions, we rather consider that any molecular junction, single-molecular or ensemble, presupposes the presence of a "molecular wire," which is thus defined by its function and not by its molecular shape (elongated or not).[20] Thus, we will not treat molecular wires as a "device" under a separate heading, but as an ubiquitous and versatile component of molecular junctions. Instead, it will be molecular junctions, with their varying implementations, that we will consider as a meaningful basic device (see below). It naturally follows that devices made from single molecules, thin films or single crystals, all fall within the scope of this work.

We should also stress that the presence of a molecular junction is not the sole prerequisite of molecular electronic devices, as molecules can be incorporated into electronic devices through other capacities, such as light-harvesting antennas in the case of dye-sensitized solar cells. From this consideration, it follows that we will consider molecules at several capacities when describing molecular electronic/spintronic devices.

Finally, regarding the application domain of molecular electronic and spintronic devices, these have been developed with two objectives in mind: (i) study of transport properties of molecules under varying external stimuli, such as temperature, electric fields (voltages) and magnetic fields (**Fig. 1**), with the longer-term objective to understand the influence of these stimuli on the molecular properties. In that sense, the transport properties are the measured quantity of the analytical method. (ii) Construction of functional devices, which carry out specific tasks. Both these categories, *analytical* and *functional*, fall within the scope of this work.

7.07.3 A Brief Overview of the Magnetism of d- and f-Metal Ions

The magnetic properties of coordination complexes arise from the presence of unpaired electrons in their valence orbitals. The type of these orbitals (d or f), the coordination number and geometry, the type of ligand atoms, etc., determine fundamental aspects of their magnetic properties. In addition, a series of other interactions define the details of their magnetic properties: (i) magnetic interactions between electronic spins through the orbitals of bridging ligands (superexchange); (ii) through-space interactions between electron spins (dipolar); (iii) interactions with magnetic nuclei of the metals themselves (hyperfine couplings) or the ligands (superhyperfine couplings). While a full theoretical treatment of these phenomena is beyond the scope of this review, a few basic remarks are useful to prepare the reader for the proper understanding of some key concepts treated in the following sections.

As mentioned above, the type of orbitals where the unpaired electrons reside, plays an important role in determining the magnetism of metal ions. A principal distinction can be drawn between d- and f-metal ions and regards the treatment of spin-orbit coupling. In both cases, the ligand field lifts the degeneracy of the valence orbitals, and orders them in a way that depends on the specific details of the LF strength and geometry. In the derived electronic configuration, apart from the quantum number S of the spin operator $\mathbf{S}$, we can also define a quantum number L for the orbital momentum operator L. For the f-series metal ions, this is straightforward to assign as it coincides with that of the free ion, while for d-ions we need to use the T-P isomorphism for the particular spectroscopic term (see p. 478 of Ref. 21).

While for both types of ions spin-orbit coupling (SOC) arises between the spin and orbital degrees of freedom of the electrons, as it is a relativistic phenomenon, its strength increases with the atomic number. In most 3d-metal ions (with the notable exception of Co^{II}) SOC is weak enough to be considered as a perturbation. In 4d and 5d metal ions this is stronger and often needs to be explicitly taken into consideration. In f-ions (with the notable exception of Gd^{III}, $\mathbf{L} = 0$), this is so strong that the good quantum number becomes that of the total angular momentum, $\mathbf{J} = \mathbf{L} + \mathbf{S}$.

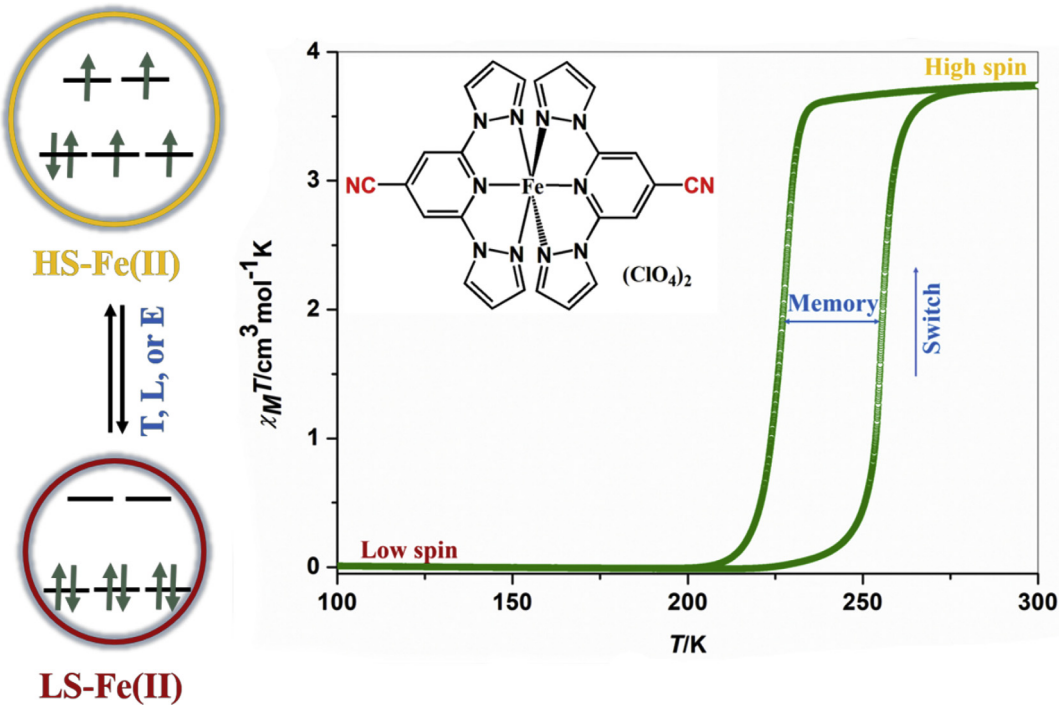

Fig. 2 Concept of Fe(II) spin crossover (SCO). A low-spin (LS) to high-spin (HS) transition, and vice versa, is induced upon application of an external stimulus, such as temperature (T), light (L), or electric field (E). Spin-state switching in an iron(II) system is shown (Left). A bistable SCO profile associated with a prototypical iron(II)-CN-BPP complex (inset); BPP stands for 2,6-bis(pyrazol-1-yl)pyridine (Right). The presence of thermal hysteresis renders the SCO systems suitable for the development of molecule-based memory architectures. Part of the image reproduced with permission from Senthil Kumar, K.; Del Giudice, N.; Heinrich, B.; Douce, L.; Ruben, M. *Dalton Trans.* 2020. https://doi.org/10.1039/D0DT02214D.

Another significant difference is that in the case of f-metal ions, valance (4f) electrons are well shielded by the 5s and 5p orbitals, and magnetic exchange interactions become very weak. Thus the principal determinant of their magnetic properties is the LF. However, depending on the sensitivity of the technique, other weaker interactions may arise, such as exchange, dipolar or hyperfine interactions, and significantly affect their magnetic properties.

Since SCO and SMM complexes will be of particular interest in this review a brief explanation of both will be presented.

Typically, SCO in a transition metal ion featuring d^4-d^7 electronic configuration—placed in a ligand field of appropriate strength—occurs upon application of an external stimulus—for example, temperature, light, or electric field (Fig. 2). SCO in transition metal complexes occurs in many different ways and is roughly classified as (i) gradual, (ii) abrupt, (iii) abrupt and hysteretic. The complexes undergoing SCO in an abrupt manner coupled with the occurrence of hysteresis are termed bistable, and such systems are desirable for the development of molecule-based memory architectures (Fig. 2). Iron(II)-based complexes are the most studied SCO systems, because the SCO in iron(II) complexes involve pure diamagnetic ($S = 0$; LS) and paramagnetic ($S = 2$; HS) states, rendering them more suitable for device applications than the SCO complexes of other transition metal ions, featuring paramagnetic LS and HS states.

Single-Molecule Magnetism is usually described phenomenologically, as the phenomenon whereby a single magnetic molecule (not experiencing long-range order) can retain its magnetization for an extended period of time in the absence of a magnetizing field. This definition is problematic as there does not exist a consensus of what constitutes an "extended period," and because certain SMMs only display this property inside a magnetic field due to a phenomenon called Quantum Tunneling of the Magnetization. It is therefore useful to accompany the above phenomenologial definition with a mechanistic explanation of the phenomenon. Thus, an SMM behavior is observed in magnetic molecules whose ground states are characterized by a high spin multiplicity and a high magnetic anisotropy of the easy-axis type, which creates an energy barrier to magnetization reversal. In 3d-metal SMMs (single ions or exchange-coupled polynuclear systems) this situation is parametrized by a large S of the ground state and a zero-field splitting parameter $D < 0$. A different class of SMMs, based on Ln^{III} ions, benefits from the very strong spin-orbit coupling (SOC), which imposes the description of their magnetic states with the J quantum number, and which induces a very strong magnetoanisotropy, making them nearly Ising spins (g_x, $g_y \sim 0$). An illustration of the SMM phenomenon in this latter family is shown in Fig. 3.

7.07.4 Survey of Molecular Device Technologies

In a seminal paper, Aviram and Ratner envisioned a molecular rectifier, consisting of one π-donor and one π-accepting system, to reproduce the rectifying functionality of silicon p-n junctions.[22] Quite often, such concept articles do not lead to the exact application of the original ideas due to unforeseen complications in their real-world implementation. However, they do give useful

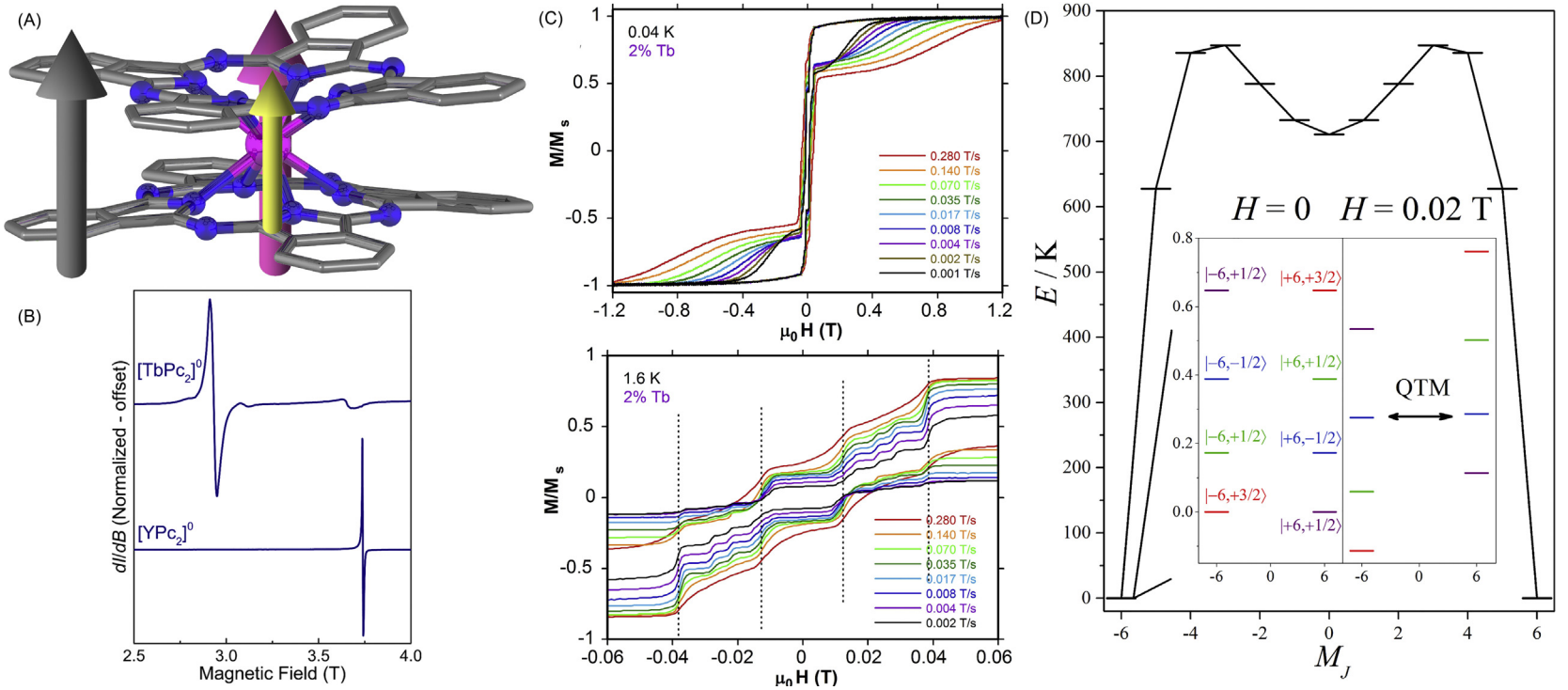

Fig. 3 The phenomenon of Single-Molecule Magnetism illustrated in the [Tb(Pc)(Pc*)] molecule (Pc^{2-} = the phtalocyaninato anion; Pc^{*-} = the reduced monoanionic radical ligand), hereafter denoted as $TbPc_2$. (A) The molecular structure of $TbPc_2$ showing the $J = 6$ spin of the Tb^{III} ion (purple), the $S = 1/2$ radical spin delocalized over the two phthalocyanine ligands (gray), and the nuclear spin $I = 3/2$ of the ^{159}Tb nucleus. (B) The EPR spectrum of $TbPc_2$ and of its YPc_2 diamagnetic analogue demonstrating the radical nature of the ligand. (Reproduced from Ref. Komijani, D.; Ghirri, A.; Bonizzoni, C.; Klyatskaya, S.; Moreno-Pineda, E.; Ruben, M.; Soncini, A.; Affronte, M.; Hill, S. *Phys. Rev. Mater.* **2018**, *2*(2). https://doi.org/10.1103/PhysRevMaterials.2.024405) (C) Magnetic hysteresis of magnetically dilute sample of $TbPc_2$. The major steps of the hysteresis loops, denoted by dashed lines in the bottom plot, correspond to accelerated relaxation due to QTM. (D) An energy-level diagram explaining the slow magnetic relaxation and QTM. Without QTM, magnetization reversal between the $M_J = J_z = -6$ to the $+6$ state occurs over a large energy barrier. QTM occurs between states $|J_z, I_z\rangle$ of opposite electron spin projections J_z and the same nuclear spin projections $\pm I_z$, when their energies tend to become degenerate at specific magnetic field strengths, under the influence of the Zeeman interaction.

insights that lead to related implementations. Thus, although molecular rectifiers are currently researched (see below), they have not reached the commercial stage. On the other hand, molecular junctions are already used in commercial applications, as are Dye-Sensitized Solar Cells (DSSCs or Grätzel cells) and Organic Light-Emitting Diodes (OLEDs).

To better place molecular electronic/spintronic devices in the current context, we will give a very brief overview of molecular device types that have the potential to influence future technologies and markets. This survey will be carried out in order of maturity, starting from already commercial technologies, going on to technologies still under research and development.

7.07.4.1 Commercial Devices

7.07.4.1.1 Organic LEDs (OLEDS)

A recent revolution in flat panel displays has been the introduction of organic LED (or OLED) technology, with Pioneer introducing the first car stereo with OLED elements in 1997,[23] and with the first commercially launched OLED TV, the Sony XEL-1, entering the market in 2008. Although the "O" in the OLED acronym stands for "organic," coordination complexes played a major role in the evolution of this technology, and still do.

At the heart of OLED displays lies a thin film of an electroluminescent material which emits light when traversed by an electric current. Electroluminescence was discovered in 1963 in anthracene single crystals[24] and the search for similar materials intensified over the years. Interestingly, an emitting material that proved extremely useful in the field was tris(8-hydroxyquinolinato) aluminum (Alq_3), widely known to freshmen chemists from gravimetric analysis of aluminum. Eastman Kodak researchers used sublimed Alq_3 as the emissive layer of a bilayer structure, thus reporting the construction of an organic light-emitting diode in 1987.[25,26] The molecular complex Alq_3 remained an important material during the advance of the field.

It was subsequently observed that doping Alq_3 with a Pt-porphyrin dye induced highly efficient electrophosphorescence.[27] This pointed researchers to the fact that the large SOC of heavy metals played a crucial role in this behavior. In the absence of SOC, the dye absorbs the excitons only from the pure singlet states of the conducting host material (fluorescence), which account only for 0.25 of the total, limiting the internal quantum efficiency, η_{int}, to 25%. SOC induces singlet-triplet mixing allowing the harvesting also of the "triplet" excitons (phosphorescence), allowing η_{int} to approach 100%. Soon after, a diode incorporating the green electrophosphorescent material $[Ir^{III}(ppy)_3]$ (ppy = 2-phenylpyridine) was shown to confirm this hypothesis, demonstrating a short phosphorescent decay (~500 ns), attributed to SOC.[28] This landmark discovery reoriented research in OLED materials. As a measure of the level of penetration of coordination and organometallic materials in OLED technology, out of 61 light-emitting materials commercialized by Sigma-Aldrich (as of July 2020),[29] 17 are based on Ir^{III}, 3 on Ru^{II}, 3 on Eu^{III}, 2 on Zn^{II}, 1 on Pt^{II}, 1 on Li^{I}, and 2 are the Alq_3 complex. Thus, almost half the proposed materials are coordination-based, and more than half among those are Ir^{III}-based.

7.07.4.1.2 Dye-sensitized solar cells

In contrast to OLED operation, molecular materials have also been used in photovoltaic devices, i.e. using light to generate electric current. The photovoltaic effect is the generation of electron-hole pairs by photons falling on a semiconductor surface. When two different semiconductors are in contact, forming a junction, this effect can create an electric potential across their interface. Ever since Henri Becquerel discovered this phenomenon,[30] the prospect of unlimited electrical energy generated by sunlight has motivated scientists in that research. However, sunlight is not fully exploited by semiconductors, as their band gaps may often fall to the high-frequency edge of the solar spectrum. This is the case with TiO_2, a particularly popular semiconductor due to its photostability, non-toxicity and abundance.

Photovoltaics have been based on the same principles and materials as photography, as pointed out by Grätzel,[31] thus benefitting from the same theoretical understandings. Thus, when it was understood that photographic films could be sensitized to longer wavelengths by organic dyes, photoelectrochemical cells followed suit shortly thereafter by Moser in 1887, using erythrosine on silver halide electrodes.[32] As semiconductors with lower band-gaps, coinciding with visible light, exhibit increased photocorrosion, photosensitization became a particularly crucial aspect for the viability of photovoltaics. The dyes absorb the light quantum, are excited and then inject an electron into the semiconducting anode. An electron from the cathode then reduces the oxidized dye, usually through a mediator redox couple. Over the next decades, and particularly in the aftermath of the 1973 oil crisis, research in organic photosensitizers was pursued, making this aspect of molecular devices the oldest to be pursued.

In a slight twist to the prevailing strategy, in 1972 Tributsch extended his research to another, actually dual, direction, by using a chlorophyll solution as a dye[33]: on the one hand he was considering "bionic" (biomimetic, in today's terms) energy generation to achieve artificial photosynthesis; on the other hand, he used a coordination dye since, as was discovered later, the photosynthetic system contains several coordination components.

Soon thereafter, the purely coordination-chemistry direction was pursued with the use of $[Ru(bpy)_3]^{2+}$ as photosensitizing dye for SnO_2[34] and TiO_2[35] single-crystal anodes. This line of research proved particularly successful after the improvement introduced from the understanding of the role of covalent linking of the dye to the anode. Carboxylate side groups in $[Ru(bpy)_2(bcpa)]$ (bpcaH = 2,2′-bipyridine-4,4′-dicarboxylic acid) were used to graft this molecule to MoS_2[36] and TiO_2[37] single-crystalline anodes. These improvements paved the way for the breakthrough by Grätzel, who succeeded in optimizing key characteristics for such cells using anodes of high surface roughness constructed from a film of sintered TiO_2 nanoparticles, and sensitized by $\{Ru(bcpa)_2(\mu\text{-}CN)_2[Ru(bpy)_2]_2\}^{2-}$,[38] and subsequently by *cis*-$[RuX_2bpca_2]$ ($X^- = Cl^-$, Br^-, I^-, CN^-, NCS^-).[39] Among the studied complexes, the $X^- = NCS^-$ analogue, also known as R3 or Ru535, achieved unprecedented efficiency of ~10%. This astounding increase in

efficiency, made Ru-polypyridyl sensitizers the most heavily studied ones. However, it also marked an approximate ceiling value for efficiency, which has only been incrementally surpassed since.[40]

Research continued to other coordination complex sensitizers, notably [ZnTCPP] ($TCPP^{2-}$ = tetracarboxyphenyl porphyrinate),[41] which exploits the strong absorptions of the Soret and Q-bands of the porphyrin chromophore. These developments paved the way for the study of a large family of porphyrin-based sensitizers,[42] which have already afforded improvements over Ru DSSCs.[43] These research findings are part of an effort to replace costly 4d and 5d metals with earth-abundant ones. More recently, an iron TiO_2 sensitizer was described, based on a Fe^{II} complex of a carboxy-substituted bisimidazole-pyridine chelating ligand. This sensitizer led to a 92% photon to electron conversion,[44] and the use of iron in this domain has gained new traction.[45–48]

DSSCs have already broken into the market and are available from companies such as Exeger,[49] Solaronix[50] and H.glass,[51] whereas the maturity of this technology is such that Do-it-yourself DSSC kits, for example, from Sol Ideas,[52] are commercially available.

Picking up on the trail of DSSCs, Perovskite Solar Cells (PSCs) have a very short history, but an explosive evolution. Lead halides such as $CsPbX_3$ have long been known to be perovskite-structure semiconductors. Since Miyasaka and coworkers reported the first PSC with $CH_3NH_3PbI_3$ in 2009,[53] the reported efficiencies of 10% in 2012[54] and of 21% in 2016,[55] illustrate the explosive progress in this research direction.

Although PSCs have already reached a pre-market stage,[56] very serious challenges remain: their dependence on Pb—a highly toxic metal—poses a major pollution risk. Their long-term stability under the influence of humidity, oxygen, temperature, and sunlight UV radiation is another ill-studied question.[57] Specialized standards for the measurement of PSC stability hadn't been defined until January 2020,[58] and conclusions from coherent application of those standards won't be available for several years.

7.07.4.1.3 Molecular junctions for sound amplification

In closing this section, we present an application which is most notable for being, to our knowledge, the first commercially available practical use of molecular junctions (MJs).

A common remark of music industry professionals on the performance of silicon-transistor amplifiers regards the timbre of the resulting sound, which is described as "cold." This evocative and subjective description is directly rooted to the shapes of the amplified signals, which determine the resulting sound. Interestingly, vacuum-tubes are still considered the highest quality technology for sound amplification, offering natural saturation and rich harmonics due to the particular signal clipping they achieve. As such, they are still preferred by the high-end part of music industry, despite their inconvenience and high cost compared to solid-state electronics.

To overcome this problem, a molecular-junction based amplifier was constructed using carbon-molecule-carbon layers, in which the molecular entities were organic azobenzene oligomers of 1–10 nm in length,[59] electrochemically grown from azobenzene diazonium salts.[60] Today this technology is marketed by Nanolog Audio.[61]

7.07.4.2 Non-commercialized Devices

7.07.4.2.1 Molecular rectifiers

As previously mentioned, molecular rectifiers were the archetypical device proposed for molecular electronics by Aviram and Ratner.[22] However, one of the main problems of such devices was the low rectification ratio of AC currents. While 10^5 rectification ratios have been reported for DC currents by rectifiers constructed from SAMs of Fc–C≡C–Fc termini tethered to long alkyl chains,[62] AC rectification ratios stood at a mere 18% for 50 Hz AC currents in 2011 for similar junctions.[63] Only recently has it been possible to construct molecular rectifiers that work in the MHz regime, consisting of composite CuPc/F16CoPc films.[64]

7.07.4.2.2 Molecular spin valves

Before describing molecular spin valves, a few words on the underlying phenomenon, giant magnetoresistance (GMR), are in order. This was discovered in 1988 independently by Fert[65] and Grünberg,[66] and led to the 2007 Nobel Prize on Physics. It is observed in layered interfaces consisting of ferromagnetic electrodes separated by a non-magnetic conductor. When the magnetizations of the electrodes are parallel, the entire device exhibits a lower resistance, up to 50%, than when the two magnetizations are antiparallel. This can be explained by considering that the electron current consists of two "fluids" with opposite spin polarizations, each flowing through two separate channels. Each current is scattered more weakly when crossing the interface of an electrode with parallel magnetization, experiencing a smaller resistance. It can be easily shown with electric circuit analogues that the resistance of the entire device when both channels are considered, is smaller when the source and drain magnetizations are parallel.

A spin valve is a device taking advantage of this phenomenon to change resistance as a function of an applied magnetic field. In order for the spin valve to discern the absolute orientation of the applied field, the magnetization of one of the magnetic layers is pinned by an antiferromagnetic layer, thus becoming a "hard" magnetic layer. In a spin valve, the spin fluid coming from the source is spin-polarized, i.e. the "parallel" electrons are more than the "antiparallel" ones.

In 2002 the first molecular spin valve was reported in which the organic semiconductor α-sexithienyl was placed between two manganite ferromagnetic electrodes.[67] In 2004 the first molecular spin valve based on a coordination material was reported, with Alq_3 used as semiconducting spacer between a manganite and a Co ferromagnetic electrodes, recording a GMR effect of up to 40%.[68] The facile sublimation of this type of complexes was the basis for the report of the first molecular spin valves based on magnetic coordination complexes, namely Ln_3q_9.[69] "Organic" spin valves subsequently drew the interest of theoretical investigations, which proposed the implementation of molecular spin valves by connecting ferromagnetic leads through organic molecules[70,71] and have since produced lively research.[72]

These findings have also given rise to the concept of "spinterface,"[73] which describes the process of spin injection from a ferromagnetic to an organic material.

7.07.5 Molecular Junction Architectures

Molecular junctions are found in an important part of molecular electronic/spintronic devices, they therefore deserve a separate section for their description, and herein we present the main technologies used to incorporate molecules in electronic and spintronic devices. As previously mentioned, a molecular junction, i.e. an electrode/molecule/electrode series, can consist of a single or many molecules (ensembles).[74–79] Several techniques have been developed to implement this fundamental concept in the cases of single-molecule or ensemble junctions.

A very extensive 2016 review by Guo and coworkers[20] gives a detailed outline of the domain of molecular electronics, whereas a 2020 review by Ruitenbeek and coworkers[80] focuses especially on the aspect of addressing single-molecule transport phenomena. As far as magnetic coordination complexes are concerned, which are the main focus of this review, an overarching issue concerns the behavior of molecules on surfaces. In particular, key questions are whether surface-deposited molecules retain their structural integrity and, if they do, whether they reflect the electronic and magnetic properties of the bulk material. These are not straightforward problems and have been the subject of numerous studies. This is beyond the scope of this work, but several specialized reviews[81–85] have touched upon aspects of surface deposition of magnetic complexes on surfaces.

7.07.5.1 Thin-Film (Ensemble) Junctions

As indicated in the discussion above, thin-film (or ensemble) molecular junctions have been around since before the field of molecular electronics was described in these terms. The first experimental demonstration was reported in 1971 by Mann and Kuhn,[86] who used double layers of fatty acid cadmium salts to study the tunneling conductance of thin insulating layers. Moreover, early implementations of OLEDs were fabricated with thin films of organic and coordination materials developed through chemical vapor deposition (see above).

In these early implementations, the top electrode was deposited through vapor deposition of the electrode materials,[25] a technique still used in more recent applications.[59] However, this method of creating the top electrode may damage the thin film. Thus alternative techniques have been developed, such as liquid flotation of the top electrode metallic leaf, use of a liquid metal drop electrode (i.e. hanging Hg electrode) and capillary electrodes made of eutectic alloys.[20] In another approach, the electrodes are preformed through high-throughput on-wire lithography, and their gap is filled by the organic material through polymerization,[87,88] a method suitable for the mass-production of molecular junctions.

7.07.5.2 Single-Molecule Junctions

The technologies covered below are currently used to implement single-molecule junctions, though it must be understood that this occurs at the ultimate stage of perfecting their use; these devices can also implement many-molecule (ensemble) junctions, although this is a generally undesired outcome.

7.07.5.2.1 Scanning tunneling microscope (STM) junctions

The invention of the STM afforded the ability to conduct transport measurements over single molecules. Thus, it may be considered that the earliest single-molecule junctions were implemented during STM experiments, such as single-molecule resolution of C_{60} carried out in 1993,[89] followed by early attempts to measure the conductance of linear molecules.[90] Such early experiments were plagued by the tendency of the, generally large, STM tip to come to contact with more than one molecules and register their net contribution. These experiments were subsequently refined by the use of a statistical treatment of thousands of individual measurements to convincingly isolate the single-molecule conductance.[91,92]

STM topography on Mn_{12} films was attempted in 2003[93] and reports of single-molecule STM observation of Mn_{12} SMMs appeared shortly thereafter,[94,95] along with similar reports on [2 × 2] Co^{II}_4 grid complexes,[96] a Fe^{III}_4 SMM,[97] a Mn^{II}_9 grid complex,[98] a nickelocene molecule,[99] etc. The role of the interest in the SMM phenomenon is illustrated by the STM study of single molecules of $TbPc_2$ in 2008.[100]

A very important advance in the technique in 1990,[101] was the use of ferromagnetic STM tips, that is, spin-polarized STM tips. Due to the tunneling magnetoresistance (TMR) effect, the conductance depends on the spin polarization of the conduction electrons, which renders the technique sensitive to surface magnetization. Spin-polarized STM (SP-STM) is closely related to the spin valve effect produced by GMR (see 6.2.1 for a brief description), and has become a powerful technique in imaging magnetic structures and molecules on surfaces.

Another breakthrough in this domain was the use of SP-STM in the study of magnetic complexes. The first such study was carried out in 2008 on CoPc molecules deposited on Co nanoislands[102] which, quite notably, took place before the first such study on C_{60}.[103] The phthalocyanine "platform" proved so adapted to such experiments that experiments with CoPc were reproduced on a Fe ferromagnetic surface,[104] as well as experiments with $Fe^{II}Pc$ molecules on a Bi_2Te_3 layer,[105] and with the $TbPc_2$ complex, both on single-molecules[106] and thin films.[107] In a similar vein, molecules of the SCO complex $[Fe(phen)_2(NCS)_2]$ deposited on Co/Cu(111) were also studied by SP-STM.[108]

SP-STM has been used to demonstrate a high magnetoresistance favored by single-molecule junctions, that may also have implications in the context of SCO complexes. A single-molecule junction was constructed from a HS *trans*-$[Fe^{II}(tzpy)_2(NCS)_2]$ (tzpy = 2-pyridyl[1,2,3]triazolo[1,5-α]pyridine) molecule anchored between a ferromagnetic Ni tip and an Au surface through the S-atoms of the NCS^- ligands. The conductance of the device was dependent on the Ni-tip polarization, and the change between up and down polarizations was 10,000%. It was also found that the spin-polarized current generated at the Au-complex interface was enhanced by the magnetic molecule. Indeed, by replacing with the LS homologous complex *trans*-$[Fe^{II}L^A(NCS)_2]$ (L^A = *N*,*N*′-bis(1-pyridin-2-ylethylidene)-2,2-dimethylpropane-1,3-diamine), no such amplification occurred. This is an intriguing finding in the context of introducing SCO complexes in molecular spin-valve devices.[109]

SP-STM studies on $TbPc_2$[106] have been particularly informative in elucidating the magnetic nature of the molecules when adsorbed on surfaces, in particular whether the radical spin in the highest occupied molecular orbital (HOMO) of the Pc ligand system is retained upon surface deposition, or whether this is quenched. By depositing $TbPc_2$ molecules on ferromagnetic Co islands on Ir (which act as hard magnets), and by studying them with a Fe-coated W tip (which acts as a soft magnet), it was possible

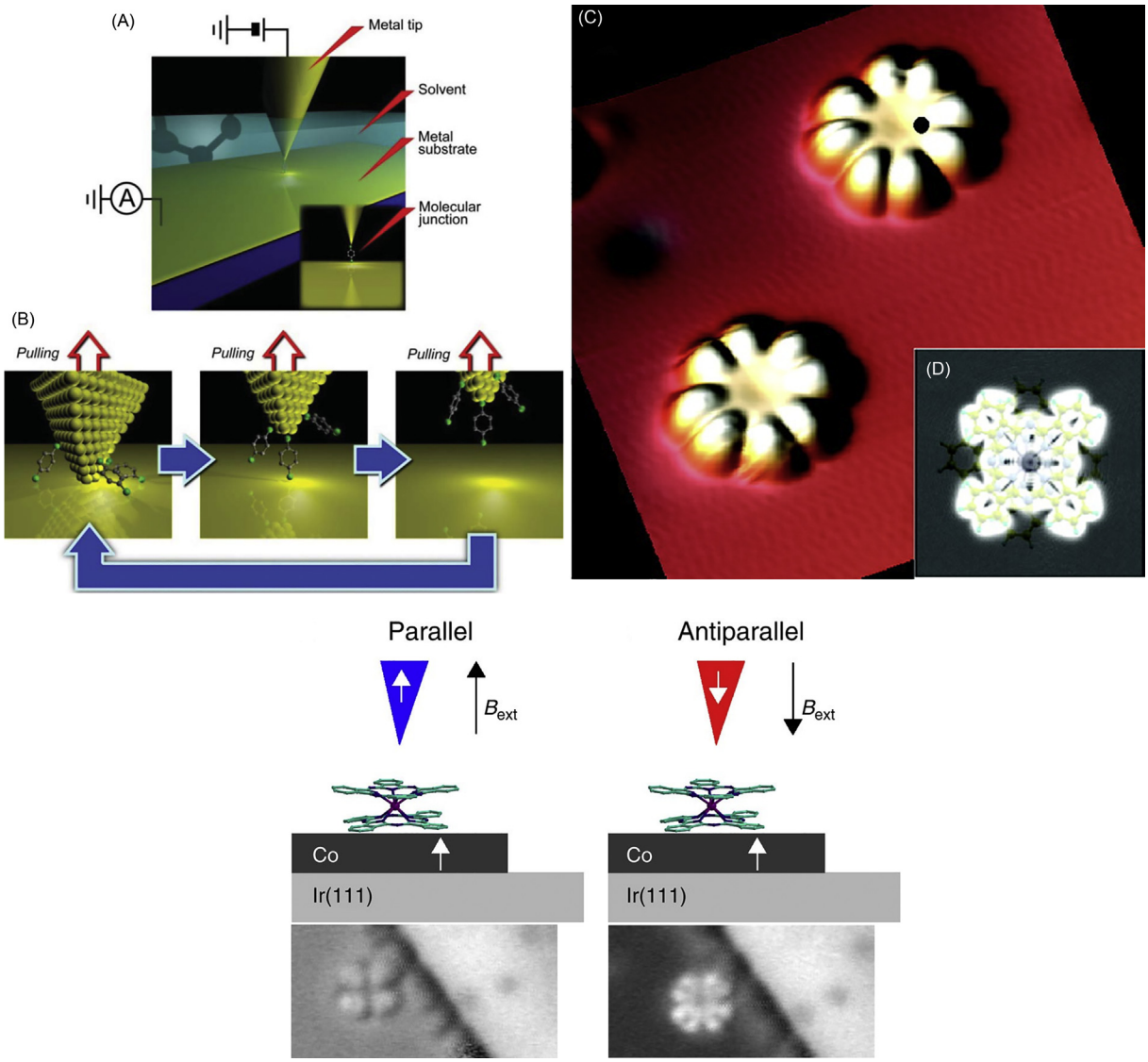

Fig. 4 The principle of an STM junction. Top left: Formed by a metallic tip connected to a conducting metallic surface through a single molecule. For a truly single-molecule junction to be acquired, repeated up-down movements of the tip may be required for a unique molecule to be in the junction. (Reproduced from Tsutsui, M.; Taniguchi, M. *Sensors* **2012**, *12*(6), 7259–7298. https://doi.org/10.3390/s120607259) Top right: Use of the technique to create single-molecule junctions with a magnetic molecule: STM images of the $TbPc_2$ SMM showing a characteristic eight-lobe pattern belonging to the ligand's frontier orbitals. (Reproduced from Vitali, L.; Fabris, S.; Conte, A. M.; Brink, S.; Ruben, M.; Baroni, S.; Kern, K. *Nano Lett.* **2008**, *8*(10), 3364–3368. https://doi.org/10.1021/nl801869b) Bottom: SP-STM of the $TbPc_2$ SMM allowing to distinguish the spin polarization of the LUMO orbitals. (Adapted from Schwöbel, J.; Fu, Y.; Brede, J.; Dilullo, A.; Hoffmann, G.; Klyatskaya, S.; Ruben, M.; Wiesendanger, R. *Nat. Commun.* **2012**, *3*(1). https://doi.org/10.1038/ncomms1953.)

to carry out conductance studies for parallel and antiparallel tip-substrate magnetizations, by varying the tip magnetization by an external magnetic field. Differential conductance SP-STM studies confirmed that the lowest unoccupied molecular (LUMO) orbitals have a zero net spin polarization, i.e. the spin of the upper Pc ligand is quenched upon adsorption. Nevertheless, these measurements revealed a spin splitting of that orbital, i.e. an energy difference between its two spin polarizations (Fig. 4).

A potential avenue for further studies on molecular systems is the single-atom EPR developed as an evolution of SP-STM, whereby a radiofrequency electric field excites spin transitions through its magnetoelectric coupling. This was demonstrated on Fe^{II} adatoms in 2015[110] and since applied to several other similar systems,[111–113] though no such studies on molecular systems have been reported to date.

In closing, based on the above definition of a single-molecule junction, STM-junctions are clearly the earliest ones implemented. Nevertheless, although they have revealed a wealth of information on transport and other phenomena of single molecules, i.e. in their analytical capacity, certain hurdles remain for their use for the construction of functioning electronic/spintronic devices. One such limitation of the technique is the gating of a single molecular junction. This latter limitation started to be removed very early on, with the description of a four-tip STM in 2001.[114] This subdomain has since evolved[115] and has the potential to host additional STM tips for the construction of specific molecular electronic/spintronic devices which require more than one elements. Still, the perspectives and limitations of such developments remain to be explored.

7.07.5.2.2 Mechanically controlled break junctions (MCBJs)

In MCBJs,[116,117] a constricted metal bridge (either a notched wire or a lithographically fabricated bridge), whose two sides will subsequently provide the source and drain, is fixed onto a flexible substrate. Under the action of a push rod acting below the substrate, and that of two counter supports on the opposite side, a deformation is created which ultimately breaks the bridge at its weak point, i.e. the constriction. Subsequently, the length of the formed gap can be precisely controlled by the push-rod's action.

MCBJs were first used for molecular transport studies in 1997, although these early studies actually studied SAMs of benzene-1,4-dithiol[79] and 4-thioacetylbiphenyl[118] and not single molecules. In a process similar to the refinement of STM junctions (see above) the transport properties of single organic[119] or H_2[120] molecules were reported in 2002.

Such devices based on coordination complexes are usually constructed with molecules properly functionalized with S-groups which assure tethering to the Au surface. The first such study was carried out in 2002 on a Pt^{II} organometallic complex,[121] followed by a ferrocene complex.[122] Interestingly, MCBJ devices allowed the direct manipulation of the ligand field parameters of metal complexes by modifying the junction distance. It was remarked that $[M(terpy)]_2$ coordination spheres are the molecular analogue of a Cardan joint, with the entire electron transport pathway passing through the metal center. Thus, by modifying the interelectrode distance, it was possible to tune the molecular conductance of a molecule of $[Ru^{II}(L)_2](PF_6)_2$ (L = thioacetic acid S-(4-[2,2′;6′,2″] terpyridin-4′-ylethynyl-phenyl ester)) placed in a MCBJ.[123] Subsequently, this principle was tested in a junction made of $[Co^{II}(tpy\text{-}SH)_2]$ (tpy-SH = 4′-mercapto-2,2′:6′,2″-terpyridine), also a demonstration of a molecular Cardan joint. Interestingly, however, this molecule proved to exhibit a Kondo peak splitting consistent with an $S = 1$ system, and not a Kramers systems predicted for a Co^{II} (d^7) ion. This result was rationalized by considering a $1e^-$ reduction, with an electron captured by the molecule from the Au electrode, thus yielding a Co^{I} metal center. The MCBJ was then used to control the magnetic anisotropy of the complex through mechanical stretching (Fig. 5).[124] Similar studies were used to detect spin-state transitions as a function of the electrical bias in an exchange-coupled dimer).[125]

While MCBJs are a powerful and simple analytical technique for single-molecule addressing, they lack the surface-topography features of STMs. The technique exhibits severe limitations from an applications perspective as it is not clear whether such devices can be scaled to create multi-junction architectures. Moreover, they lack the ability of a voltage gate that can tune the electrodes' Fermi levels with respect to the energy states of the molecule, constitutes a severe functional handicap (see below).

7.07.5.2.3 Electromigrated junctions

The latest addition to the molecular electronic/spintronic technologies are electromigrated junctions (Fig. 6). Electromigration is the transport of the conductor's material under the influence of high-density DC currents due to momentum exchange with the moving electrons. It was first described by Gérardin in 1861[126] but became of practical importance only during the development of microelectronics. It was a suspected source of failures of early integrated circuits, manifested as cracks of the metallic conductors, and correctly identified as such through the works of Jim Black.[127,128]

However, from being a problem, electromigration has been adapted as a solution for the fabrication of junctions with nm-sized gaps. In the first such demonstration in 1999,[129] McEuen and coworkers were able to reproducibly break an Au nanowire by ramping the electric bias. As in the creation of MCBJs, electromigrated junctions also require the fabrication of a "weak point," which also is a constriction of the wire/bridge. However, in this case the increased current density creates the "stress," as it leads to resistive heating that melts the constriction. Electromigrated junctions have been particularly useful in the fabrication of single-molecule spintronic devices, such as spin transistors.

Electromigrated junctions offer an additional advantage which goes far beyond the method of producing a clean and precise break in the conductor. Since the breaking takes place without mechanical movement, like in MCBJS, the conducting strip/wire may be lithographically placed on any desirable substrate. Fabrication of this strip on top an insulating layer, followed by a third electrode right below, gives the possibility to fabricate an electrical gate below the junction, the additional component required for the construction of a transistor. Given the particular importance of this particular junction architecture in the construction of molecular transistors, the relevant literature will be reviewed under its own heading (see Section 7.07.6.2.3).

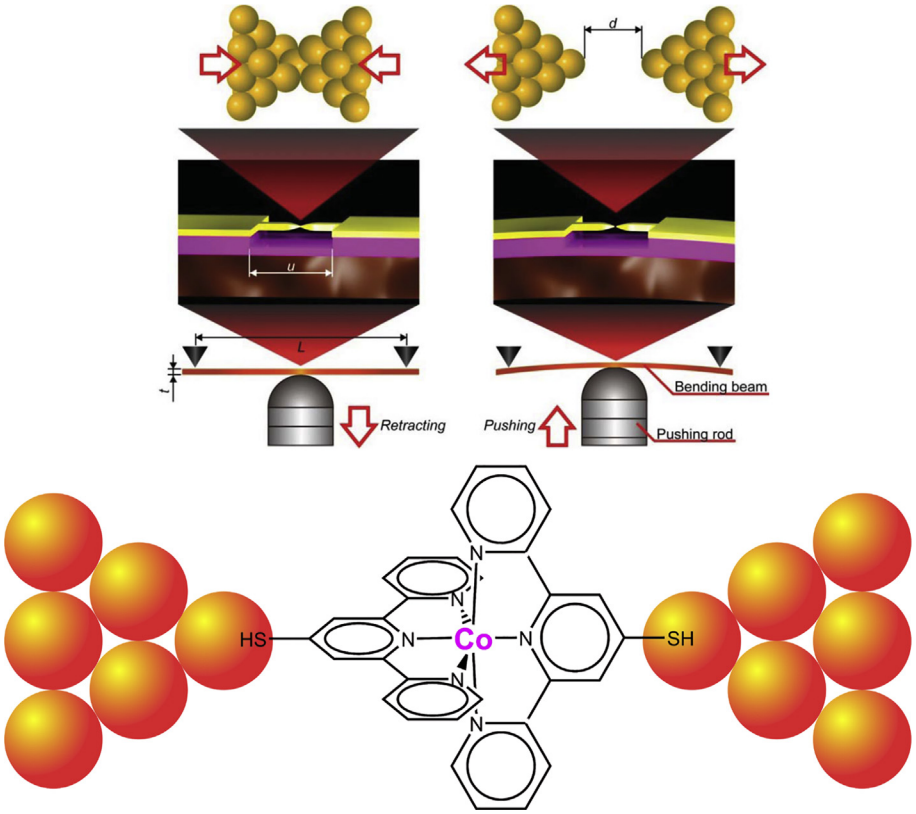

Fig. 5 Top: The principle of a mechanically-controlled break-junction (MCBJ). The mechanical bending of the substrate breaks the junction, and the gap is controlled to pm precision by the movement of the pushing rod. (Reproduced from Tsutsui, M.; Taniguchi, M. *Sensors* **2012**, *12*(6), 7259–7298. https://doi.org/10.3390/s120607259) Bottom: A Co^{II} complex of an S-functionalized terpy ligand placed in an MCBJ gap.[124] Movements of the electrodes modulate the ligand-field parameters by direct mechanical deformation of the ligand sphere.

7.07.6 Spintronic Devices Based on Magnetic Coordination Complexes

7.07.6.1 SCO Spintronic Devices

7.07.6.1.1 Electron transport characteristics of SCO junctions

The occurrence of spin-state change in SCO complexes is coupled with physical property variations—such as, thermochromism and volume expansion—due to the modulation of electronic population in the orbitals concerned. For example, the SCO in a d^6 iron(II) complex involves t_{2g}^6, e_g^0 LS and $t_{2g}^4e_g^2$ HS configurations. Such a variation in electronic population, coupled with the SCO, alters the frontier molecular energetics, which in turn tune the alignment of frontier molecular orbitals with respect to the Fermi level of electrodes on which the complexes are deposited. The modulated coupling between the electrodes and frontier molecular orbitals commensurate with the spin-state of a complex causes spin-state dependence of conductivity in SCO junctions. Such variation of transport characteristics with respect to the spin-state of SCO complexes renders the complexes suitable to harness molecular electronics and spintronics devices based on SCO complexes. Importantly, the transport in HS-SCO complex junctions is spin-polarized with major contributions arising from β-spin electrons residing in the t_{2g} orbital. Thus, SCO complexes could be used as ON-OFF switchable spin filters in spintronic circuitry.

Apart from transport junctions, the utility of SCO complexes as solvent sensors, actuating elements in MEMS devices, temperature and pressure sensors have also been demonstrated.[130–132] Furthermore, spin-state switching properties of the complexes have also been studied on 2D materials such as graphene[130,133–135] and hybrid graphene-SCO device architectures have been fabricated, as discussed in Section 7.07.6.1.2. Overall, the device-suitable nature of SCO complexes is well elucidated by a range of experimental and theoretical investigations. In the following sections, we provide an overview on the transport properties of single molecule, nanoparticle (NP), thin film, and hybrid device architectures incorporating SCO complexes.

7.07.6.1.2 Single molecule SCO junctions

Electrical transport characteristics of single SCO molecules can be studied by trapping them in (i) STM junctions, (ii) MCBJs or electromigration junctions, and (iii) graphene-molecule-graphene (GMG) junctions. Important conceptual insights describing spin-state switching at a single molecule level and the associated transport characteristics modulations have been obtained from the studies, as depicted in Fig. 7.

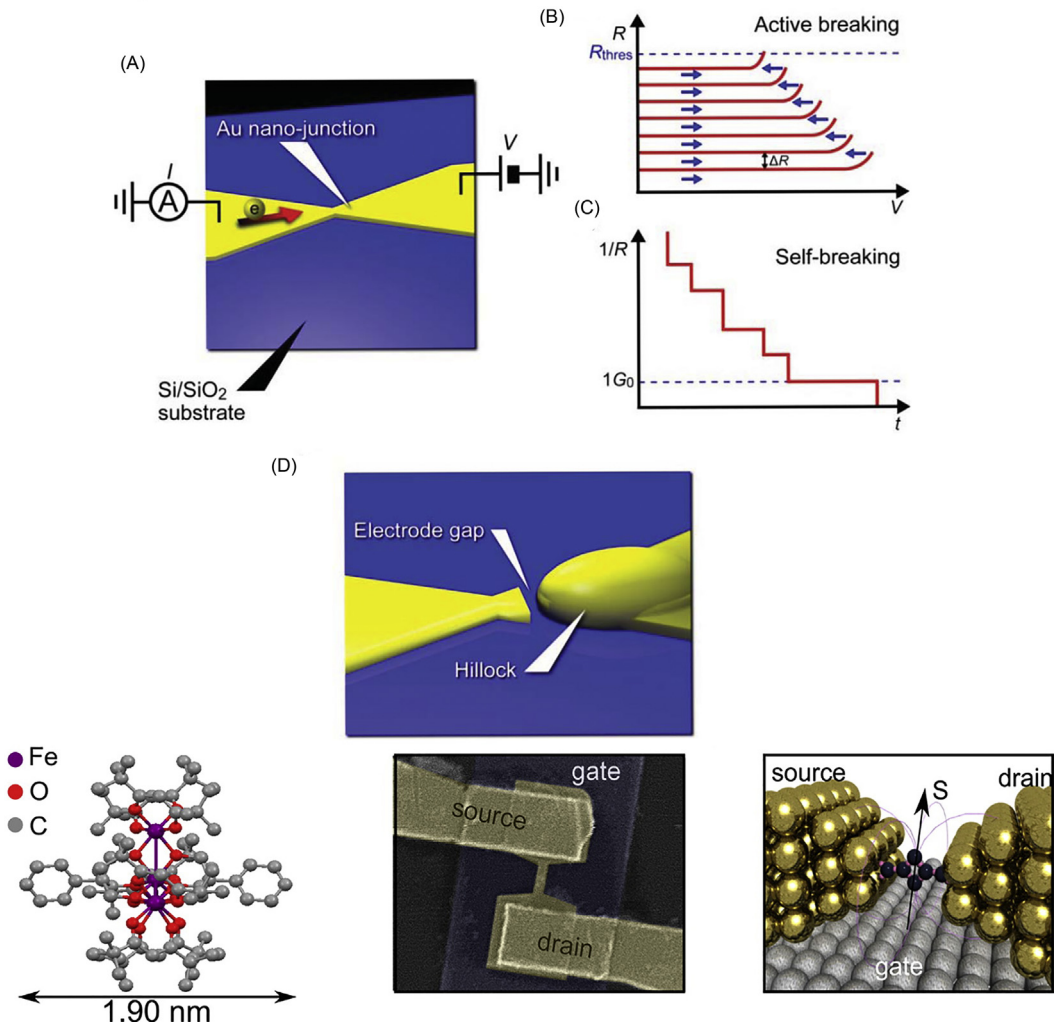

Fig. 6 Top: The principle of an electromigrated junction. Repeated rampings of the applied voltage gradually increase the resistivity due to electromigration and narrowing of the constriction. A final current under constant voltage causes the constriction to self-break due to Ohmic heating. (Reproduced from Tsutsui, M.; Taniguchi, M. *Sensors* **2012**, *12*(6), 7259–7298. https://doi.org/10.3390/s120607259) Bottom: Use of the method to construct a spin transistor with an Fe_4 SMM molecule. The molecule is shown on the left, a SEM image of the transistor in the middle and an artistic view the transistor on the right. (Reproduced from Burzurí, E.; Yamamoto, Y.; Warnock, M.; Zhong, X.; Park, K.; Cornia, A.; van der Zant, H. S. J. *Nano Lett.* **2014**, *14*(6), 3191–3196. https://doi.org/10.1021/nl500524w)

Theoretical studies of single SCO molecule junctions had predicted the more conductive nature of the HS-state relative to its LS counterpart and spin-polarized nature of the electron transmission.[136–139] Moreover, the utility of electric fields as a stimulus in inducing spin-state switching at a molecular level and a large resistance variation coupled with spin-state switching have also been theoretically proposed.[140,141] Such theoretical attributes of conductance states of HS and LS SCO complexes have been experimentally verified in single molecule junctions. In a seminal study, bias polarity dependence of spin-state switching of a prototypical SCO complex—$[Fe(phen)_2(NCS)_2]$ (phen = 1,10-phenanthroline)—in an STM junction was demonstrated (Fig. 7A). Application of negative bias polarity ($V > -0.8$ V) induced the LS to HS switching, whereas the HS to LS switching proceeded upon application of positive bias polarity ($V > +1.2$ V). Remarkably, the experiments revealed the more conductive nature of the HS-state of $[Fe(phen)_2(NCS)_2]$ relative to its LS counterpart. The bias polarity-dependent spin-state switching is associated with a hysteretic current switching behavior, rendering $[Fe(phen)_2(NCS)_2]$ as a single molecule memristor. The elucidation of voltage-induced combined spin and conductance tunability at molecular level augurs well for the development of molecule-based memory elements.[142]

The bias polarity dependence of spin-state switching in $[Fe(phen)(bpz)_2]$ (bpz^- = dihydrobis(1-pyrazolyl)borate), was also demonstrated at a molecular scale in an STM junction. Application of positive voltages exceeding +2.5 V ($I = 50$ pA) by placing the STM tip in an arbitrary position induced the LS to HS switching of molecules located at nm distances away from the tip position. The reverse HS to LS was induced by applying a voltage pulse of +1.8 V ($I = 500$ pA) by placing the tip directly above a HS complex.

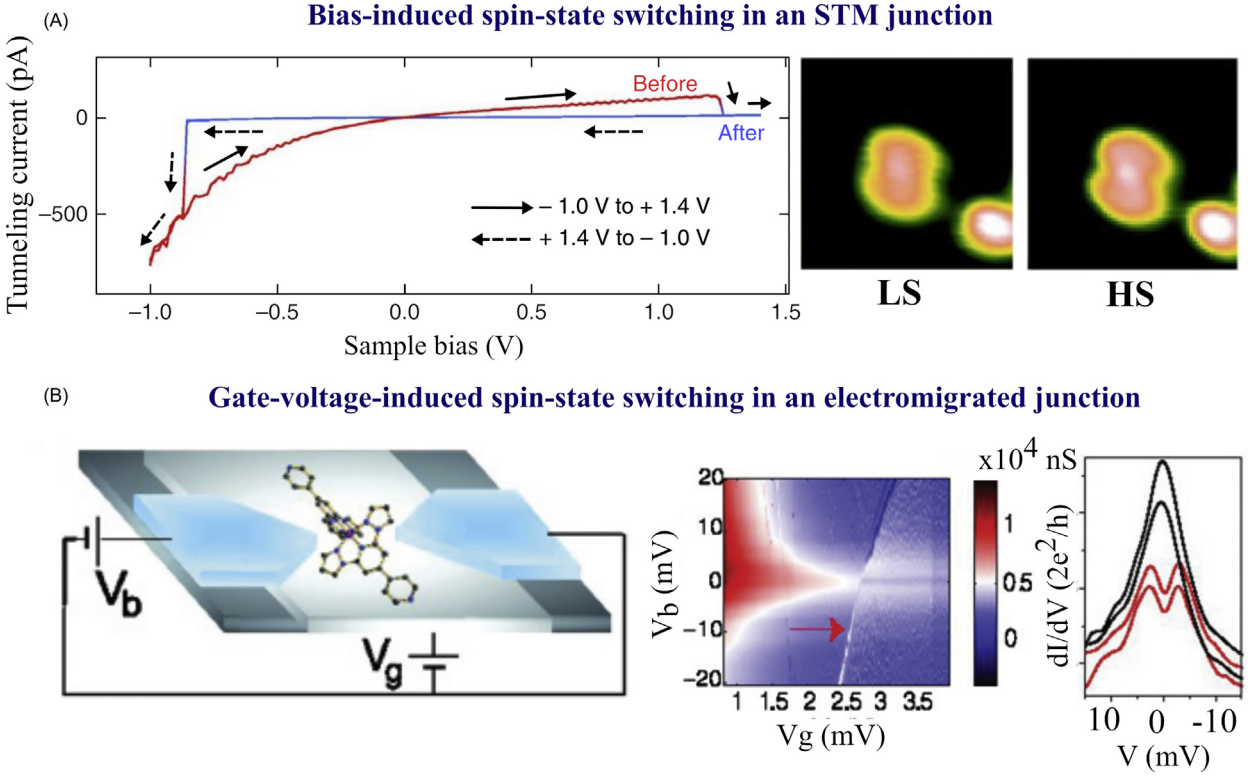

Fig. 7 Spin-state switching in single molecule SCO junctions. (A) Bias-induced spin-state switching observed for $[Fe(phen)_2(NCS)_2]$ at the single molecule level in an STM junction. In a typical experiment involving single $[Fe(phen)_2(NCS)_2]$ molecules, the HS to LS, and vice versa, switching is induced by varying the bias polarity of the CuN/Cu(100) substrate on which the molecule is anchored. At $V > -0.8$ V, LS to HS switching is observed; the reverse HS to LS switching is observed at $V > +1.2$ V. The hysteretic nature of the switching process endows the $[Fe(phen)_2(NCS)_2]$ with single molecule memristor characteristics. An STM tip placed above a single molecule, identified the spin-state of the molecule, as shown in the figures next to the I–V plot. (Reproduced with permission from Miyamachi, T.; Gruber, M.; Davesne, V.; Bowen, M.; Boukari, S.; Joly, L.; Scheurer, F.; Rogez, G.; Yamada, T. K.; Ohresser, P.; Beaurepaire, E.; Wulfhekel, W. *Nat. Commun.* **2012**, *3*(1). https://doi.org/10.1038/ncomms1940) (B) Gate voltage (V_g) mediated—via charging of ligand—SCO in an electromigrated junction comprising a single $[Fe(bpp)_2]^{2+}$ complex. At $V_g > 2.5$ V (red arrow), the overall spin of the system changes from $S = 0$ to $S = 1$. This was reflected as splitting of the zero bias conductance peak, shown as red traces in the d*I*/d*V* versus *V* plot. The black and red traces are measured at $V_g < 2.5$ V and $V_g > 2.5$ V, respectively. (Reproduced with permission from Meded, V.; Bagrets, A.; Fink, K.; Chandrasekar, R.; Ruben, M.; Evers, F.; Bernand-Mantel, A.; Seldenthuis, J. S.; Beukman, A.; van der Zant, H. S. J. *Phys. Rev. B* **2011**, *83*(24). https://doi.org/10.1103/PhysRevB.83.245415.)

A sudden decrease of current accompanied the HS to LS switching, which indicates the more conductive nature of the HS-state of $[Fe(phen)(bpz)_2]$ than its LS counterpart.[143]

Electric field-induced spin-state switching and the associated spin-state dependent conductance switching in single-SCO molecule junctions have been demonstrated for an $[Fe(bpp)_2]^{2+}$ (bpp = bis-pyrazolyl pyridine) complex trapped in a field effect transistor (FET) device architecture. Application of electric fields via the gate led to the charging of the ligands, which in turn induced the formation of the HS-state. A triplet ground state was proposed for the complex—extra electrons ($2 \times S = ½$) residing in the ligands are antiferromagnetically coupled with the S = 2 HS iron(II) center. Such assignment was verified by the experimental observation of split Kondo resonance peak (see **Fig. 7**B). An explicit difference between the conductance of the LS and HS states of $[Fe(bpp)_2]^{2+}$ complex was not presented in the study.[144]

While all the three examples illustrate the possibility of voltage-induced spin-state switching at single molecule scale, there are remarkable differences. The spin-state switching of $[Fe(phen)_2(NCS)_2]$ is polarity dependent: the LS to HS switching is induced by applying a negative voltage, whereas the HS to LS switching requires the application of positive voltage. Moreover, the switching is induced by placing the STM tip directly above the $[Fe(phen)_2(NCS)_2]$ molecule. On the other hand, spin-state switching of $[Fe(phen)(bpz)_2]$ was induced in both directions (i.e. LS to HS and HS to LS) upon application of positive voltage pulses. Moreover, unlike the situation in the case of $[Fe(phen)_2(NCS)_2]$, the LS to HS switching of $[Fe(phen)(bpz)_2]$ was realized by applying a positive voltage pulse at a remote position. The transportation of hot electrons by surface resonances as far as 13 nm from the tip position caused the LS to HS switching, indicating the electron-induced nature of the switching process. The possibility of electric field-induced switching is ruled-out based on the orientation of the dipole moment of $[Fe(phen)(bpz)_2]$, which is oriented 45 degrees relative to the surface normal. Such an orientation facilitates the field-induced switching at positive and negative polarities, which is not observed experimentally, as described above. To describe the electron-induced switching in $[Fe(phen)(bpz)_2]$, a new term

electron-induced spin-state trapping (ELIESST) was coined, which is analogous to the light-induced excited spin-state trapping (LIESST). In ELIESST mediated switching of $[Fe(phen)(bpz)_2]$, the initially injected electron occupies an unoccupied orbital of the LS complex generating an intermediate-state (IS^-), from which the complex can statistically relax to either HS or LS state, and the excess electron tunnels to the substrate. Since the experiments were performed at 5 K, which is well below the $T_{1/2}$ value of the bulk samples, some of the metastable HS complexes, formed via the relaxation of the IS^-, remain trapped on the surface for hours. The reverse HS to LS switching of metastable HS complexes were selectively induced via a charged intermediate similar to the IS^- described above. The ELIESST mediated spin-state switching process is analogous to the electron-induced excitation of LS $[Fe(bpp)_2]^{2+}$ complex to a HS-state.

A similar mechanistic pathway is proposed to explain the switching in $[Fe(phen)_2(NCS)_2]$. The HS to LS switching occurred after a time delay upon application of +1.5 V voltage pulse, indicating the presence of an intermediate state during the spin-state switching. The average switching rate (R) upon application of voltage pulse is related to current (I) as $R = I^N$. The observation of $N \approx 8$ for the LS to HS switching process indicates role of vibrational heating mediated excitation of LS state due to inelastic scattering of tunneling electrons. A linear relation between switching rate and current, that is, $N = 1$, was observed for the HS to LS switching; a single electron process involving the charging of a state present around +1.1 eV caused the HS to LS switching process. An electron-induced excitation of HS $[Fe(phen)_2(NCS)_2]$ into an intermediate excited state and subsequent relaxation of the excited state to the LS state was proposed as a mechanistic pathway involved in the HS to LS switching.

Overall, all three studies discussed above converge on an electron-induced spin-state switching process. Mechanistically, charging of bpp ligands facilitates the LS to HS switching in $[Fe(bpp)_2]^{2+}$ and such an attribute was well proved via experimental and computational studies.[144,145] Moreover, the LS to HS switching is reported to be bias polarity independent due to the symmetric nature of $[Fe(bpp)_2]^{2+}$ complex featuring two identical bpp ligands coordinated with the iron(II) SCO center. The equal coupling strength of the ligands with the left and right electrodes rendered the spin-state switching bias polarity independent. The magnetic interactions—antiferromagnetic—between the additional electrons centered in the ligand and the metal centered HS electrons were well established for $[Fe(bpp)_2]^{2+}$. A point noteworthy here is only the LS to HS switching is observed for $[Fe(bpp)_2]^{2+}$ complex trapped in an FET junction.

In the cases of $[Fe(phen)_2(NCS)_2]$ and $[Fe(phen)(bpz)_2]$ both the LS to HS and HS to LS switching were experimentally demonstrated but the nature of magnetic interaction between the metal centered HS electrons and extra electron(s) residing in the ligand-based orbitals were not elucidated. Moreover, the spin-state switching is bias polarity dependent in both the cases due to the inherently asymmetric nature of the complexes—the unequal coupling of the ligand with the left and right electrodes rendered the spin-state switching bias polarity dependent. Mechanistically, the spin-state switching process in junctions composed of $[Fe(phen)_2(NCS)_2]$ or $[Fe(phen)(bpz)_2]$ is caused by inelastic cotunneling of electrons mediated creation of metal to ligand charge transfer (MLCT) and metal centered (MC) electronic excitons. Decay of the MLCT exciton via an intermediate state facilitates the LS to HS switching. On the other hand, the HS to LS transition involves the decay of the excited MC state via an intermediate state, as established in a recent computational study.[146]

While the above studies detail controlled spin-state switching at single molecule junctions, random—telegraph-like—spin-state switching and the associated conductance modulations have also been reported for iron(II) complexes trapped in between graphene/metallic electrodes and in STM junctions. Transport characteristics of a pyrene tethered iron(II) SCO complex was probed at a single molecule level by placing it between graphene electrodes (Fig. 8D). A reproducible and random switching between two different conductance states caused by SCO was demonstrated. Unlike the bulk sample, the SCO is induced at any temperature, even at 4 K, in the absence of external stimuli.

The dI/dV plots showed the opening of conductance channels at lower threshold voltages for the HS state than the LS state. The close proximity of the LUMO of the HS state to the Fermi level relative to the energetic proximity of the LS state is the reason behind the low current blockade gap associated with the HS state. Moreover, the transport characteristics of the HS state is spin-resolved, rendering the SCO molecules suitable to develop switchable spin polarizers.[6] Similar SCO mediated switching of resistance states was reported for an iron(III) complex trapped between gold electrodes. Unlike the relatively larger −0.6 V bias used in graphene SCO junctions, a smaller 8 mV bias voltage is applied in the Au–SCO junction, thus the role of electric field as stimulus in inducing SCO is ruled out. Remarkably, some of the devices fabricated using the complex showed multilevel switching characteristics, this is attributed to the presence of two SCO complexes within the nanogap.[147] Random switching between three different conductance states was also demonstrated for an iron(III) complex—$[Fe(pap)_2]^+$ (pap^- = N-2-pyridylmethylidene-2-hydroxyphenylaminate)—deposited on $Cu_2N/Cu(100)$ surface by sublimation. Topographical analysis of the surface bound $[Fe(pap)_2]^+$ complexes revealed the presence of HS conformer A on the surface. Application of 2.5 V voltage by placing the tip above conformer A resulted in the random switching between three current levels: the high current level is associated with HS conformer A, and the two other low current levels correspond to LS conformers B and C. The three different current states corresponding to configurations A, B, and C rendered the system as memristor. The selective nature of the switching process, that is, the deterministic nature of the memory, is demonstrated by selectively switching the configuration of a molecule (A → B) without affecting its nearest neighbors. Note, the charge state of the surface deposited $[Fe(pap)_2]^+$ is ambiguous and the assignment of the spin-state is not solely based on the conductance state.[148] A caged iron(II)-terpyridine complex electro-spray deposited on Au(111) substrate have also shown two-level tunneling current variations—under a constant applied bias of 0.9 V—characteristic of SCO-induced switching discussed above.[149] Overall, single molecule transport characteristics of SCO complexes trapped in between graphene and gold electrodes reveal small structural perturbations in metal-ligand distances contributing to the random switching between spin-states and the

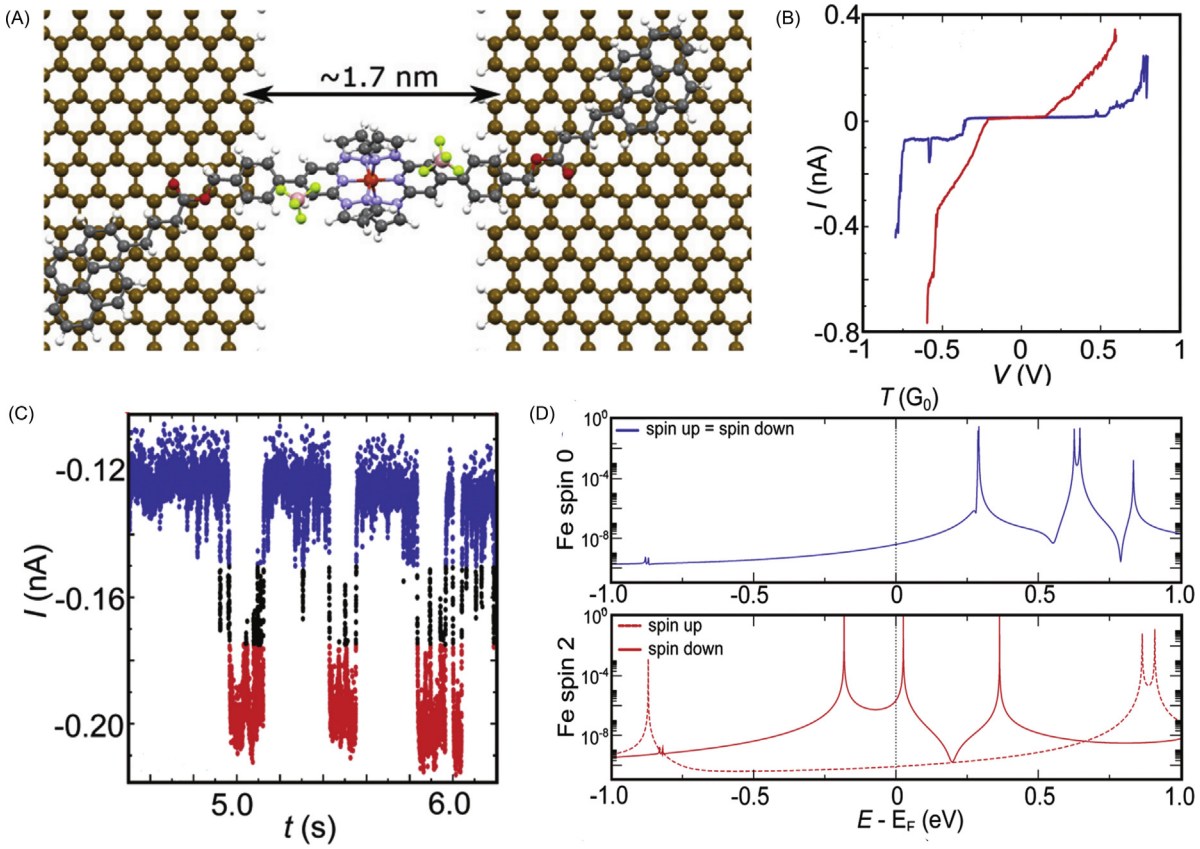

Fig. 8 Random spin-state switching in a single SCO molecule-graphene junction. (A) Schematic of a graphene-SCO complex junction: A pyrene-decorated SCO complex was anchored in between single-layer graphene electrodes. (B) Current (I) versus voltage (V) plots of LS (blue) and HS (red) states of the complex, showing spin-state dependent conductance variation. (C) At $T = 2$ K, a telegraph-like conductance variation attributed to random spin-state switching was observed. (D) The transport is spin-polarized in the HS-junctions due to the closer proximity of HS-LUMO level (solid red trace) to the Fermi level than the LS-LUMO (dotted red trace). Images reproduced with permission from Burzurí, E.; García-Fuente, A.; García-Suárez, V.; Senthil Kumar, K.; Ruben, M.; Ferrer, J.; van der Zant, H. S. J. *Nanoscale* **2018**, *10*(17), 7905–7911. https://doi.org/10.1039/C8NR00261D.

associated telegraph-like conductance switching. The studies also indicate the drastically different nature of SCO process at the individual level when compared with the cooperative nature of SCO in the bulk scale.

Electric field and stretching induced spin-state switching and the associated conductance variations have also been demonstrated in molecular junctions embedding single iron(II) complexes. A dipole placed in an electric field undergoes a torque, thus spin-state switching could be induced by placing an iron(II) complex composed of ligands featuring a large dipole moment. This concept was demonstrated for a heteroleptic iron(II) complex placed in a gold MCBJ.[150] The complex is composed of differently functionalized terpyridine ligands arranged perpendicular around the central iron(II) switching entity. One of the terpyridine ligands features terminal anchoring groups, which anchor the complex in the MCBJ junction. The other ligand is endowed with a permanent dipole moment by functionalizing it with electron donating (NMe_2) and withdrawing (CN) groups. Application of electric field across the junction distorts the complex structure due to the coupling between the electric field and dipole carrying push-pull ligand. Such coupling distorts the perpendicular organization of the ligands around the iron(II) core, consequently a LS to HS switching ensued. The LS to HS switching coupled with molecular structure reorganization, perpendicular to distorted, triggered by electric filed evidences the utility electric filed as a stimulus in inducing spin-state switching at single-molecule level.

Spin-state switching between HS and LS, and vice versa, involves metal-ligand bond length elongation—the Fe−N bond lengths are longer in HS complexes than in their LS counterparts. In retrospect, spin-state switching could be induced by stretching a single molecule placed in between metallic leads. Such stretching-induced spin-state switching in metal-molecule-metal MCBJ junction was demonstrated for a homoleptic iron(II)-terpyridine complex. The complex was fixed on the metallic leads via sulfur-anchoring groups, and a gradual stretching of the junction induced LS to HS switching. The related zero bias conductance measurements indicate the more conductance nature of HS state than the LS state, a fact also supported by theoretical calculations.[151] Similar stretching-induced spin-state switching is demonstrated for a single Fe-porphyrin complex in an STM junction. At narrow junction gaps, the macrocyclic complex adsorbed on an Au(111) surface adopts a saddle conformation and is in HS state ($S = 2$). Retracting the STM tip away from the substrate, while in contact with the complex, stretches the complex and an intermediate triplet

spin configuration (S = 1) with planar conformation is obtained.[152] The above studies demonstrate the mechanical triggering of SCO in single molecule MCBJ and STM junctions.

In an interesting study, controlled spin-state switching of a nickelocene molecule attached to an STM tip was demonstrated. The $S = 1$ to $S = 1/2$ spin-state switching is observed upon moving from the tunneling to the contact regime, that is, when the nickelocene is in contact with the underlying Cu(100) substrate, $S = 1/2$ spin-state is stabilized. Retracting the nickelocene-functionalized STM tip away from the substrate induces $S = 1/2$ to $S = 1$ spin-state switching. Thus, surface-state mediated triggering of spin-state switching at single molecule level was demonstrated.[99]

Ideally speaking, some of the complexes underwent spin-state switching at a molecular level under the influence of electric field, mechanical, and surface-state stimuli are not SCO active at the bulk scale. Thus the elucidation of spin-state switching of the complexes at single molecule level serves as the proof of the concept that spin-state switching can be induced at a single molecule level even for the complexes that are not SCO active at bulk scale. Overall, although SCO is a bulk state phenomenon in molecular solids, the above discussion demonstrates the possibility of inducing SCO in single molecule junctions with the help of appropriate switching mechanisms. Application of voltage pulses induced SCO either by charging the ligand or by exciting the LS or HS molecule to an electronically excited state. The relaxation of the excited state either to a stable LS or meta-stable HS state completed the spin-state switching process. Such mechanistic insights obtained from single molecule measurements and the possibility of voltage induced switching augurs well for the development of switching and memory elements based on SCO complexes, as demonstrated in the case of $[Fe(phen)_2(NCS)_2]$ in an STM junction. On the other hand, stochastic switching between spin-states in the absence of any particular external stimulus in single molecule junctions indicates the role of small perturbations, most probably molecular vibrations, effecting spin-state switching; this makes sense considering spin-phonon coupling associated with the SCO in bulk samples. Apart from these, the utility of electric field and molecular stretching stimuli employed to modulate spin-state of designer iron(II) complexes elucidates the conceptually rich landscape of single molecule experiments associated with functional coordination complexes.

7.07.6.1.2.1 SCO Nanostructures

The occurrence of thermal hysteresis upon LS to HS transition renders the SCO systems as switching and memory elements in nanoscale device architectures. However, hysteretic I–V profiles were not observed, except for the case of $[Fe(phen)_2(NCS)_2]$, in the single molecule SCO complex junctions discussed in the previous section. The demonstration of hysteretic SCO in nanostructured materials and the size dependence of SCO characteristics indicates the usefulness of such materials as nanoscale switching and memory elements.[153,154] An intriguing quest is: can the temperature-dependent hysteretic SCO behavior reflect as hysteretic switching in nanoscale junctions composed of nanostructured SCO systems? Indeed, hysteretic temperature-dependent current switching behavior has been demonstrated in such junctions. Nano-structured objects of the one-dimensional polymeric SCO complex $[Fe(Htrz)_2(trz)](BF_4)$ are one of the most studied SCO-active nano systems, because such systems show bistable SCO characteristics above room temperature. Initial studies of the spherical and rod-shaped nano structures of the as-synthesized 1D-complex powders revealed an above RT hysteretic conductance switching due to temperature-induced LS to HS switching (C1-C3 in **Fig. 9**A).[155] To study the particle size dependent SCO properties and the associated conductance switching parameters, pristine spherical and rod-shaped nanoparticles (NPs) of $[Fe(Htrz)_2(trz)](BF_4)$ were prepared employing a reverse-micelle-based technique. Transport characteristics of such NPs organized between gold electrodes using dielectrophoresis (DEP)[156] or 2D-self-assembly[157] directing methods revealed hysteretic current switching characteristics attributed to temperature-induced spin-state switching. Importantly, in all the junctions discussed above, the HS state is found to be less conductive than the LS state.

Transport characteristics of core-shell type NP assemblies of $[Fe(Htrz)_2(trz)](BF_4)$ have also been studied. Temperature-dependent conductance measurements of a single 10 nm core-shell NP composed of polymeric $[Fe(Htrz)_2(trz)](BF_4)$ core and surfactant shell, referred to as SCO@surfactant NP, placed in between Au electrodes revealed an above RT hysteretic conductance switching attributed to spin-state switching.[158] Remarkably, voltage-induced conductance switching was also demonstrated in the single SCO@surfactant NP junction. Sweeping of voltage beyond a threshold voltage triggered the switching from the low-conductance state to the high-conductance state. Such voltage induced conductance switching is attributed to a voltage-induced spin-state switching mediated by several plausible mechanisms including the ELIESST mechanism discussed in **Section 7.07.6.1.2** for single molecule SCO junctions. In contrast to the transport measurements involving multiparticle junctions, the HS state is more conductive than the LS state in single SCO@surfactant NP junctions. A similar hysteretic and more conductive HS-state than the LS-state was reported for a hybrid film composed of $[Fe(Htrz)_2(trz)](BF_4)$ NPs and single walled carbon nanotubes (SWNTs).[159] Mechanistically, transport in multiparticle and single NP junctions is mediated by thermally activated hopping and single electron tunneling, respectively, of charge carriers. Smaller thermal activation energy of conductivity associated with the LS form of $[Fe(Htrz)_2(trz)](BF_4)$ than the HS form rendered the LS form more conductive in multiparticle junctions.

While above RT hysteretic switching is demonstrated in NP junctions of $[Fe(Htrz)_2(trz)](BF_4)$, the current values remained low prohibiting the practical applications of such devices. To circumvent the issue, core-shell Au@SCO NP arrays composed of an Au-core (12 nm) and 4 nm thick $[Fe(Htrz)_2(trz)](BF_4)$ shell were prepared, and the electrical characteristics of NP arrays were studied by placing them in between Au electrodes.[160] At an applied voltage of 2 V, a hysteretic conductance switching was observed upon temperature variation. However, unlike the single particle SCO@surfactant junctions, high conductance values are observed for Au@SCO junctions when the SCO shell is in the LS-state. Moreover, a larger ON/OFF conductance switching ratio of 5300 were observed in the Au@SCO devices than the conductance ratio of 2 observed in the SCO@surfactant devices. The increased switching ratio observed in Au@SCO device is due to the intrinsically conductive nature of the metallic Au core.

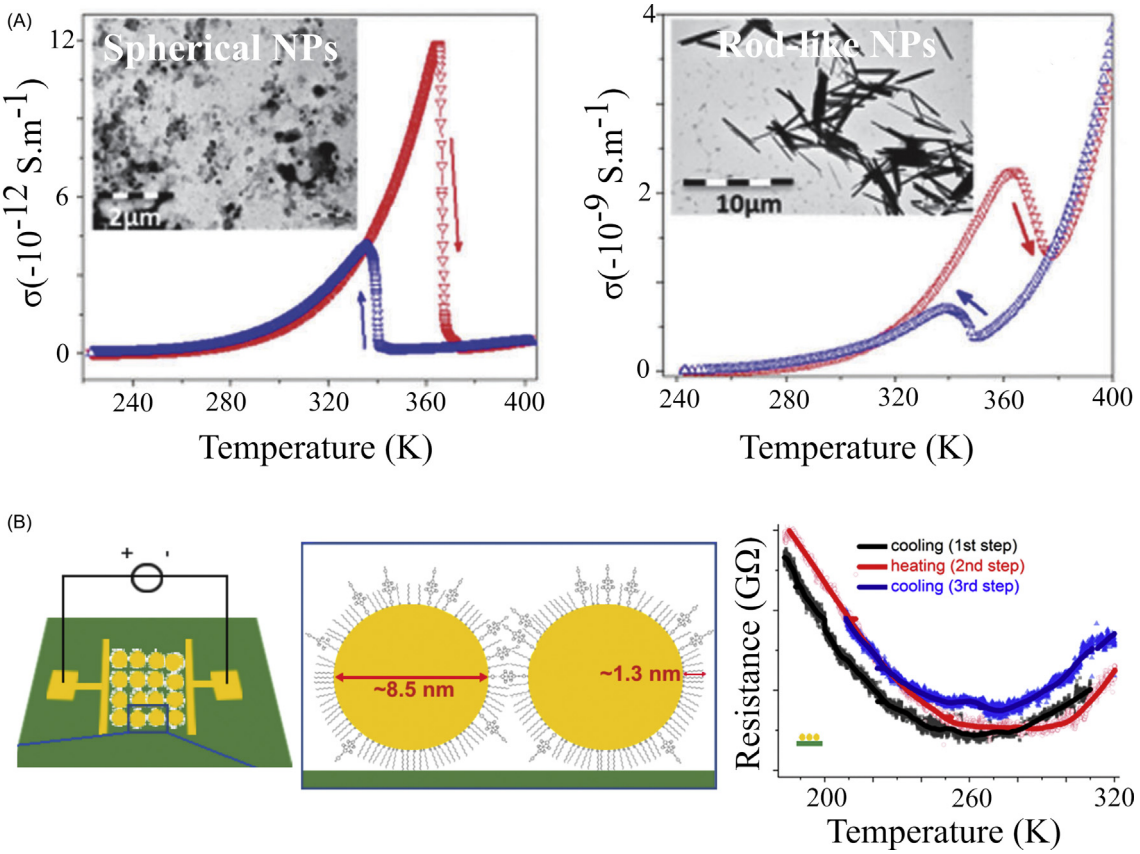

Fig. 9 Transport characteristics of nanostructured SCO architectures. (A) Temperature versus dc conductivity plots of spherical (C1) and needle-like (C2) $[Fe(Htrz)_2(trz)](BF_4)$ nanostructures, showing hysteretic conductance switching. (Reproduced with permission from Rotaru, A.; Gural'skiy, I. A.; Molnár, G.; Salmon, L.; Demont, P.; Bousseksou, A. *Chem. Commun.* **2012**, *48*(35), 4163–4165. https://doi.org/10.1039/C2CC30528C.) (B) Schematic of an SCO molecule-Au nanoparticle array device; the Au nanoparticles (box) are protected by a mixed layer of SCO complex and octanethiol ligands. The minimum in the resistance observed, around the $T_{1/2}$, in the temperature-dependent resistance plots is attributed to spin-state switching. (Reproduced with permission from Devid, E. J.; Martinho, P. N.; Kamalakar, M. V.; Šalitroš, I.; Prendergast, Ú.; Dayen, J.-F.; Meded, V.; Lemma, T.; González-Prieto, R.; Evers, F.; Keyes, T. E.; Ruben, M.; Doudin, B.; van der Molen, S. J. *ACS Nano* **2015**, *9*(4), 4496–4507. https://doi.org/10.1021/acsnano.5b01103.)

While the transport characteristics of NP junctions composed of polymeric $[Fe(Htrz)_2(trz)](BF_4)$ complex are well investigated, studies on NP architectures composed of monomeric SCO complexes decorated around metallic cores are scarce. Functionalization of Au NPs with a molecular SCO complex $[Fe(AcSBPP)_2](ClO_4)_2$ featuring sulfur-based anchoring groups and octane thiol alkyl chains resulted in the formation of mixed-ligand protected Au-NPs (Fig. 9B). The particles were arranged as arrays in between Au electrodes separated by 100 nm. Temperature dependent transport characteristics, at an applied bias of 0.3 V, of Au-NP array junction indicated the high resistance (R) state of the HS complexes decorated around the Au core. Unlike the studies involving the $[Fe(Htrz)_2(trz)](BF_4)$ complex, a gradual resistance versus T profiles were observed in the Au@SCO molecule junctions. Remarkably, a resistance minimum in the R versus T plots were observed in the Au@SCO molecule junctions close proximity to the $T_{1/2}$ value observed for the molecular complex in the bulk state. Such appearance of the resistance minimum could be used to probe SCO temperature in electrical devices incorporating SCO molecules.[161]

Overall, the hysteretic conductance versus temperature profiles recorded for $[Fe(Htrz)_2(trz)](BF_4)$ junctions are promising towards the fabrication of realistic SCO-based switching and memory elements. Moreover, the low conductance nature of HS state observed in junctions bridged by large nm sized $[Fe(Htrz)_2(trz)](BF_4)$ particles and core-shell arrays and high conductance nature of HS $[Fe(Htrz)_2(trz)](BF_4)$ core studied in single particle junction indicate different mechanistic pathways guiding transport in the junctions.

7.07.6.1.2.2 Thin film junctions

The transport characteristics of SCO complexes deposited as thin films of various thicknesses have been studied to fabricate large area molecular electronic and spintronics junctions. Upon deposition of an SCO complex on to a substrate, the SCO properties of the complex in direct contact with the surface are heavily altered due to the molecule-surface interactions.[131,162] The situation is more pronounced for the complexes deposited on metallic substrates. A classic example is the pinning of spin-states of

$[Fe(phen)_2NCS_2]$ in direct contact with Cu(100) substrate, that is, a coexistence of LS- and HS-states were observed due to the differing nature of interactions of the complexes with the surface. As discussed in Section 7.07.6.1.2, deposition of the complex over a CuN intermediate layer reduced the interaction between the underlying Cu(100) substrate and the complex, enabling spin-state manipulation at single-molecule level. Apart from the surface-mediated blocking of SCO, the fragmentation of complexes upon interacting with the substrates have also been reported. Detailed descriptions of the role of molecule-surface (spinterface) interactions in tuning the SCO of adsorbed molecules can be found in the recent reviews and reports.[131,163–168] Increasing the thickness of the films mitigates the surface-induced perturbations on SCO starting from the second layer, and complete SCO is observed in nm thick films, as observed in the bulk-state. Several recent reviews elaborately discuss the spin-state switching properties of the surface deposited SCO complexes and the transport characteristics of thin film SCO junctions.[131,139,163,164,169,170] Consequently, a brief description of the transport characteristics of thin film SCO devices covering salient features are presented in the following sections.

In general, thin films of SCO complexes on suitable substrates are deposited employing vacuum sublimation. The technique is useful to produce impurity-free submonolayer to multilayer SCO films, and the advances made in the field has been reviewed recently.[131] The single-molecule level spin-state switching studies of $[Fe(phen)_2NCS_2]$ and $[Fe(phen)(bpz)_2]$ presented in Section 7.07.6.1.2 was also carried out on thin molecular deposits of the complexes. Since the experiments are performed by selectively switching single molecules, the studies are better placed in Section 7.07.6.1.2.

In a first ever study, transport properties of 240 nm thick film of the prototypical iron(II) complex $[Fe(phen)_2NCS_2]$ were probed by fabricating a thin complex film on an Au substrate using sublimation.[171] Current-voltage characteristics of the film sandwiched between Au electrodes at RT revealed that the space charge-limited current (SCLC) transport characteristic was mediated by the HOMO of the HS-state of the complex. Note, the complex is in the HS-state at RT, and no temperature dependent I–V characteristics were measured. A similar SCLC mediated transport in junctions composed of 50 nm film of $[Fe(qnal)_2]$ ($qnal^- =$ quinoline-naphthaldehyde), sandwiched between Ag and LiF/Au electrodes were observed. Temperature-dependent transport studies indicated a spin-state mediated switching of transport mechanism. In the LS-state of the film the transport is characterized by a shallow-trap mediated SCLC transport, whereas in the HS-state, the SCLC transport is characterized by exponential distribution of traps.[172]

Apart from the temperature dependent studies, the transport characteristics of thin SCO-active films have also been studied in optoelectronic junctions. Variable temperature transport characteristics of $[Fe(phen)(bpz)_2]$ films sandwiched between electrodes such as indium tin oxide (ITO) and aluminum (Al) indicated more conductive nature of the HS-state of the complex obtained upon temperature variation. On the other hand, the HS-state obtained at 5 K via visible light irradiation is less conductive than the corresponding LS-state, signifying different charge transport pathways associated with the device architecture in the presence or absence of visible light irradiation.[173] While the above studies indirectly elucidate the role of iron(II) centers in mediating transport, a recent device-centric in operando synchrotron X-ray absorption spectroscopic (XAS) study unambiguously proves the involvement of iron(II) centers in mediating transport.[174]

Bistable switching characteristics of SCO complexes render them useful for the fabrication of molecule-based memory elements. However, the so far studied SCO complexes in the thin film state have shown gradual SCO characteristics not appealing for applications. To mitigate this issue, thin films of $[Fe(bpy)(bpz)_2]$ (bpy = 2,2′-bipyridine), were deposited on ferroelectric substrates and a non-volatile resistance switching was demonstrated.[175] The spin-state of the complex is pinned either in the LS or HS-state depending on the ferroelectric polarization of the substrate and the spin-state is retained in the absence of applied voltage. The switching between the low and high resistance state corresponding to the HS and LS states, respectively, was induced by changing the ferroelectric polarization of the underlying ferroelectric substrates via voltage poling. The bistable nature of the resistance switching conferred the devices with memory function. A read-only memory, similar to the NP-based memory architectures discussed in Section 7.07.6.1.2.1, based on 200 nm thick film of $[Fe(HB(pz)_3)_2]$ deposited between interdigitated Au-electrodes, was also demonstrated. Remarkably, the experiments revealed the more conductive nature of the LS-state of $[Fe(HB(pz)_3)_2]$ than the HS-state.[176]

Overall, spin-state dependent conductance switching is established in thin film junctions in line with the single molecule and nanoparticles junctions discussed in the previous sections. The utility of the SCO complexes as non-volatile and read-only memory elements have also been demonstrated in the thin film junctions. A point noteworthy here is that the high- or low-conductance nature of a particular spin-state dependents on the nature of experiment performed, as well-established for thermal and optoelectronic junctions composed of $[Fe(phen)(bpz)_2]$ films.

7.07.6.1.3 Graphene-SCO hybrid device architectures

The sensitivity of SCO to interfacial interactions is a well-known phenomenon, especially for mono or submonolayer thick films of SCO complexes in direct contact with metallic electrodes. On the other hand, the intrinsically insulating nature of the molecular and nanostructured SCO materials hamper the realistic device integration of SCO materials. To circumvent these issues, graphene-SCO hybrid materials are proposed, considering the device suitable electrical conductance characteristics of graphene. Such proposition is also based on the recent reports elucidating the preservation of spin-state switching of molecular complexes in direct contact with graphene/highly oriented pyrolytic graphene (HOPG) substrate[135,165] and the observation of modulated electrical transport properties of graphene due to spin-state switching of adsorbed SCO nanoparticles.

Three main directions, namely, (i) studying of spin-state switching characteristics of molecule and nanoparticles anchored or adsorbed on graphene, elucidating the graphene/molecule/nanoparticle interface in tuning SCO, (ii) non-invasive spin-state

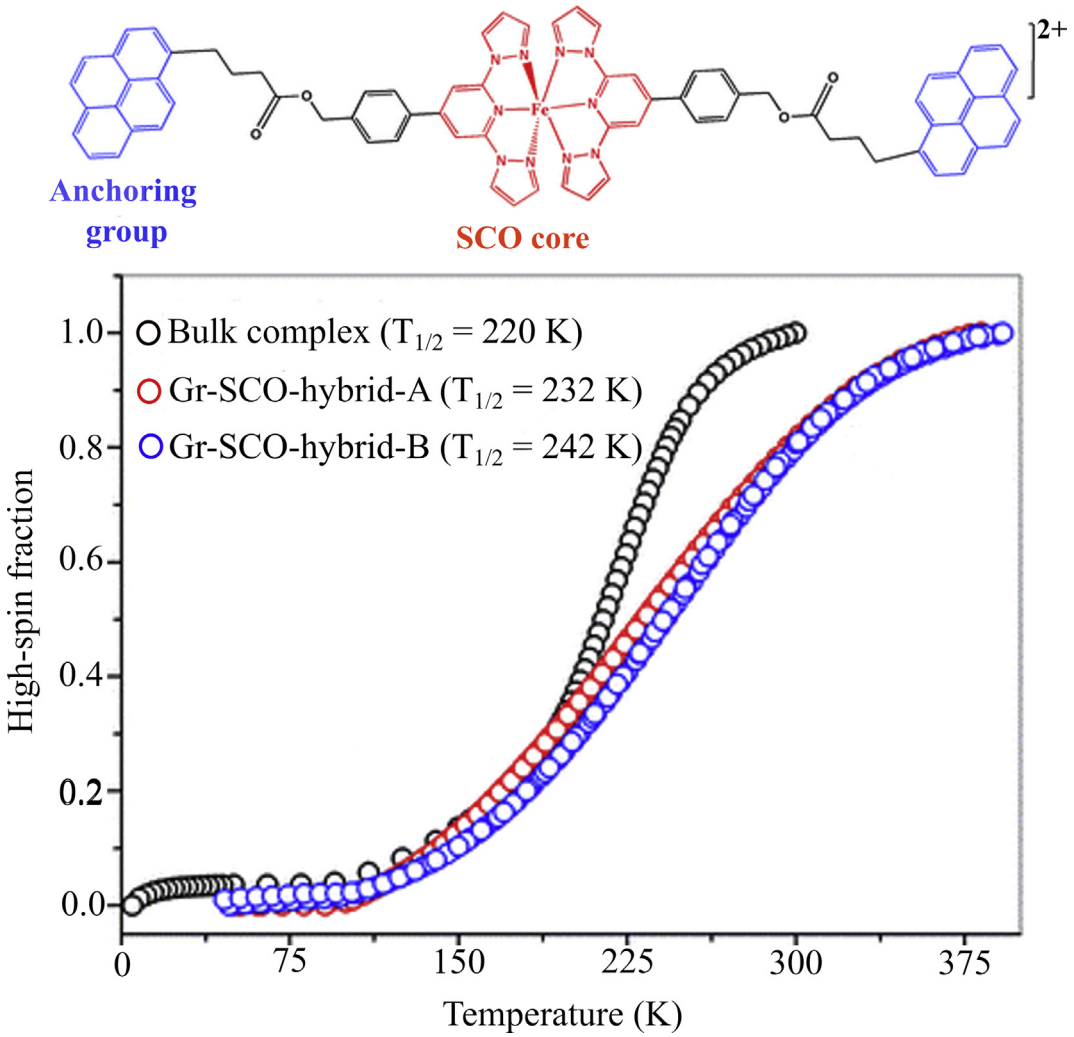

Fig. 10 Spin-state switching in a graphene-SCO hybrid material. (A) Molecular structure of an SCO complex tethered with pyrene anchoring groups. (B) Spin-state switching characteristics of the complex in the bulk-state and graphene-SCO complex hybrids. The similar SCO profiles of graphene-SCO complex hybrids Gr-SCO-A and Gr-SCO-B indicate the reproducible nature of the hybrid material preparation. Images reproduced with permission from Senthil Kumar, K.; Šalitroš, I.; Boubegtiten-Fezoua, Z.; Moldovan, S.; Hellwig, P.; Ruben, M. A *Dalton Trans.* **2018**, *47*(1), 35–40. https://doi.org/10.1039/C7DT03623J.

probing using graphene-transport measurements, and (iii) the elucidation of SCO-based memory architectures have been developed over time.

In comparison with the bulk SCO characteristics, notable variations in the SCO characteristics of nanoparticles and molecular complexes upon anchoring with graphene have been demonstrated.[133,135] In a typical study, SCO characteristics of a graphene-SCO complex hybrid was probed and the preservation of SCO of the complex was elucidated (Fig. 10).[135] Such experimental observations encouraged the fabrication of graphene-based devices, facilitating non-invasive readout of spin-state of nanoparticles and single crystals, employing graphene-transport measurements.

The sensitivity of graphene's electrical transport characteristics to the spin state of surface-deposited SCO active materials is the underlying principle of such a proposition. Consequently, non-invasive spin-state detection of a $[Fe(Htrz)_2(trz)](BF_4)$ nanoparticle thin film deposited on a CVD graphene was demonstrated. The coupling between the graphene charge-carrier scattering mechanism and dielectric modulation of SCO film induced by spin-state change enabled spin-state detection.[177] Recently, the spin state of an SCO complex crystal was probed (see Fig. 11) in a graphene field effect transistor (GFET) device using a concept called chemo-electric gating (CEG).[178] In the GEC-based GFET, electric dipole fluctuations (arising upon SCO) associated with the molecules inside the crystal caused electrostatic potential variations inside the graphene sheet and the Dirac point of the sheet was altered accordingly, paving the way for the direct electrical probing of the spin-state of the SCO crystal. The tri-layer GFET device consists of an SCO crystal and a graphene layer separated by a polymeric spacer. The polymeric spacer is permeable to electrostatic effects and minimizes mechanical stress-induced conductivity variation of the graphene sheet due to SCO. Heat-cool cycles of the device in

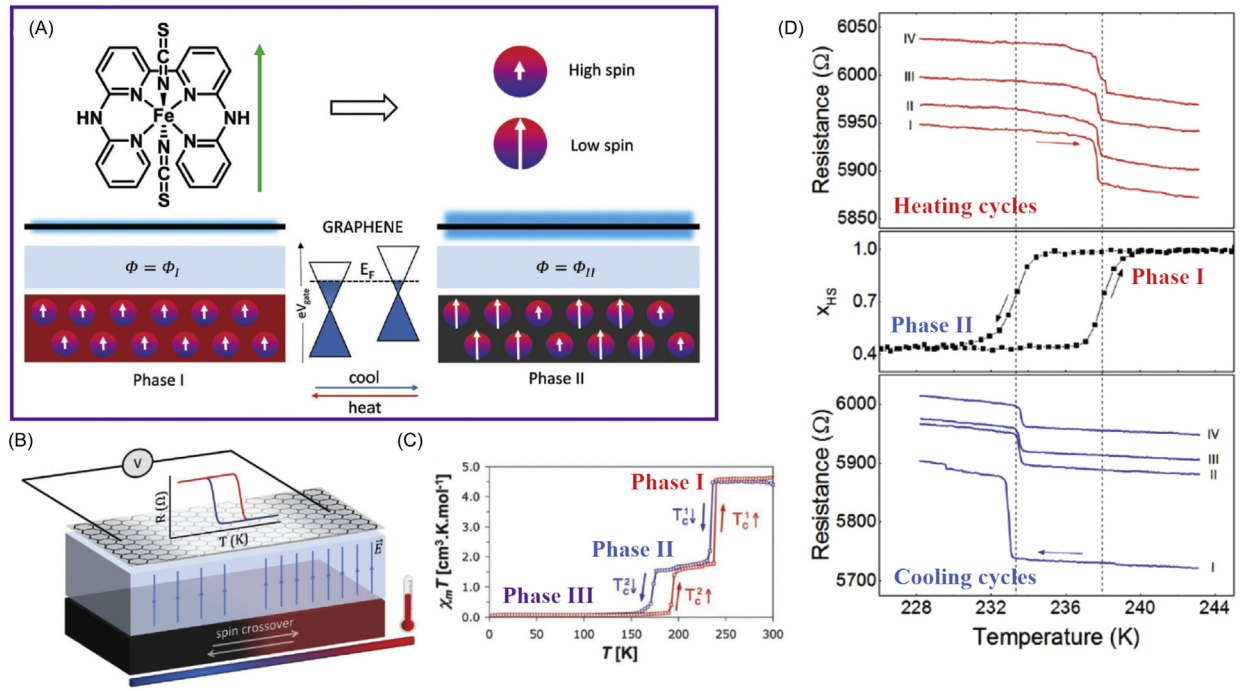

Fig. 11 Contactless sensing of SCO in GFET device. (A) Molecular structure of the iron(II) complex—the direction of dipole moment associated with the complex is shown as a green arrow—and the mechanism of CEG mediated sensing of spin-state of the complex crystals: the dipole moment variation associated with the SCO modulates the Dirac points of graphene, facilitating spin-state detection. (B) Schematic of the GFET device structure. The presence of dielectric polymeric spacer between the SCO crystal substrate and graphene sheet renders the device as contactless spin-state sensor. (C) $\chi_m T$ versus T plot showing the stepwise and hysteretic spin-state characteristic of the complex crystal. The HS, intermediate spin, and LS states of the crystal are denoted as phase I, II, and III, respectively. (D) Resistance versus temperature plots of the device in the heating (top) and cooling (bottom) modes. The resistance drop/increase of the device coinciding with the midpoints of phase II to phase I/phase I to phase II transitions (middle) in the heating/cooling cycles facilitates spin-state detection. Reproduced from Geest, E. P.; Shakouri, K.; Fu, W.; Robert, V.; Tudor, V.; Bonnet, S.; Schneider, G. F. *Adv. Mater.* **2020**, *32*(10), 1903575. https://doi.org/10.1002/adma.201903575.

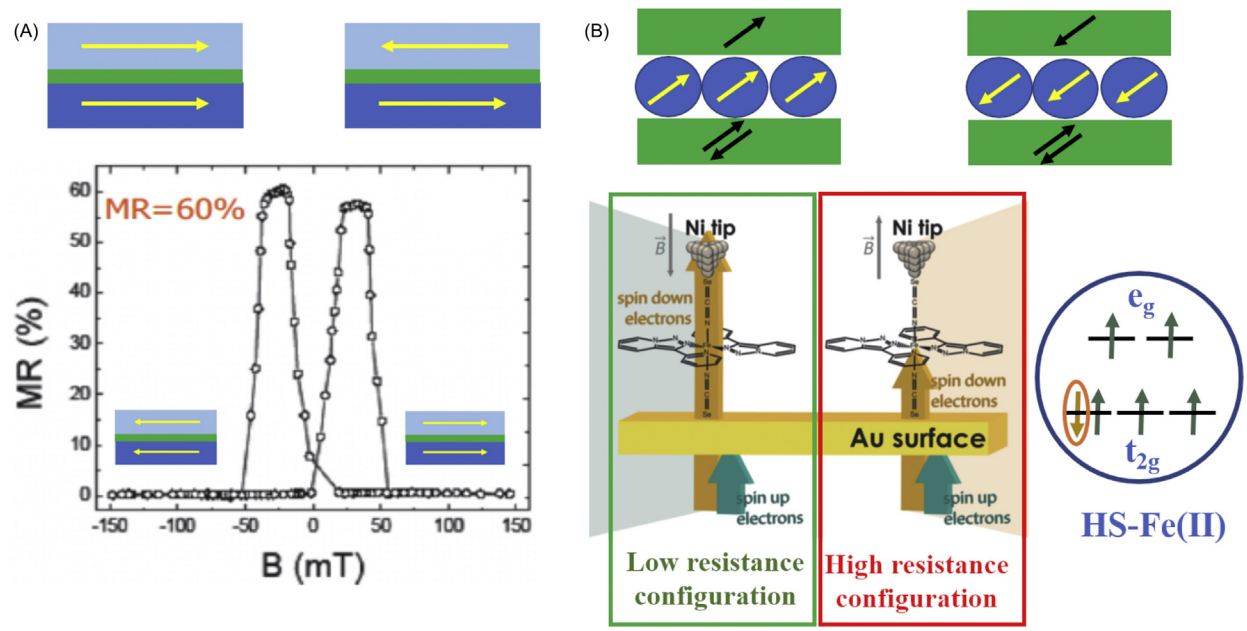

Fig. 12 Spintronics junctions. (A) In a solid-state junction a nonmagnetic conducting spacer is sandwiched between two ferromagnetic electrodes. The magnetization direction of the hard (bottom) ferromagnetic electrode is fixed, whereas the magnetization direction of the soft (top) electrode could be reversibly modulated by applying a magnetic field (top schematic). Low (R_P) and high (R_{AP}) resistance states are observed for the parallel and antiparallel alignment, respectively, of magnetization direction of top and bottom ferromagnetic electrodes. Magneto resistance (MR) is calculated

the SCO region induced resistivity variation of the GFET device commensurate with the spin-state switching, exemplifying a contactless spin-state sensing mechanism using graphene transport measurement.

7.07.6.1.4 Spin-polarized transport in SCO junctions

Solid-state spintronics relies on the spin polarized nature of charge carriers. Spintronics concepts such as giant magneto resistance (GMR) and tunnel magneto resistance (TMR) paved the way for the realization of magnetic memories. In a typical GMR device, a nm thick nonmagnetic conducting metallic sheet is placed in between two (bottom and top) ferromagnetic electrodes (Fig. 12A). The resistance of the device depends on the magnetic orientation of the bottom and top electrodes: low and high resistance states are obtained for parallel and anti-parallel orientations, respectively.

In molecular spintronics, an offspring of solid-state spintronics, molecules are used as a nonmagnetic layer to separate bottom and top magnetic electrodes (Fig. 12B). The topic came to the fore after the observation of spin-polarized charge injection from a magnetic electrode to an organic semiconductor; a strong magnetoresistance and spin diffusion length of 200 nm were reported.[67] Subsequently, the generic nature of spin-polarized transport in molecular spintronic device architectures composed of ferromagnetic electrodes and non-magnetic molecules was demonstrated.[179] Use of magnetic molecules, such as SMMs and SCO complexes, adds another dimension to the molecular spintronics research. For example, molecular spintronics junctions solely relying on the magnetic property—namely, magnetic anisotropy, HS-state—of a molecule could be developed. In such junctions, a magnetic molecule is sandwiched between metallic and nonmagnetic electrodes and a spin polarized current output could be observed with the polarization state of the output determined by the magnetic state of the molecule. In a rare example, a spintronic junction solely composed of organic components (i.e. without metallic electrodes) was achieved. The junction termed as "supramolecular spin value" is composed of $TbPc_2$-SMMs anchored on single walled carbon nanotube (SWNT) and charge carrier transport is dictated by the magnetic state of SMMs anchored on SWNTS, see Section 7.07.6.2.1 for more details. While conceptually interesting, the low temperature operation limit of SMM-based spintronics devices hinder the realization of practical RT operable spintronics devices. SCO complexes capable of undergoing reversible spin-state switching at around RT are ideal choices to obtain ambient temperature operable molecular spintronics junctions. Moreover, the tunable nature of spin-state at single molecule level (as discussed in Section 7.07.6.2.1) renders the SCO complexes suitable for the development of switchable spintronics junctions—an ON-OFF switching of polarized current output is envisioned.

As elucidated in computational studies, HS iron(II) SCO complexes sandwiched between nonmagnetic metallic electrodes act as spin filters, whereas transport in LS complex is not spin polarized due to the equal number of spin-up and spin-down electrons. After electron injection from an electrode to a HS complex, only spin-down electrons are transported through the molecule due to the close proximity of spin-down electron-containing t_{2g} orbitals to the Fermi level of the electrode. Despite many computational studies predicting spin filtering by HS SCO complexes, not much has been reported on experimental confirmationsof such predictions.

In a rare experimental study, a large conductance switching and spin polarized transport was reported for a device composed of a $[Fe(tzpy)_2(NCS)_2]$ SCO complex (Fig. 12B, tzpy = 2-pyridyl[1,2,3]triazolo[1,5-α]pyridine). When the HS complex is sandwiched between a nonmagnetic Au electrode and spin polarized nickel (Ni) tip, only spin-down electrons are transported through the HS complex and the spin-up electrons are scattered due to the close energetic alignment of spin-down electron-containing t_{2g} orbital to the Au Fermi level. The resistance state of the device is controlled by the polarity of the Ni tip. When the polarity is down, the spin down electrons passing through the HS complex are transported without scattering, thus a low-resistance state of the device is achieved. On the other hand, a high-resistance state is obtained in the case of a spin-up polarized Ni tip. Overall, the spin filtering nature of HS $[Fe(tzpy)_2(NCS)_2]$ was demonstrated through these experiments.

7.07.6.2 SMM Spintronic Devices

In this section, we will describe recent advances in the construction of SMM-based spintronic devices. We note that while electrically conducting SMMs have been recently reviewed in the context of bulk samples,[72] this is not the focus of the current discussion, as we will focus on single-molecule devices.

using the relation: $MR = (R_{AP}\text{-}R_P/R_P) \times 100$ (bottom graph). (Part of the image reproduced with permission from Fert, A. *Rev. Mod. Phys.* **2008**, *80*(4), 1517–1530. https://doi.org/10.1103/RevModPhys.80.1517 (B) In an ideal molecular spintronic junction spin polarization of the conducting electrons are determined by the magnetic molecule sandwiched between nonmagnetic electrodes (top schematic). Preferential transport of spin-down electron in a spintronics junction involving a HS SCO complex. In this particular example, a spin-polarized Ni tip is used as a top electrode. The spin-down electrons, shown inside the orange circle, are preferentially transported via the HS complex, rendering the HS Fe(II) complex as a spin filter. The polarization of the Ni tip is used as a detection mechanism: a low resistance state is obtained for spin-down tip polarization (bottom figure). (Part of the image reproduced with permission from Aragonès, A. C.; Aravena, D.; Cerdá, J. I.; Acís-Castillo, Z.; Li, H.; Real, J. A.; Sanz, F.; Hihath, J.; Ruiz, E.; Díez-Pérez, I. *Nano Lett.* **2016**, 16(1), 218–226. https://doi.org/10.1021/acs.nanolett.5b03571

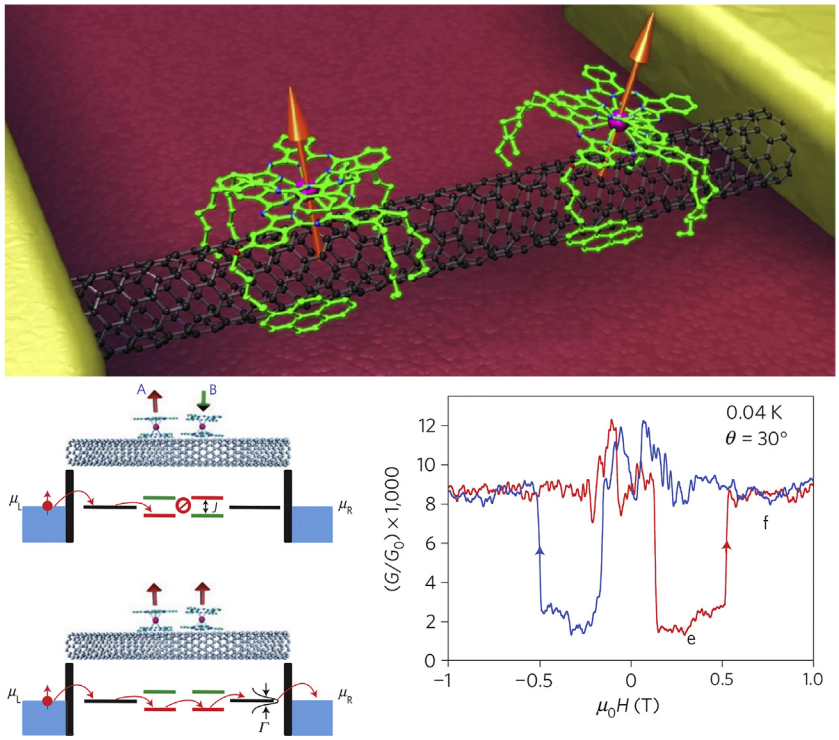

Fig. 13 Top: Artistic view of the supramolecular spin valve. The pyrene-substituted Pc ligand shown in the image assures π-π interactions with the SWCNT, stabilizing the SMM through a supramolecular assembly. Bottom Left: Representation of the spin filtering mechanism. When two consecutive SMMs have opposite spin polarizations, the energy mismatch of the channels decreases the conductance. Under stronger external magnetic fields all spin polarizations are parallel, which triggers the high conductance state. Right: Magnetoresistance as a function of field sweeps for an angle of 30° relative to the SWCNT axis. Reproduced from Krainov, I. V.; Klier, J.; Dmitriev, A. P.; Klyatskaya, S.; Ruben, M.; Wernsdorfer, W.; Gornyi, I. V. *ACS Nano* **2017**, *11*(7), 6868–6880. https://doi.org/10.1021/acsnano.7b02014.

7.07.6.2.1 Supramolecular spin valves

The devices described herein are closely related to molecular spin valves (see Section 7.07.4.2.2), with the difference that of interest here are single-molecule variations of this concept. It should be noted that theoretical investigations have dealt with SMM-based spin-valve transistors (SVTs) between non-magnetic electrodes in which an SMM acts as a conducting and spin-filtering component.[180,181] However, experimental work has shown that SWNTs are good conductors for spin-polarized currents, either injected at the ferromagnet-SWNT interface in spin valves,[182] or polarized on the SWNTs themselves by SMMs grafted upon them (see below).

Before describing such devices constructed with SMMs, it is useful to point out the overarching concept of an SVT. This was invented in 1995[183] to solve the problem of measurement of the spin-valve effect, until then carried out in the experimentally more expedient current-in-plane (CIP) geometry. CIP measurements reduce the measured effect to only the electrons that are shunted between layers, while those channeled in a single layer do not participate. The current-perpendicular-to-plane (CPP) geometry allows all electrons to cross the various layers, but then the very thin multilayer device only exhibits a small resistance which is difficult to measure. The SVT solved this problem, though the discussion falls beyond the scope of this chapter.

Conceptually, single-molecule SVTs are a variation of molecular spin transistors (MSTs, see Section 7.07.6.2.3). However, it was discovered that the same polarization effect could be achieved by a single molecule of the $TbPc_2$ SMM, where the spin filtering and conducting functions are handled separately by the SMM and by a SWCNT, respectively. In a modification of the MST described in Section 7.07.6.2.3, spin valves were constructed by connecting two non-magnetic Pd electrodes with a SWCNT.[184] This junction sat atop an insulating SiO_2 layer, with a gate below. Chemically modified $TbPc_2$ SMMs were then attached onto the SWCNT through π-π interactions through a pyrene-substituent grafted on one of the phtalocyanine ligands (Fig. 13). During previous studies it had been determined[185] that a $TbPc_2$ per 11 nm of SWCNT was on average attached, giving an average number of four SMMs anchored atop the SWCNT in the SVT device. In such a device, the first SMM acts as the spin polarizer, whereas the subsequent ones act as spin analyzers, giving a smaller or larger resistance to the SWCNT depending on their spin polarization (parallel or antiparallel) with respect to their previous SMM. Spin filtering was hysteretic as a function of magnetic field sweeps: for strongly negative fields, all SMMs were polarized parallel to one another giving a low resistance. Upon sweeping the field to the opposite direction, at some point one of the SMMs reversed its magnetization first, leading to the high-resistance regime. Upon further increase another SMM followed suit recovering the low-R regime. This behavior was strongly dependent on the field-sweep rate according to Landau-Zener statistics,[186] with slower field sweeps leading to a zero-field spin reversal via quantum tunneling of magnetization

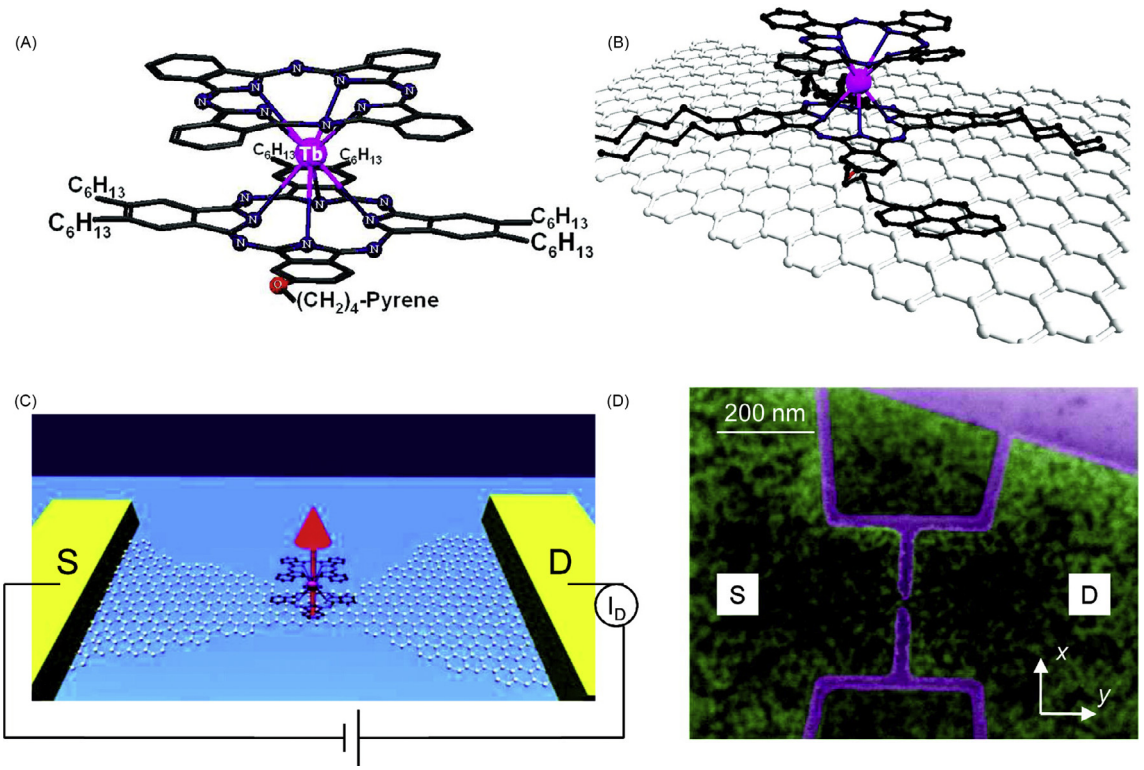

Fig. 14 Representation of the pyrene-substituted $TbPc_2$ molecule (A) adsorbed on a graphene sheet (B). A graphene nanocostriction with adsorbed $TbPc_2$ is connecting the source and drain of a molecular transistor. An artistic representation of the device is shown in (C) and a false-color SEM image in (D). Reproduced from Candini, A.; Klyatskaya, S.; Ruben, M.; Wernsdorfer, W.; Affronte, M. *Nano Lett.* **2011**, *11*(7), 2634–2639. https://doi.org/10.1021/nl2006142.

(QTM) reducing the hysteresis, and faster sweeps favoring spin reversal at higher fields through a direct process. Another statistically intriguing aspect of these few-molecule experiments is that for the same device, spin flips do not occur at precisely the same field, but can vary from sweep to sweep.

In effect, these experiments showed that a single SMM molecule reproduced the function of an entire ferromagnetic layer of spin valves. The ferromagnet-electrode-like function of SMM is due to the hybridization of the $S = 1/2$ $Pc^{\bullet-}$ radical with the nanotube walls which allowed a very efficient transfer of polarization between the Tb^{III} electron spin and the SWCNT through the Tb-Pc magnetic coupling, effectively creating localized quantum dots. This phenomenon was subsequently theoretically investigated in greater detail.[187–189] A more advanced adaptation of this experiment, involving transverse magnetic fields and three lateral side-gates was used to demonstrate the magnetic exchange coupling between the electronic spins of the Tb^{III} ion and the $Pc^{\bullet-}$ radical.[190] However, a few remarks are also in order: (i) The devices showed strong variability, with GMR ratios ranging from 2% to 300%.[191] (ii) The number of SMMs per device is not easy to control.

It is worth noting that a very related, though not identical, device was reported involving $TbPc_2$ molecules deposited on graphene. The adsorption of the pyrene-substituted $TbPc_2$ on graphene was demonstrated using spatially resolved Raman spectroscopy (Fig. 14).[192] Based on these findings, a device consisting of a graphene nanoconstriction connecting two electrodes, was constructed, on which $TbPc_2$ was deposited.[193] This device exhibited a magnetoresistance that was highly sensitive to the magnetization orientation of the SMM molecules, and in principle could form the basis for highly sensitive magnetic sensors.

As these developments demonstrate, graphene is acquiring increasing importance in the construction of molecular devices, something that has been extensively reviewed[194] and further stressed in the context of a graphene-electrodes molecular transistor implementation (see Section 7.07.6.2.3).

7.07.6.2.2 Molecular magnetomechanical resonators

Building upon the design of the supramolecular spin valve, but taking it to an entirely different direction, the SWCNT was considered as a nanoelectromechanical system (NEMS), and its mechanical oscillations were used as a measured quantity. It had been predicted that the spin degree of freedom of a magnetic molecule or nanoparticle, rigidly grafted on a nanomechanical resonator (such as a SWCNT), could couple to the mechanical oscillations of that resonator.[195,196] At the same time, it had been proposed that a highly anisotropic magnetic species of magnetic moment $\mathbf{m}$, could exert a magnetic torque $\boldsymbol{\Gamma}_{mag} = \mathbf{m} \times \mathbf{H}_{ext}$ under the influence of an external magnetic field $\mathbf{H}_{ext}$, thus producing an S-shaped deformation (Fig. 15, top).[197] This model suggests that the strain would modify the resonance frequency of the mechanical oscillation by a quantity Δf. Theoretically, the spin reversal at the

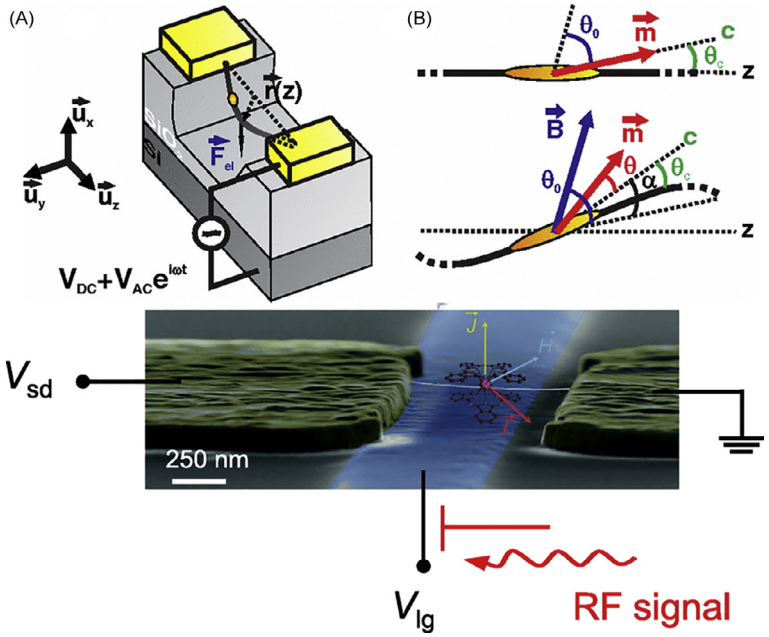

Fig. 15 Top: the principle of a molecular magnetomechanical resonator. A SWCNT is suspended between two points and under the influence of a periodic RF excitation $V_{AC}(t)$ undergoes an oscillation of amplitude **r**(z). Under the influence of a magnetic field, a magnetic molecule grafted onto the oscillator exerts a torque, twisting the oscillator thus modifying its resonance frequency. In the figure, **c** is the magnetic anisotropy vector, **B** is the magnetic field and **m** is the magnetic moment vector under the influence of **B**. (Reproduced from Lassagne, B.; Ugnati, D.; Respaud, M. *Phys. Rev. Lett.* **2011**, 107 (13). https://doi.org/10.1103/PhysRevLett.107.130801 Bottom: SEM image showing a molecular resonator consisting of a $TbPc_2$ molecule rigidly grafted on a SWCNT. The molecular structure of the SMM is overlayed on the SEM image, indicating the magnetic moment vector **J**. The excitation-detection were conducted through the transistor gate and source-drain voltages, respectively. (Adapted from Ganzhorn, M.; Klyatskaya, S.; Ruben, M.; Wernsdorfer, W. *Nat. Nanotechnol.* **2013**, *8*(3), 165–169. https://doi.org/10.1038/nnano.2012.258; Ganzhorn, M.; Klyatskaya, S.; Ruben, M.; Wernsdorfer, W. *ACS Nano* **2013**, *7*(7), 6225–6236. https://doi.org/10.1021/nn402968k

appropriate field should be associated with a discontinuity of the Δf value, also associated with hysteretic behavior. Also, the Δf versus $\mathbf{H}_{ext}$ profile was predicted to be dependent on the angle between the $\mathbf{H}_{ext}$ vector and the molecular easy axis, with the hysteretic behavior disappearing entirely when the magnetic field is normal to the anisotropy axis.

An implementation of this idea was demonstrated using the pyrene-substituted $TbPc_2$ molecule described above (see Section 7.07.6.2.1). The device consisted of the spin transistor described above, whose bias and gate voltages were used to control the resonance frequency of the SWCNT oscillation (Fig. 15, bottom). Field sweeps parallel to the molecule's easy axis were carried out and the spin reversals were monitored through conductance measurements, demonstrating that the spin system could indeed couple to the SWCNT's oscillation modes.[198]

Subsequently, the possibility of a torque-based mechanical magnetometer was tested using this device. For that implementation the magnetic moment of the $TbPc_2$ molecule can be expressed as $\mathbf{m} = (g\mu_B/\hbar)\mathbf{J}$, and can be expected to induce a magnetomechanical response. A radiofrequency (RF) driving signal ($\sim$112 MHz) was injected through the gate voltage by means of a home-made bias *T*, and was superposed to the DC gate voltage, at a temperature of 20 mK. Indeed, the induced mechanical oscillations were detected by the source-drain electrodes through the changes they produced on the charge flow. At low powers, a pristine SWCNT behaved as a harmonic oscillator, implementing a high-quality resonator ($Q \sim 18{,}000$). At higher powers, a $TbPc_2$-grafted SWCNT behaved as a Dufing oscillator, exhibiting strong nonlinearity and a bistability between two oscillation modes. The spin reversal could trigger a sudden transition between the two modes, which could be detected with a very good signal to noise (S/N) ratio by the source-drain voltage change.[199] Incidentally, a larger-scale approach of this principle was subsequently reported using a 140 nm layer of a SCO complex deposited on a MEMS resonator, hysteretically modifying its oscillation characteristics.[200]

7.07.6.2.3 Molecular spin transistors

At a fundamental level, a molecular transistor (MT) follows the design principles of MOSFETs, with the molecular junction sitting atop a gate that can apply a controlled electric field on the molecule. The electric field modifies the electronic states of the molecule and subsequently its transport properties. In what follows, it is assumed that MTs are single-molecule ones: although SAM-based large-area MTs have recently started to be considered, they still constitute a very minor part of current research.[201,202]

The first implementation of a molecular transistor was reported in 2000, and consisted of C_{60} molecules placed between Au electrodes fabricated through the electromigration technique.[19] This study revealed that the transport properties of the molecule could couple with additional degrees of freedom, vibrational in that case, hence allowing their study via the conductance measurements.

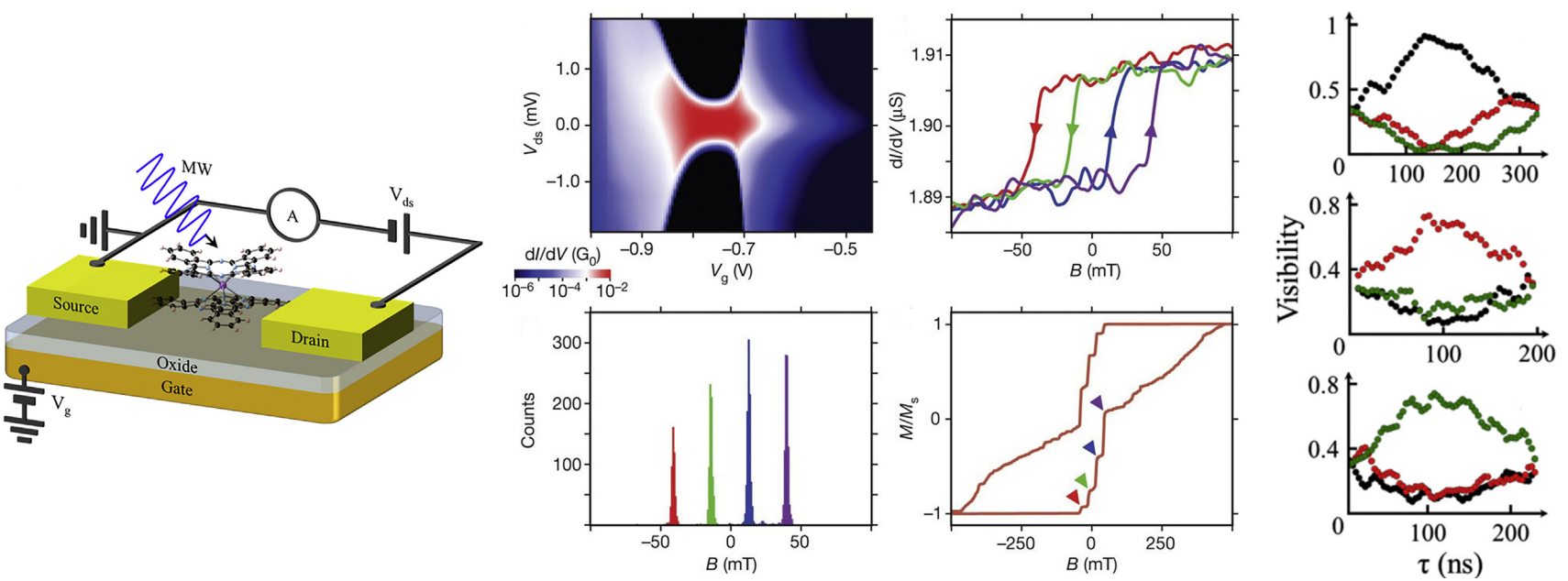

Fig. 16 Left: Design principle of the molecular spin transistor, including a microwave (MW) irradiation enhancement. (Reproduced from Godfrin, C.; Lumetti, S.; Biard, H.; Bonet, E.; Klyatskaya, S.; Ruben, M.; Candini, A.; Affronte, M.; Wernsdorfer, W.; Balestro, F. *J. Appl. Phys.* **2019**, *125*(14), 142801. https://doi.org/10.1063/1.5064593.) Middle: Electrical readout of the nuclear qubit state. The position of the conductance jump is characteristic of the spin-state. (Reproduced from Vincent, R.; Klyatskaya, S.; Ruben, M.; Wernsdorfer, W.; Balestro, F. *Nature* **2012**, *488*(7411), 357–360. https://doi.org/10.1038/nature11341 Right: A database quantum search by implementation of the Grover algorithm: starting from a superposition of three states (the "database" entries), manipulation of the spin qubit with specially designed MW pulses can selectively populate the desired state, i.e. can "pull" a particular database entry. (Reproduced from Godfrin, C.; Ferhat, A.; Ballou, R.; Klyatskaya, S.; Ruben, M.; Wernsdorfer, W.; Balestro, F. *Phys. Rev. Lett.* **2017**, *119*(18), 187702. https://doi.org/10.1103/PhysRevLett.119.187702.)

This concept was extended to the magnetic degrees of freedom of the MJ molecule in 2002. In two back-to-back papers, molecular spin transistors were used to study the magnetotransport properties of a paramagnetic $[Co^{II}(terpy)_2]^{2+}$ complex,[203] and of an antiferromagnetic $[(Me_3tacn)_2V^{IV}{}_2(CN)_4(\mu\text{-}C_4N_4)]$ dinuclear complex.[204]

This technique was soon applied to the study of Mn_{12} SMMs, in two 2006 studies. In one case researchers studied junctions prepared from the archetypical Mn_{12}-acetate and for the Mn_{12}-chloroacetato SMM,[205] whereas in the other the authors studied an Mn_{12} SMM with the S-terminated 4-(acetylthio)benzoato ligand ($Me(O{=}C)S\text{-}Ph\text{-}CO_2^-$).[206] In both those studies the junctions were fabricated through electromigration of Au wires, sitting atop an Al/Al_2O_3 gate/insulator, and in both reports Coulomb blockade features appeared in about 10% of the fabricated junctions. However, the excitation energies determined by the two works varied by an order of magnitude (14 vs 1.1–1.3 meV, respectively). It should be noted that neither the precise identity of the molecular species between the electrodes nor its oxidation state were confirmed.

Subsequently, spin transistors constructed through the same method with Fe_4-SMMs revealed field-dependent excitations at 1.5 meV, comparable to the U_{eff} value, and the differential conductance plots showed regions of Coulomb blockade and of single-electron tunneling.[207] In this case the authors were more sure of the stability of the molecules on the Au electrode based on the results of prior studies of surface-deposited samples. Researchers observed the magnetic anisotropy by sample rotations inside the magnetic field,[208] and a Franck-Condon blockade.[209] At the same time, these results inspired studies on Mn_4 SMMs.[210]

Such devices were not only constructed with SMMs. The $[2 \times 2]$ $Co^{II}{}_4$ molecular grid complex $[Co^{II}{}_4L_4](BF_4)_8$ (L = 4,6-bis(2′,2″-bipyrid-6′-yl)-2-phenylpyrimidine) was used to construct such devices, and their conductance characteristics revealed vibrational effects related to the molecule and the appearance of two distinct oxidation states as a function of the gate voltage.[211]

However, the SMM that was most studied in the context of spin transistors is $TbPc_2$, in experiments reported in 2012[212] and illustrated in (Fig. 3). Due to QTM, magnetic relaxation at low temperatures is accelerated at magnetic fields which induce level crossings between the $J_z = +6$ and -6 states; for $TbPc_2$ this occurs at four positions (two for increasing and two for decreasing fields), in particular at ± 14 and ± 40 mT. These experiments showed that due to its ferromagnetic coupling to the Tb^{III} spin, the conductance of the $Pc^{\bullet-}$ radical ligand, which can be considered as a quantum dot, acquires a different value for each of the two J_z states of the Tb^{III} ions, effectively allowing the electrical readout of the nuclear spin state. This exchange-induced dependence of the conductance on the spin-state was further elaborated subsequently (Fig. 16).[213]

For these experiments, a crucial device component was a 3D vector magnet that could align the applied magnetic field to the molecular easy axis, which was not possible to control during the fabrication of the junction. Measurements of the differential conductance dI/dV revealed a Kondo effect due to the $S = 1/2$ radical spin, and a Kondo temperature T_K calculated at 0.6 K. Measurements under swept magnetic fields revealed changes in conductance between two values, at the magnetic field strengths associated with the spin flips. This being a unique molecule, the spin flip would occur only at a single magnetic field for each field sweep, so the experiments were repeated 75,000 times, and histograms revealed peaks of the spin-flip fields at the four different positions mentioned above.

Further statistical analysis of a larger number of such experiments involving 2.5 s sweeps and zero waiting time,[214] revealed that when spin flips occurred they were only characterized by $\Delta m_I = 0, \pm 1$. Further analysis of the dwell time of the system at each nuclear spin state revealed a T_1 values of $\sim$25 s for the $m_I = \pm 3/2$ states and $\sim$ 13 s for the $m_I = \pm 1/2$ ones. These differences were correlated with the number of transition paths for each state, which were two for the $m_I = \pm 1/2$ states (excitation *and* relaxation) and only one for the for the $m_I = \pm 3/2$ states (excitation *or* relaxation). The relaxation mechanism was determined to be spin-lattice relaxation through a Weger process which involves the conduction electrons, and associated with their number per unit time, thus suggesting a way of electrical control of the relaxation by the current density.

Reversal statistics for different waiting times between each sweep revealed that for waiting time up to ca. 20 s led to spin flips of $\Delta m_I = 0$, indicating a long lifetime of the hyperfine states. Only for waiting times above 50 s did $\Delta m_I = \pm 1, \pm 2$ and ± 3 transitions start becoming statistically significant, indicating that spin-flips occurred between two successive field sweeps, i.e. during the waiting time. This experiment demonstrated the single-shot readout of the nuclear spin state of a unique molecule by purely electric means, a first step in passing from the use of molecular spin transistors as purely analytical devices to functional ones.

In a next step, the authors used an updated version of the device, which incorporated the ability to irradiate the molecule with microwave pulses.[7] They found that the MW pulses interacted with the spin system and excited transitions between its nuclear states. However, it was not the magnetic component of the MW radiation that was absorbed, as this was determined to be too weak to achieve such an effect. Instead, it was the electric component (ca. 1 mV/nm) which interacted with the spin system through the hyperfine Stark effect. Since the effective magnetic field $\mathbf{B}_{eff}$ at the nucleus is a function of the spin (J) and the hyperfine interaction (A), modifying A by a time-dependent electric field can in principle lead to oscillations of $\mathbf{B}_{eff}$ that can be used to control the spin state. Moreover, it was found that the static HF Stark effect from the gate voltage modified the resonance frequency, providing with an additional lever for electric control. After initializing it at its $m_I = +3/2$ state, MW pulses were used to excite the transition to the $m_I = +1/2$ nuclear state. By varying the pulse duration, Rabi oscillations were recorded. By applying a pulse sequence of two $\pi/2$ pulses separated by a time τ, the authors recorded Ramsay fringes whose fit allowed them to determine $T_2{}^* = 64$ μs.

These groundbreaking experiments started bringing closer to realization a goal outlined almost two decades previously, and which provided a major impetus for the study of SMMs, i.e. their use for the encoding of spin qubits. SMMs, with their molecular nature and facile preparation, promised to overcome limitations relating to scaling, and were examined by theoreticians as potential qubit candidates.[215,216] Moreover, the possibility of a Hilbert space of a dimension $d > 2$ (e.g. in polynuclear MNMs like Mn_{12}, or mononuclear ones with hyperfine interactions), allows to envisage the generalization of the qubit concept beyond the two-level paradigm, i.e. to qu*d*its.[217]

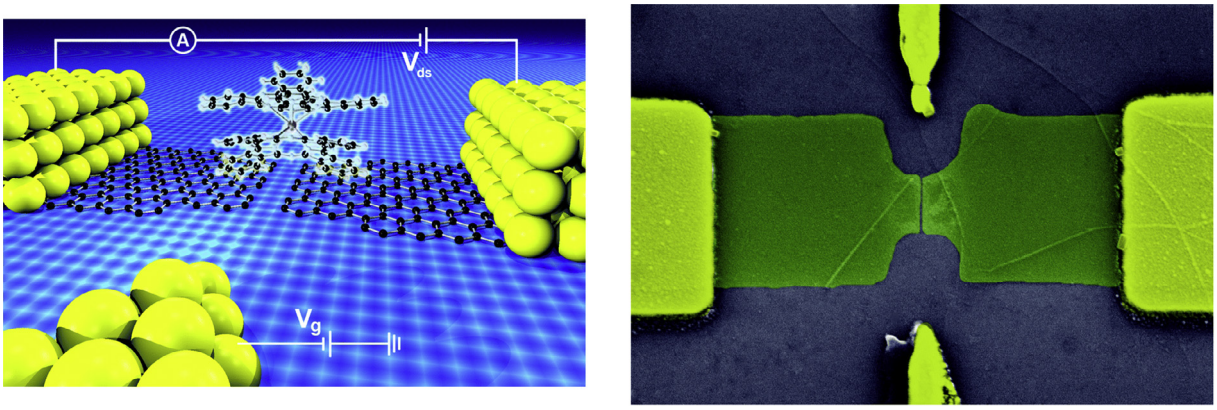

Fig. 17 Left: Artistic view of the spin transistor consisting of graphene source-drain electrodes. Right: false-color SEM image of the device. Reproduced from Lumetti, S.; Candini, A.; Godfrin, C.; Balestro, F.; Wernsdorfer, W.; Klyatskaya, S.; Ruben, M.; Affronte, M. *Dalton Trans.* **2016**, *45* (42), 16570–16574. https://doi.org/10.1039/C6DT02445A with permission from The Royal Society of Chemistry.

Based on these principles and taking their implementation a step further to a functioning device, these researchers used the $TbPc_2$ transistor as a spin qu*d*it, by utilizing the $d = 4$ dimensionality of the Hilbert subspace of its ground state.[8] In particular, they set off from the previous proposition that the Grover algorithm could be implemented by a unique multilevel quantum system,[218] foregoing the need of entangling qubits. By using a multichromatic MW pulse which could excite all three transitions ($+3/2 \rightarrow +1/2$, $+1/2 \rightarrow -1/2$, $-1/2 \rightarrow -3/2$), it was possible to create a coherent superposition of two, three, or four states (Hadamard gate) corresponding to a "database." Starting from the three-state superposition, it was possible to use another specially designed pulse to selectively amplify each of the states, thus selectively accessing the "database."

By adapting the electromigration technique from gold to graphene (see **Section 7.07.6.2.1**), it was also possible to create nanometer-separated graphene electrodes using a feedback-controlled electroburning technique in air and at room temperature. By ramping up the voltage over several cycles it was possible to create precise nanometer-scale gaps at 87% yields, on which $TbPc_2$ could be deposited by drop-casting (**Fig. 17**).[219] One of the advantages of using graphene instead of gold is that the increased mobility of Au atoms at room temperature is avoided, thus greatly facilitating the construction of devices and increasing their life time.

In closing, a few remarks are in order regarding the challenges of MSTs in their current implementation: (i) Electromigrated STs have a low yield per chip (ca. 10%) which limits their high throughput fabrication. (ii) The molecules are stabilized in the interelectrode gap with random molecular orientations, which hinders multiqubit architectures experiencing the same external magnetic field. (iii) STs have the potential of aging at elevated temperatures due to the mobility of the molecules and/or the Au atoms. Aging also occurs under high source-drain voltages. (iv) Different device preparations of $TbPc_2$ transistors have shown sample-dependent Kondo temperatures, Pc-Tb exchange couplings and T_1 times, thus putting into question the ability to construct arrays of identical systems.

7.07.7 Perspectives and Conclusions

In this section we attempt to assess the perspectives of molecular devices based on coordination complexes, taking into account developments in related fields.

7.07.7.1 Hybrid Molecular-Superconducting Devices

The development of molecular devices based on coordination complexes stands to benefit from experimentation with different types of materials as substrates/electrodes, in particular superconductors. An early attempt to study the effects of such hybrid structures involved microcrystalline Mn_{12}-acetate, coprecipitated with a microcrystalline sample of a YBaCuO superconductor.[220] Recently, more elaborate studies involved the UHV deposition and magnetic study of a Fe_4 SMM on the (111) surface of a Pb crystal, a type I superconductor. This was chosen to study its SMM behavior inside and outside the superconducting window of Pb ($T_C < 7.2$ K, $B_C < 0.08$ T). Indeed, for $B > B_C$ QTM was suppressed and a thermally activated magnetic relaxation dominated, seen as hysteresis loops. When the magnetic field was gradually reduced below $B < B_C$, the superconductor transitioned to its intermediate state, characterized by growing Meissner-state islands which repel the external applied field. This transition was observed as an increasing fraction of SMMs undergoing tunneling relaxation, since in their immediate vicinity $B_{loc} = 0$.[221]

Superconducting coplanar waveguide (or microstrip) resonators have been used to increase the sensitivity of EPR spectroscopy and have been tried on molecular materials, such as a chromium(III) spin triangle,[222] and organic radicals.[223] However, the same problem can be recast as the coherent coupling of the modes of these resonators with the molecular spins, which might allow the

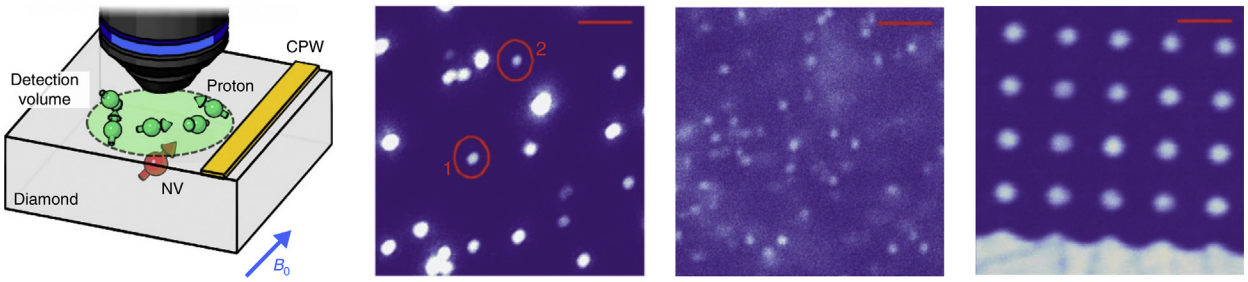

Fig. 18 New technologies in single-spin readout. Left: Single-spin magnetic resonance uses NVs to detect nearby nuclear or electronic spins by virtue of dipolar interactions. (Reproduced from Staudacher, T.; Raatz, N.; Pezzagna, S.; Meijer, J.; Reinhard, F.; Meriles, C. A.; Wrachtrup, J. *Nat. Commun.* **2015**, *6*(1). https://doi.org/10.1038/ncomms9527.) Right: Single-spin optical addressing uses light detection to directly detect by optical means Ln^{III} impurities inside a diamagnetic matrix. (Reproduced from Kolesov, R.; Xia, K.; Reuter, R.; Stöhr, R.; Zappe, A.; Meijer, J.; Hemmer, P. R.; Wrachtrup, J. *Nat. Commun.* **2012**, *3*(1). https://doi.org/10.1038/ncomms2034.)

information transfer between superconducting qubits and spin qubits. The interest would be that use of spin qubits that are also capable of acting as color centers, might provide additional benefits such as the optical addressing of such hybrid systems,[224–228] an issue also considered in Section 7.07.7.2.

7.07.7.2 Qubits Beyond Spintronics?

To date, attempts at SMM-qubit implementations have been carried out by using spin transistors for SMM-qubit readout and/or control (see Section 7.07.6.2.3). In that sense, the distinction between an SMM qubit and an SMM spin transistor is currently trivial. However, this does not necessarily need to remain the case, as new emerging principles could be used for a more efficient single-qubit control and readout. Not only have new types of magnetic molecules, and not just SMMs, been examined for the purpose,[229] but new theoretical understandings (e.g. the role of vibronic degrees of freedom,[230] couplings to surfaces,[231] magnetoelectric couplings[232]) are starting to shape the design of molecules and devices, and recent review articles have outlined several of these new tasks and perspectives.[233,234]

As far as device architecture is concerned, such a new paradigm may be a necessity considering the limitations of spin transistors, at least in their current implementation. While molecular species are generally praised for their ability to form large arrays, a principal problem of current technologies is their inability to individually address the molecules of such large arrays. For example, multi-tip STMs (see Section 7.07.5.2.1) can address a small number of pre-positioned molecules, but scaling would be highly challenging. On the other hand, incorporating molecular species on prefabricated nanoelectronic devices (e.g. on electromigrated junctions through drop casting) suffers from low yields, typically in the order of a few percent per chip, as well as difficult to control aging of the device (see Section 7.07.6.2.3).

To remedy these deficiencies and regain the essential advantages of molecular objects (e.g. the facile preparation of large arrays of identical objects through molecular engineering[235]), it would be ideal to be able to optically address such arrays. Two developments in single-molecule detection may provide answers to these problems:

7.07.7.2.1 Single-spin magnetic resonance

In this detection method, NV centers are brought into close contact with the molecules whose magnetic resonance needs to be studied. The magnetic fields produced by the electronic or nuclear spins interact with the NVs, slightly modifying their Zeeman shift. The detection is then carried out optically, by examining the intensity of the fluorescence under irradiation of a 532 nm laser (Fig. 18, left). This approach, referred to as single-spin magnetic resonance, has produced impressive sensitivities, going as far as the detection of a few nuclear spins with a single NV.[236–239]

Clearly, the detection of electronic spins with magnetizations as strong as those of Ln^{III} ions is within the reach of this technique. However, the need to controllably approach the SMM molecule to a NV introduces an additional engineering complication.

7.07.7.2.2 Single-spin optical addressing

It might be more interesting to entirely forego the use of the NV by directly reading the spin of the SMM. In that regard, and considering the relevance of Ln-based SMMs, a very interesting work was the use of visible-to-ultraviolet upconversion for optical detection of a single Pr^{III}-ion impurities implanted in an yttrium aluminum garnet (YAG) crystal (Fig. 18, right).[240]

One of the problems of achieving single-shot optical readout of Ln^{III} impurities was the lack of cyclicity of these transitions: due to the admixtures of crystal-field states, there is an absence of strictly allowed and forbidden transitions, with all of them being weakly allowed. Thus, relaxation can occur through multiple pathways, making it difficult to cycle a specific transition. A way to resolve this was proposed by using strong magnetic fields.[241]

Recently, the single-shot detection of such impurities was reported in two works appearing simultaneously.[242,243] In particular, Raha et al.[242] reported the non-demolition readout of an Er^{III} impurity in yttrium silicate (Y_2SiO_5, YSO) with 94.6% fidelity.

Kindem et al.[243] reported the single-shot readout of $^{173}Yb^{III}$ ions in an yttrium orthovanadate (YVO_4 or YVO) crystal with over 95% fidelity.

7.07.7.2.3 Optically addressable spin qubits

These readout schemes achieve the readout of spin qubits without recourse to conductance measurements. Such measurements, as was mentioned above, suffer from significant issues of reproducibility, yield and stabilities. In effect, removing the requirement for conducting electrons to couple with the spin degree of freedom, would *stricto* sensu remove these spin qubits from the realm of spintronics.

Such schemes require optically addressable spin qubits, which may function in a capacity similar to that of color centers, such as nitrogen vacancies (NVs) in diamonds, with an added benefit that of a higher spatial precision in their fabrication. These qubits could be optically initialized in the desired state, manipulated with MW pulses, and then read out optically (optically-detected magnetic resonance, ODMR). Significance progress has been made in this direction by the group of Danna Freedman (see a review of some early achievements[244] and more recent results).[245] Very recently, more elaborate experiments were reported on molecular ($S = 1$, $D > 0$) analogues of NVs based on organometallic $[Cr^{IV}R_4]$ complexes ($R = o$-tolyl, 2,3-dimethylphenyl, 2,4-dimethylphenyl).[246] These complex molecular qubits were initialized through optical pumping, manipulated with MW pulses administered through a CPW and finally read out by ODMR, demonstrating the functioning principles of such a qubit.

These studies were carried out on magnetically dilute samples (in a diamagnetic SnR_4 matrix) and on ensembles of spin qubits. Eventually, the single-spin addressing techniques may be applied to develop molecule-based optically controlled devices.

7.07.7.3 Conclusions

The computational and experimental investigations discussed in the preceding sections elucidate the utility of magnetic coordination complexes as go-to systems to replicate device architectures achieved with solid-state devices. For example, the demonstration of molecular spin valves and the implementation of Grover's algorithm at a molecular scale are some of the salient examples in which the potential of molecular components is unanbiguously illustrated. The tuning of physical properties and the bottom-up self-assembly facilitated by molecular engineering principles, render these molecular components very attractive for the practical implementation of future devices. A case-by-case sum up of challenges ahead for molecular systems is presented as follows.

On the SCO front, the experimental demonstrations of spin-state switching at single-molecule junctions upon application of bias voltage, electric field, and stretching are encouraging both in terms of conceptual understanding of switching mechanisms at the single molecule scale and of spintronics applications. A missing link is the comprehensive experimental elucidation of computationally predicted spin-polarized transport in HS junctions and ON-OFF switchability of polarized electron transport. To achieve the observation of spin-polarized transport, an SCO molecule could be connected between ferromagnetically polarized electrodes and the transport characteristics analyzed. In a similar vein, the spin-polarized transport could be studied in thin-film junctions by sandwiching an SCO molecule in between ferromagnetic electrodes.

On the SMM front, a series of tasks remains to be tackled. First, the temperature range where the SMM effect is operative still remains quite low, just having overtaken liquid nitrogen temperatures in one case.[247] While this is not forbidding per se the development of certain devices (e.g. spin qubits), increase of this temperature would facilitate the more straightforward construction and wider adoption of such devices. Another issue just having begun to be appreciated, and which is critical for device fabrication, is the importance of SMM-substrate spin-phonon interactions[231,248] and of vibronic degrees of freedom[230] on the SMM phenomenon. While magnetoanisotropy-engineering has been a main focus for the increase of the spin-reversal barrier over the past three decades, these are issues that will need to be addressed for the future SMM-device conception. Finally, with the importance of the nuclear spin degree of freedom, fabricating identical devices translates to synthesizing isotopically pure SMMs.

In conclusion, isotopologue coordination chemistry, which takes into account the impact of the nuclear spin degree of the central atom on the physical properties, respectively the device function, will therefore become a key factor in the practical implementation of coordination complexes.[5]

References

1. Werner, A. *Z. Anorg. Chem.* **1893,** *3* (1), 267–330. https://doi.org/10.1002/zaac.18930030136.
2. Werner, A. *Neuere Anschauungen Auf Dem Gebiete Der Anorganischen Chemie*, F. Vieweg und Sohn: Braunschweig, 1905.
3. Cotton, F. A.; Wilkinson, G. *Advanced Inorganic Chemistry: A Comprehensive Text*, 4th edn.; Wiley: New York, 1980. completely rev. from the original literature.
4. Bogani, L.; Wernsdorfer, W. *Nat. Mater.* **2008,** *7* (3), 179–186. https://doi.org/10.1038/nmat2133.
5. Wernsdorfer, W.; Ruben, M. *Adv. Mater.* **2019,** *31* (26), 1806687. https://doi.org/10.1002/adma.201806687.
6. Burzurí, E.; García-Fuente, A.; García-Suárez, V.; Senthil Kumar, K.; Ruben, M.; Ferrer, J.; van der Zant, H. S. J. *Nanoscale* **2018,** *10* (17), 7905–7911. https://doi.org/10.1039/C8NR00261D.
7. Thiele, S.; Balestro, F.; Ballou, R.; Klyatskaya, S.; Ruben, M.; Wernsdorfer, W. *Science* **2014,** *344* (6188), 1135–1138. https://doi.org/10.1126/science.1249802.
8. Godfrin, C.; Ferhat, A.; Ballou, R.; Klyatskaya, S.; Ruben, M.; Wernsdorfer, W.; Balestro, F. *Phys. Rev. Lett.* **2017,** *119* (18), 187702. https://doi.org/10.1103/PhysRevLett.119.187702.
9. Dietrich-Buchecker, C. O.; Sauvage, J. P.; Kintzinger, J. P. *Tetrahedron Lett.* **1983,** *24* (46), 5095–5098. https://doi.org/10.1016/S0040-4039(00)94050-4.
10. Anelli, P. L.; Spencer, N.; Stoddart, J. F. *J. Am. Chem. Soc.* **1991,** *113* (13), 5131–5133. https://doi.org/10.1021/ja00013a096.
11. Koumura, N.; Zijlstra, R. W. J.; van Delden, R. A.; Harada, N.; Feringa, B. L. *Nature* **1999,** *401* (6749), 152–155. https://doi.org/10.1038/43646.

12. Wilson, M. R.; Solà, J.; Carlone, A.; Goldup, S. M.; Lebrasseur, N.; Leigh, D. A. *Nature* **2016,** *534* (7606), 235–240. https://doi.org/10.1038/nature18013.
13. Erbas-Cakmak, S.; Fielden, S. D. P.; Karaca, U.; Leigh, D. A.; McTernan, C. T.; Tetlow, D. J.; Wilson, M. R. *Science* **2017,** *358* (6361), 340–343. https://doi.org/10.1126/science.aao1377.
14. Iino, R.; Kinbara, K.; Bryant, Z. *Chem. Rev.* **2020,** *120* (1), 1–4. https://doi.org/10.1021/acs.chemrev.9b00819.
15. Peplow, M. *Nature* **2015,** *525* (7567), 18–21. https://doi.org/10.1038/525018a.
16. De Cola, L., Chiorboli, C., Eds.; *Molecular Wires: From Design to Properties. Topics in Current Chemistry*, Springer: Berlin; New York, 2005.
17. James, D. K.; Tour, J. M. *Molecular Wires and Electronics; Topics in Current Chemistry*; ; Springer Berlin Heidelberg: Berlin, Heidelberg, 2005; pp 33–62. https://doi.org/10.1007/b136066.
18. Weiss, E. A.; Wasielewski, M. R.; Ratner, M. A. *Molecular Wires and Electronics; Topics in Current Chemistry*; ; Springer Berlin Heidelberg: Berlin, Heidelberg, 2005; pp 103–133. https://doi.org/10.1007/b136068.
19. Park, H.; Park, J.; Lim, A. K. L.; Anderson, E. H.; Alivisatos, A. P.; McEuen, P. L. *Nature* **2000,** *407* (6800), 57–60. https://doi.org/10.1038/35024031.
20. Xiang, D.; Wang, X.; Jia, C.; Lee, T.; Guo, X. *Chem. Rev.* **2016,** *116* (7), 4318–4440. https://doi.org/10.1021/acs.chemrev.5b00680.
21. Boča, R. *Theoretical Foundations of Molecular Magnetism*, 1st edn.; In: *Current Methods in Inorganic Chemistry* Elsevier: New York, 1999.
22. Aviram, A.; Ratner, M. A. Molecular Rectifiers. *Chem. Phys. Lett.* **1974,** *29* (2), 277–283. https://doi.org/10.1016/0009-2614(74)85031-1.
23. Pioneer Corporation. History of Pioneer Corporation | Brand/History | Corporate Information | Pioneer Corporation https://global.pioneer/en/info/history/chronology/ (accessed Jul 22, 2020).
24. Pope, M.; Kallmann, H. P.; Magnante, P. *J. Chem. Phys.* **1963,** *38* (8), 2042–2043. https://doi.org/10.1063/1.1733929.
25. Tang, C. W.; VanSlyke, S. A. *Appl. Phys. Lett.* **1987,** *51* (12), 913–915. https://doi.org/10.1063/1.98799.
26. Tang, C. W.; VanSlyke, S. A.; Chen, C. H. *J. Appl. Phys.* **1989,** *65* (9), 3610–3616. https://doi.org/10.1063/1.343409.
27. Baldo, M. A.; O'Brien, D. F.; You, Y.; Shoustikov, A.; Sibley, S.; Thompson, M. E.; Forrest, S. R. *Nature* **1998,** *395* (6698), 151–154. https://doi.org/10.1038/25954.
28. Baldo, M. A.; Lamansky, S.; Burrows, P. E.; Thompson, M. E.; Forrest, S. R. *Appl. Phys. Lett.* **1999,** *75* (1), 4–6. https://doi.org/10.1063/1.124258.
29. Light Emitters and Dopants – OLED and PLED Materials. https://www.sigmaaldrich.com/materials-science/material-science-products.html?TablePage=19353482 (accessed Jul 21, 2020).
30. Becquerel, H. *C. R. Acad. Sci.* **1839,** *9*, 145–149.
31. Grätzel, M. *Nature* **2001,** *414* (6861), 338–344. https://doi.org/10.1038/35104607.
32. Moser, J. *Monatsh. Chem.* **1887,** *8* (1), 373. https://doi.org/10.1007/BF01510059.
33. Tributsch, H. *Photochem. Photobiol.* **1972,** *16* (4), 261–269. https://doi.org/10.1111/j.1751-1097.1972.tb06297.x.
34. Gleria, M.; Memming, R. *Z. Phys. Chem.* **1975,** *98* (1–6), 303–316. https://doi.org/10.1524/zpch.1975.98.1-6.303.
35. Clark, W. D. K.; Sutin, N. *J. Am. Chem. Soc.* **1977,** *99* (14), 4676–4682. https://doi.org/10.1021/ja00456a025.
36. Tributsch, H. *Z. Naturforsch. A* **1977,** *32* (9). https://doi.org/10.1515/zna-1977-0911.
37. Dare-Edwards, M. P.; Goodenough, J. B.; Hamnett, A.; Seddon, K. R.; Wright, R. D. *Faraday Discuss. Chem. Soc.* **1980,** *70,* 285. https://doi.org/10.1039/dc9807000285.
38. O'Regan, B.; Grätzel, M. *Nature* **1991,** *353* (6346), 737–740. https://doi.org/10.1038/353737a0.
39. Nazeeruddin, M. K.; Kay, A.; Rodicio, I.; Humphry-Baker, R.; Mueller, E.; Liska, P.; Vlachopoulos, N.; Graetzel, M. *J. Am. Chem. Soc.* **1993,** *115* (14), 6382–6390. https://doi.org/10.1021/ja00067a063.
40. Carella, A.; Borbone, F.; Centore, R. *Front. Chem.* **2018,** *6*. https://doi.org/10.3389/fchem.2018.00481.
41. Tachibana, Y.; Haque, S. A.; Mercer, I. P.; Durrant, J. R.; Klug, D. R. *J. Phys. Chem. B* **2000,** *104* (6), 1198–1205. https://doi.org/10.1021/jp992774b.
42. Higashino, T.; Imahori, H. *Dalton Trans.* **2015,** *44* (2), 448–463. https://doi.org/10.1039/C4DT02756F.
43. Mathew, S.; Yella, A.; Gao, P.; Humphry-Baker, R.; Curchod, B. F. E.; Ashari-Astani, N.; Tavernelli, I.; Rothlisberger, U.; Nazeeruddin, M. K.; Grätzel, M. *Nat. Chem.* **2014,** *6* (3), 242–247. https://doi.org/10.1038/nchem.1861.
44. Harlang, T. C. B.; Liu, Y.; Gordivska, O.; Fredin, L. A.; Ponseca, C. S.; Huang, P.; Chábera, P.; Kjaer, K. S.; Mateos, H.; Uhlig, J.; Lomoth, R.; Wallenberg, R.; Styring, S.; Persson, P.; Sundström, V.; Wärnmark, K. *Nat. Chem.* **2015,** *7* (11), 883–889. https://doi.org/10.1038/nchem.2365.
45. Chábera, P.; Liu, Y.; Prakash, O.; Thyrhaug, E.; Nahhas, A. E.; Honarfar, A.; Essén, S.; Fredin, L. A.; Harlang, T. C. B.; Kjær, K. S.; Handrup, K.; Ericson, F.; Tatsuno, H.; Morgan, K.; Schnadt, J.; Häggström, L.; Ericsson, T.; Sobkowiak, A.; Lidin, S.; Huang, P.; Styring, S.; Uhlig, J.; Bendix, J.; Lomoth, R.; Sundström, V.; Persson, P.; Wärnmark, K. A. *Nature* **2017,** *543* (7647), 695–699. https://doi.org/10.1038/nature21430.
46. Liu, Y.; Persson, P.; Sundström, V.; Wärnmark, K. *Acc. Chem. Res.* **2016,** *49* (8), 1477–1485. https://doi.org/10.1021/acs.accounts.6b00186.
47. Wenger, O. S. *J. Am. Chem. Soc.* **2018,** *140* (42), 13522–13533. https://doi.org/10.1021/jacs.8b08822.
48. Wenger, O. S. *Chem. A Eur. J.* **2019,** *25* (24), 6043–6052. https://doi.org/10.1002/chem.201806148.
49. Technology – Exeger. https://exeger.com/technology (accessed Aug 25, 2020).
50. Solaronix – Solar Cells. Technology. https://www.solaronix.com/solarcells/technology/ (accessed Aug 25, 2020).
51. Technology. https://h.glass/technology/ (accessed Aug 25, 2020).
52. How to Build Your Own Solar Cell – Sol Ideas Technology Development. https://www.solideas.com/solrcell/english.html (accessed Aug 25, 2020).
53. Kojima, A.; Teshima, K.; Shirai, Y.; Miyasaka, T. *J. Am. Chem. Soc.* **2009,** *131* (17), 6050–6051. https://doi.org/10.1021/ja809598r.
54. Lee, M. M.; Teuscher, J.; Miyasaka, T.; Murakami, T. N.; Snaith, H. J. *Science* **2012,** *338* (6107), 643–647. https://doi.org/10.1126/science.1228604.
55. Bi, D.; Yi, C.; Luo, J.; Décoppet, J.-D.; Zhang, F.; Zakeeruddin, S. M.; Li, X.; Hagfeldt, A.; Grätzel, M. *Nat. Energy* **2016,** *1* (10). https://doi.org/10.1038/nenergy.2016.142.
56. Why perovskite photovoltaics? | Oxford PV. https://www.oxfordpv.com/perovskite-pv-transform-global-solar-market (accessed Aug 24, 2020).
57. Grätzel, M. *Nat. Mater.* **2014,** *13* (9), 838–842. https://doi.org/10.1038/nmat4065.
58. Khenkin, M. V.; Katz, E. A.; Abate, A.; Bardizza, G.; Berry, J. J.; Brabec, C.; Brunetti, F.; Bulović, V.; Burlingame, Q.; Di Carlo, A.; Cheacharoen, R.; Cheng, Y.-B.; Colsmann, A.; Cros, S.; Domanski, K.; Dusza, M.; Fell, C. J.; Forrest, S. R.; Galagan, Y.; Di Girolamo, D.; Grätzel, M.; Hagfeldt, A.; von Hauff, E.; Hoppe, H.; Kettle, J.; Köbler, H.; Leite, M. S.; Liu, S.; Loo, Y.-L.; Luther, J. M.; Ma, C.-Q.; Madsen, M.; Manceau, M.; Matheron, M.; McGehee, M.; Meitzner, R.; Nazeeruddin, M. K.; Nogueira, A. F.; Odabaşı, Ç.; Osherov, A.; Park, N.-G.; Reese, M. O.; De Rossi, F.; Saliba, M.; Schubert, U. S.; Snaith, H. J.; Stranks, S. D.; Tress, W.; Troshin, P. A.; Turkovic, V.; Veenstra, S.; Visoly-Fisher, I.; Walsh, A.; Watson, T.; Xie, H.; Yıldırım, R.; Zakeeruddin, S. M.; Zhu, K.; Lira-Cantu, M. *Nat. Energy* **2020,** *5* (1), 35–49. https://doi.org/10.1038/s41560-019-0529-5.
59. Bergren, A. J.; Zeer-Wanklyn, L.; Semple, M.; Pekas, N.; Szeto, B.; McCreery, R. L. *J. Phys. Condens. Matter* **2016,** *28* (9), 094011. https://doi.org/10.1088/0953-8984/28/9/094011.
60. Supur, M.; Smith, S. R.; McCreery, R. L. *Anal. Chem.* **2017,** *89* (12), 6463–6471. https://doi.org/10.1021/acs.analchem.7b00362.
61. Nanolog Technology. https://www.nanologaudio.com/technology.html (accessed Aug 26, 2020).
62. Chen, X.; Roemer, M.; Yuan, L.; Du, W.; Thompson, D.; del Barco, E.; Nijhuis, C. A. *Nat. Nanotechnol.* **2017,** *12* (8), 797–803. https://doi.org/10.1038/nnano.2017.110.
63. Nijhuis, C. A.; Reus, W. F.; Siegel, A. C.; Whitesides, G. M. *J. Am. Chem. Soc.* **2011,** *133* (39), 15397–15411. https://doi.org/10.1021/ja201223n.
64. Li, T.; Bandari, V. K.; Hantusch, M.; Xin, J.; Kuhrt, R.; Ravishankar, R.; Xu, L.; Zhang, J.; Knupfer, M.; Zhu, F.; Yan, D.; Schmidt, O. G. *Nat. Commun.* **2020,** *11* (1). https://doi.org/10.1038/s41467-020-17352-9.
65. Baibich, M. N.; Broto, J. M.; Fert, A.; Van Dau, F. N.; Petroff, F.; Etienne, P.; Creuzet, G.; Friederich, A.; Chazelas, J. *Phys. Rev. Lett.* **1988,** *61* (21), 2472--2475. https://doi.org/10.1103/PhysRevLett.61.2472.
66. Binasch, G.; Grünberg, P.; Saurenbach, F.; Zinn, W. *Phys. Rev. B* **1989,** *39* (7), 4828–4830. https://doi.org/10.1103/PhysRevB.39.4828.

67. Dediu, V.; Murgia, M.; Matacotta, F. C.; Taliani, C.; Barbanera, S. *Solid State Commun.* **2002,** *122* (3–4), 181–184. https://doi.org/10.1016/S0038-1098(02)00090-X.
68. Xiong, Z. H.; Wu, D.; Valy Vardeny, Z.; Shi, J. *Nature* **2004,** *427* (6977), 821–824. https://doi.org/10.1038/nature02325.
69. Bedoya-Pinto, A.; Prima-García, H.; Casanova, F.; Coronado, E.; Hueso, L. E. *Adv. Electron. Mater.* **2015,** *1* (6), 1500065. https://doi.org/10.1002/aelm.201500065.
70. Rocha, A. R.; García-suárez, V. M.; Bailey, S. W.; Lambert, C. J.; Ferrer, J.; Sanvito, S. *Nat. Mater.* **2005,** *4* (4), 335–339. https://doi.org/10.1038/nmat1349.
71. Waldron, D.; Haney, P.; Larade, B.; MacDonald, A.; Guo, H. *Phys. Rev. Lett.* **2006,** *96* (16), 166804. https://doi.org/10.1103/PhysRevLett.96.166804.
72. Cosquer, G.; Shen, Y.; Almeida, M.; Yamashita, M. *Dalton Trans.* **2018,** *47* (23), 7616–7627. https://doi.org/10.1039/C8DT01015C.
73. Sanvito, S. *Nat. Phys.* **2010,** *6* (8), 562–564. https://doi.org/10.1038/nphys1714.
74. McCreery, R. L. *Chem. Mater.* **2004,** *16* (23), 4477–4496. https://doi.org/10.1021/cm049517q.
75. Tao, N. J. *Nat. Nanotechnol.* **2006,** *1* (3), 173–181. https://doi.org/10.1038/nnano.2006.130.
76. Akkerman, H. B.; Blom, P. W. M.; de Leeuw, D. M.; de Boer, B. *Nature* **2006,** *441* (7089), 69–72. https://doi.org/10.1038/nature04699.
77. Puebla-Hellmann, G.; Venkatesan, K.; Mayor, M.; Lörtscher, E. *Nature* **2018,** *559* (7713), 232–235. https://doi.org/10.1038/s41586-018-0275-z.
78. Thoss, M.; Evers, F. *J. Chem. Phys.* **2018,** *148* (3), 030901. https://doi.org/10.1063/1.5003306.
79. Reed, M. A. *Science* **1997,** *278* (5336), 252–254. https://doi.org/10.1126/science.278.5336.252.
80. Evers, F.; Korytár, R.; Tewari, S.; van Ruitenbeek, J. M. *Rev. Mod. Phys.* **2020,** *92* (3). https://doi.org/10.1103/RevModPhys.92.035001.
81. Domingo, N.; Bellido, E.; Ruiz-Molina, D. *Chem. Soc. Rev.* **2012,** *41* (1), 258–302. https://doi.org/10.1039/C1CS15096K.
82. Cornia, A.; Mannini, M. In *Molecular Nanomagnets and Related Phenomena;* Gao, S., Ed.; ; Springer Berlin Heidelberg: Berlin, Heidelberg, 2014; pp 293–330. https://doi.org/10.1007/430_2014_150.
83. Holmberg, R. J.; Murugesu, M. *J. Mater. Chem. C* **2015,** *3* (46), 11986–11998. https://doi.org/10.1039/C5TC03225C.
84. Dreiser, J. *J. Phys. Condens. Matter* **2015,** *27* (18), 183203. https://doi.org/10.1088/0953-8984/27/18/183203.
85. Huang, Z.; Zhang, Y.; He, Y.; Song, H.; Yin, C.; Wu, K. *Chem. Soc. Rev.* **2017,** *46* (7), 1955–1976. https://doi.org/10.1039/C6CS00891G.
86. Mann, B.; Kuhn, H. *J. Appl. Phys.* **1971,** *42* (11), 4398–4405. https://doi.org/10.1063/1.1659785.
87. Qin, L. *Science* **2005,** *309* (5731), 113–115. https://doi.org/10.1126/science.1112666.
88. Chen, X.; Jeon, Y.-M.; Jang, J.-W.; Qin, L.; Huo, F.; Wei, W.; Mirkin, C. A. *J. Am. Chem. Soc.* **2008,** *130* (26), 8166–8168. https://doi.org/10.1021/ja800338w.
89. Berndt, R.; Gaisch, R.; Gimzewski, J. K.; Reihl, B.; Schlittler, R. R.; Schneider, W. D.; Tschudy, M. *Science* **1993,** *262* (5138), 1425–1427. https://doi.org/10.1126/science.262.5138.1425.
90. Bumm, L. A.; Arnold, J. J.; Cygan, M. T.; Dunbar, T. D.; Burgin, T. P.; Jones, L.; Allara, D. L.; Tour, J. M.; Weiss, P. S. *Science* **1996,** *271* (5256), 1705–1707. https://doi.org/10.1126/science.271.5256.1705.
91. Cui, X. D. *Science* **2001,** *294* (5542), 571–574. https://doi.org/10.1126/science.1064354.
92. Xu, B. *Science* **2003,** *301* (5637), 1221–1223. https://doi.org/10.1126/science.1087481.
93. Cornia, A.; Fabretti, A. C.; Pacchioni, M.; Zobbi, L.; Bonacchi, D.; Caneschi, A.; Gatteschi, D.; Biagi, R.; Del Pennino, U.; De Renzi, V.; Gurevich, L.; Van der Zant, H. S. J. *Angew. Chem. Int. Ed.* **2003,** *42* (14), 1645–1648. https://doi.org/10.1002/anie.200350981.
94. Naitabdi, A.; Bucher, J.-P.; Gerbier, P.; Rabu, P.; Drillon, M. *Adv. Mater.* **2005,** *17* (13), 1612–1616. https://doi.org/10.1002/adma.200401623.
95. Coronado, E.; Forment-Aliaga, A.; Romero, F. M.; Corradini, V.; Biagi, R.; De Renzi, V.; Gambardella, A.; del Pennino, U. *Inorg. Chem.* **2005,** *44* (22), 7693–7695. https://doi.org/10.1021/ic0508021.
96. Alam, M. S.; Strömsdörfer, S.; Dremov, V.; Müller, P.; Kortus, J.; Ruben, M.; Lehn, J.-M. *Angew. Chem. Int. Ed.* **2005,** *44* (48), 7896–7900. https://doi.org/10.1002/anie.200502743.
97. Saalfrank, R. W.; Scheurer, A.; Bernt, I.; Heinemann, F. W.; Postnikov, A. V.; Schünemann, V.; Trautwein, A. X.; Alam, M. S.; Rupp, H.; Müller, P. *Dalton Trans.* **2006**, (23), 2865–2874. https://doi.org/10.1039/B515980F.
98. Milway, V. A.; Abedin, S. M. T.; Niel, V.; Kelly, T. L.; Dawe, L. N.; Dey, S. K.; Thompson, D. W.; Miller, D. O.; Alam, M. S.; Müller, P.; Thompson, L. K. *Dalton Trans.* **2006**, (23), 2835–2851. https://doi.org/10.1039/B515801J.
99. Ormaza, M.; Abufager, P.; Verlhac, B.; Bachellier, N.; Bocquet, M.-L.; Lorente, N.; Limot, L. *Nat. Commun.* **2017,** *8* (1). https://doi.org/10.1038/s41467-017-02151-6.
100. Vitali, L.; Fabris, S.; Conte, A. M.; Brink, S.; Ruben, M.; Baroni, S.; Kern, K. *Nano Lett.* **2008,** *8* (10), 3364–3368. https://doi.org/10.1021/nl801869b.
101. Wiesendanger, R.; Güntherodt, H.-J.; Güntherodt, G.; Gambino, R. J.; Ruf, R. *Phys. Rev. Lett.* **1990,** *65* (2), 247–250. https://doi.org/10.1103/PhysRevLett.65.247.
102. Iacovita, C.; Rastei, M. V.; Heinrich, B. W.; Brumme, T.; Kortus, J.; Limot, L.; Bucher, J. P. *Phys. Rev. Lett.* **2008,** *101* (11). https://doi.org/10.1103/PhysRevLett.101.116602.
103. Kawahara, S. L.; Lagoute, J.; Repain, V.; Chacon, C.; Girard, Y.; Rousset, S.; Smogunov, A.; Barreteau, C. *Nano Lett.* **2012,** *12* (9), 4558–4563. https://doi.org/10.1021/nl301802e.
104. Brede, J.; Atodiresei, N.; Kuck, S.; Lazić, P.; Caciuc, V.; Morikawa, Y.; Hoffmann, G.; Blügel, S.; Wiesendanger, R. *Phys. Rev. Lett.* **2010,** *105* (4). https://doi.org/10.1103/PhysRevLett.105.047204.
105. Song, Y. R.; Zhang, Y. Y.; Yang, F.; Zhang, K. F.; Liu, C.; Qian, D.; Gao, C. L.; Zhang, S. B.; Jia, J.-F. *Phys. Rev. B* **2014,** *90* (18). https://doi.org/10.1103/PhysRevB.90.180408.
106. Schwöbel, J.; Fu, Y.; Brede, J.; Dilullo, A.; Hoffmann, G.; Klyatskaya, S.; Ruben, M.; Wiesendanger, R. *Nat. Commun.* **2012,** *3* (1). https://doi.org/10.1038/ncomms1953.
107. Ara, F.; Oka, H.; Sainoo, Y.; Katoh, K.; Yamashita, M.; Komeda, T. *J. Appl. Phys.* **2019,** *125* (18), 183901. https://doi.org/10.1063/1.5079964.
108. Gueddida, S.; Gruber, M.; Miyamachi, T.; Beaurepaire, E.; Wulfhekel, W.; Alouani, M. *J. Phys. Chem. Lett.* **2016,** *7* (5), 900–904. https://doi.org/10.1021/acs.jpclett.6b00172.
109. Aragonès, A. C.; Aravena, D.; Cerdá, J. I.; Acís-Castillo, Z.; Li, H.; Real, J. A.; Sanz, F.; Hihath, J.; Ruiz, E.; Díez-Pérez, I. *Nano Lett.* **2016,** *16* (1), 218–226. https://doi.org/10.1021/acs.nanolett.5b03571.
110. Baumann, S.; Paul, W.; Choi, T.; Lutz, C. P.; Ardavan, A.; Heinrich, A. J. *Science* **2015,** *350* (6259), 417–420. https://doi.org/10.1126/science.aac8703.
111. Yang, K.; Paul, W.; Phark, S.-H.; Willke, P.; Bae, Y.; Choi, T.; Esat, T.; Ardavan, A.; Heinrich, A. J.; Lutz, C. P. *Science* **2019,** *366* (6464), 509–512. https://doi.org/10.1126/science.aay6779.
112. Choi, T.; Lutz, C. P.; Heinrich, A. J. *Curr. Appl. Phys.* **2017,** *17* (11), 1513–1517. https://doi.org/10.1016/j.cap.2017.08.011.
113. Willke, P.; Yang, K.; Bae, Y.; Heinrich, A. J.; Lutz, C. P. *Nat. Phys.* **2019,** *15* (10), 1005–1010. https://doi.org/10.1038/s41567-019-0573-x.
114. Shiraki, I.; Tanabe, F.; Hobara, R.; Nagao, T.; Hasegawa, S. *Surf. Sci.* **2001,** *493* (1–3), 633–643. https://doi.org/10.1016/S0039-6028(01)01276-6.
115. Voigtländer, B.; Cherepanov, V.; Korte, S.; Leis, A.; Cuma, D.; Just, S.; Lüpke, F. *Rev. Sci. Instrum.* **2018,** *89* (10), 101101. https://doi.org/10.1063/1.5042346.
116. Moreland, J.; Ekin, J. W. *Appl. Phys. Lett.* **1985,** *47* (2), 175–177. https://doi.org/10.1063/1.96253.
117. Moreland, J.; Ekin, J. W. *J. Appl. Phys.* **1985,** *58* (10), 3888–3895. https://doi.org/10.1063/1.335608.
118. Zhou, C.; Deshpande, M. R.; Reed, M. A.; Jones, L.; Tour, J. M. *Appl. Phys. Lett.* **1997,** *71* (5), 611–613. https://doi.org/10.1063/1.120195.
119. Reichert, J.; Ochs, R.; Beckmann, D.; Weber, H. B.; Mayor, M.; Löhneysen, H.v. *Phys. Rev. Lett.* **2002,** *88* (17). https://doi.org/10.1103/PhysRevLett.88.176804.
120. Smit, R. H. M.; Noat, Y.; Untiedt, C.; Lang, N. D.; van Hemert, M. C.; van Ruitenbeek, J. M. *Nature* **2002,** *419* (6910), 906–909. https://doi.org/10.1038/nature01103.
121. Mayor, M.; von Hänisch, C.; Weber, H. B.; Reichert, J.; Beckmann, D. *Angew. Chem. Int. Ed.* **2002,** *41* (7), 1183–1186. https://doi.org/10.1002/1521-3773(20020402)41:7<1183::AID-ANIE1183>3.0.CO;2-Z.
122. Getty, S. A.; Engtrakul, C.; Wang, L.; Liu, R.; Ke, S.-H.; Baranger, H. U.; Yang, W.; Fuhrer, M. S.; Sita, L. R. *Phys. Rev. B* **2005,** *71* (24). https://doi.org/10.1103/PhysRevB.71.241401.

123. Ruben, M.; Landa, A.; Lörtscher, E.; Riel, H.; Mayor, M.; Görls, H.; Weber, H. B.; Arnold, A.; Evers, F. *Small* **2008,** *4* (12), 2229–2235. https://doi.org/10.1002/smll.200800390.
124. Parks, J. J.; Champagne, A. R.; Costi, T. A.; Shum, W. W.; Pasupathy, A. N.; Neuscamman, E.; Flores-Torres, S.; Cornaglia, P. S.; Aligia, A. A.; Balseiro, C. A.; Chan, G. K.-L.; Abruna, H. D.; Ralph, D. C. *Science* **2010,** *328* (5984), 1370–1373. https://doi.org/10.1126/science.1186874.
125. Wagner, S.; Kisslinger, F.; Ballmann, S.; Schramm, F.; Chandrasekar, R.; Bodenstein, T.; Fuhr, O.; Secker, D.; Fink, K.; Ruben, M.; Weber, H. B. *Nat. Nanotechnol.* **2013,** *8* (8), 575–579. https://doi.org/10.1038/nnano.2013.133.
126. Garardin, L. *C. R. Acad. Sci.* **1861,** *53,* 727–730.
127. Black, J. R. The proceedings of the 6th Annual Reliability Physics Symposium, p. 148; 1967.
128. Black, J. R. *IEEE Trans. Electron Dev.* **1969,** *16* (4), 338–347. https://doi.org/10.1109/T-ED.1969.16754.
129. Park, H.; Lim, A. K. L.; Alivisatos, A. P.; Park, J.; McEuen, P. L. *Appl. Phys. Lett.* **1999,** *75* (2), 301–303. https://doi.org/10.1063/1.124354.
130. Senthil Kumar, K.; Ruben, M. *Coord. Chem. Rev.* **2017,** *346,* 176–205. https://doi.org/10.1016/j.ccr.2017.03.024.
131. Ruben, M.; Kumar, K. S. *Angew. Chem. Int. Ed.* **2019.** https://doi.org/10.1002/anie.201911256.
132. Miller, R. G.; Brooker, S. *Chem. Sci.* **2016,** *7* (4), 2501–2505. https://doi.org/10.1039/C5SC04583E.
133. Qiu, D.; Ren, D.-H.; Gu, L.; Sun, X.-L.; Qu, T.-T.; Gu, Z.-G.; Li, Z. *RSC Adv.* **2014,** *4* (59), 31323–31327. https://doi.org/10.1039/C4RA04257C.
134. Murashima, Y.; Karim, M. R.; Saigo, N.; Takehira, H.; Ohtani, R.; Nakamura, M.; Koinuma, M.; Lindoy, L. F.; Kuroiwa, K.; Hayami, S. *Inorg. Chem. Front.* **2015,** *2* (10), 886–892. https://doi.org/10.1039/C5QI00097A.
135. Senthil Kumar, K.; Šalitroš, I.; Boubegtiten-Fezoua, Z.; Moldovan, S.; Hellwig, P.; Ruben, M. *Dalton Trans.* **2018,** *47* (1), 35–40. https://doi.org/10.1039/C7DT03623J.
136. Huang, J.; Xie, R.; Wang, W.; Li, Q.; Yang, J. *Nanoscale* **2016,** *8* (1), 609–616. https://doi.org/10.1039/C5NR05601B.
137. Yan, Q.; Zhou, L.; Cheng, J.-F.; Wen, Z.; Han, Q.; Wang, X.-F. *J. Chem. Phys.* **2016,** *144* (15), 154304. https://doi.org/10.1063/1.4946803.
138. Aravena, D.; Ruiz, E. *J. Am. Chem. Soc.* **2012,** *134* (2), 777–779. https://doi.org/10.1021/ja2090096.
139. Ruiz, E. *Phys. Chem. Chem. Phys.* **2014,** *16* (1), 14–22. https://doi.org/10.1039/C3CP54028F.
140. Baadji, N.; Sanvito, S. *Phys. Rev. Lett.* **2012,** *108* (21). https://doi.org/10.1103/PhysRevLett.108.217201.
141. Baadji, N.; Piacenza, M.; Tugsuz, T.; Sala, F. D.; Maruccio, G.; Sanvito, S. *Nat. Mater.* **2009,** *8* (10), 813–817. https://doi.org/10.1038/nmat2525.
142. Miyamachi, T.; Gruber, M.; Davesne, V.; Bowen, M.; Boukari, S.; Joly, L.; Scheurer, F.; Rogez, G.; Yamada, T. K.; Ohresser, P.; Beaurepaire, E.; Wulfhekel, W. *Nat. Commun.* **2012,** *3* (1). https://doi.org/10.1038/ncomms1940.
143. Gopakumar, T. G.; Matino, F.; Naggert, H.; Bannwarth, A.; Tuczek, F.; Berndt, R. *Angew. Chem. Int. Ed.* **2012,** *51* (25), 6262–6266. https://doi.org/10.1002/anie.201201203.
144. Meded, V.; Bagrets, A.; Fink, K.; Chandrasekar, R.; Ruben, M.; Evers, F.; Bernand-Mantel, A.; Seldenthuis, J. S.; Beukman, A.; van der Zant, H. S. J. *Phys. Rev. B* **2011,** *83* (24). https://doi.org/10.1103/PhysRevB.83.245415.
145. Hao, H.; Jia, T.; Zheng, X.; Zeng, Z. *Phys. Chem. Chem. Phys.* **2017,** *19* (11), 7652–7658. https://doi.org/10.1039/C6CP08265C.
146. Hao, H.; Jia, T.; Zheng, X.; Liu, P.; Zeng, Z. *J. Chem. Phys.* **2020,** *152* (13), 134301. https://doi.org/10.1063/1.5126968.
147. Gee, A.; Jaafar, A. H.; Brachňaková, B.; Massey, J.; Marrows, C. H.; Šalitroš, I.; Kemp, N. T. *J. Phys. Chem. C* **2020,** *124* (24), 13393–13399. https://doi.org/10.1021/acs.jpcc.0c03824.
148. Jasper-Toennies, T.; Gruber, M.; Karan, S.; Jacob, H.; Tuczek, F.; Berndt, R. *Nano Lett.* **2017,** *17* (11), 6613–6619. https://doi.org/10.1021/acs.nanolett.7b02481.
149. Brandl, T.; Johannsen, S.; Häussinger, D.; Suryadevara, N.; Prescimone, A.; Bernhard, S.; Gruber, M.; Ruben, M.; Berndt, R.; Mayor, M. *Angew. Chem. Int. Ed.* **2020.** https://doi.org/10.1002/anie.202006340.
150. Harzmann, G. D.; Frisenda, R.; van der Zant, H. S. J.; Mayor, M. *Angew. Chem. Int. Ed.* **2015,** *54* (45), 13425–13430. https://doi.org/10.1002/anie.201505447.
151. Frisenda, R.; Harzmann, G. D.; Celis Gil, J. A.; Thijssen, J. M.; Mayor, M.; van der Zant, H. S. J. *Nano Lett.* **2016,** *16* (8), 4733–4737. https://doi.org/10.1021/acs.nanolett.5b04899.
152. Kuang, G.; Zhang, Q.; Lin, T.; Pang, R.; Shi, X.; Xu, H.; Lin, N. *ACS Nano* **2017,** *11* (6), 6295–6300. https://doi.org/10.1021/acsnano.7b02567.
153. Salmon, L.; Catala, L. *C. R. Chim.* **2018,** *21* (12), 1230–1269. https://doi.org/10.1016/j.crci.2018.07.009.
154. Molnár, G.; Rat, S.; Salmon, L.; Nicolazzi, W.; Bousseksou, A. *Adv. Mater.* **2018,** *30* (5), 1703862. https://doi.org/10.1002/adma.201703862.
155. Rotaru, A.; Gural'skiy, I. A.; Molnár, G.; Salmon, L.; Demont, P.; Bousseksou, A. *Chem. Commun.* **2012,** *48* (35), 4163–4165. https://doi.org/10.1039/C2CC30528C.
156. Rotaru, A.; Dugay, J.; Tan, R. P.; Guralskiy, I. A.; Salmon, L.; Demont, P.; Carrey, J.; Molnár, G.; Respaud, M.; Bousseksou, A. *Adv. Mater.* **2013,** *25* (12), 1745–1749. https://doi.org/10.1002/adma.201203020.
157. Dugay, J.; Giménez-Marqués, M.; Kozlova, T.; Zandbergen, H. W.; Coronado, E.; van der Zant, H. S. J. *Adv. Mater.* **2015,** *27* (7), 1288–1293. https://doi.org/10.1002/adma.201404441.
158. Prins, F.; Monrabal-Capilla, M.; Osorio, E. A.; Coronado, E.; van der Zant, H. S. J. *Adv. Mater.* **2011,** *23* (13), 1545–1549. https://doi.org/10.1002/adma.201003821.
159. Tanaka, D.; Aketa, N.; Tanaka, H.; Horike, S.; Fukumori, M.; Tamaki, T.; Inose, T.; Akai, T.; Toyama, H.; Sakata, O.; Tajiri, H.; Ogawa, T. *Dalton Trans.* **2019,** *48* (21), 7074–7079. https://doi.org/10.1039/C8DT02923G.
160. Torres-Cavanillas, R.; Sanchis-Gual, R.; Dugay, J.; Coronado-Puchau, M.; Giménez-Marqués, M.; Coronado, E. *Adv. Mater.* **2019,** *31* (27), 1900039. https://doi.org/10.1002/adma.201900039.
161. Devid, E. J.; Martinho, P. N.; Kamalakar, M. V.; Šalitroš, I.; Prendergast, Ú.; Dayen, J.-F.; Meded, V.; Lemma, T.; González-Prieto, R.; Evers, F.; Keyes, T. E.; Ruben, M.; Doudin, B.; van der Molen, S. J. *ACS Nano* **2015,** *9* (4), 4496–4507. https://doi.org/10.1021/acsnano.5b01103.
162. Bairagi, K.; Iasco, O.; Bellec, A.; Kartsev, A.; Li, D.; Lagoute, J.; Chacon, C.; Girard, Y.; Rousset, S.; Miserque, F.; Dappe, Y. J.; Smogunov, A.; Barreteau, C.; Boillot, M.-L.; Mallah, T.; Repain, V. *Nat. Commun.* **2016,** *7* (1). https://doi.org/10.1038/ncomms12212.
163. Gruber, M.; Berndt, R. *Magnetochemistry* **2020,** *6* (3), 35. https://doi.org/10.3390/magnetochemistry6030035.
164. Gruber, M.; Miyamachi, T.; Davesne, V.; Bowen, M.; Boukari, S.; Wulfhekel, W.; Alouani, M.; Beaurepaire, E. *J. Chem. Phys.* **2017,** *146* (9), 092312. https://doi.org/10.1063/1.4973511.
165. Bernien, M.; Naggert, H.; Arruda, L. M.; Kipgen, L.; Nickel, F.; Miguel, J.; Hermanns, C. F.; Krüger, A.; Krüger, D.; Schierle, E.; Weschke, E.; Tuczek, F.; Kuch, W. *ACS Nano* **2015,** *9* (9), 8960–8966. https://doi.org/10.1021/acsnano.5b02840.
166. Pronschinske, A.; Chen, Y.; Lewis, G. F.; Shultz, D. A.; Calzolari, A.; Buongiorno Nardelli, M.; Dougherty, D. B. *Nano Lett.* **2013,** *13* (4), 1429–1434. https://doi.org/10.1021/nl304304e.
167. Kumar, K. S.; Studniarek, M.; Heinrich, B.; Arabski, J.; Schmerber, G.; Bowen, M.; Boukari, S.; Beaurepaire, E.; Dreiser, J.; Ruben, M. *Adv. Mater.* **2018,** *30* (11), 1705416. https://doi.org/10.1002/adma.201705416.
168. Kipgen, L.; Bernien, M.; Ossinger, S.; Nickel, F.; Britton, A. J.; Arruda, L. M.; Naggert, H.; Luo, C.; Lotze, C.; Ryll, H.; Radu, F.; Schierle, E.; Weschke, E.; Tuczek, F.; Kuch, W. *Nat. Commun.* **2018,** *9* (1). https://doi.org/10.1038/s41467-018-05399-8.
169. Lefter, C.; Davesne, V.; Salmon, L.; Molnár, G.; Demont, P.; Rotaru, A.; Bousseksou, A. *Magnetochemistry* **2016,** *2* (1), 18. https://doi.org/10.3390/magnetochemistry2010018.
170. Rubio-Giménez, V.; Tatay, S.; Martí-Gastaldo, C. *Chem. Soc. Rev.* **2020,** *49* (15), 5601–5638. https://doi.org/10.1039/C9CS00594C.
171. Shi, S.; Schmerber, G.; Arabski, J.; Beaufrand, J.-B.; Kim, D. J.; Boukari, S.; Bowen, M.; Kemp, N. T.; Viart, N.; Rogez, G.; Beaurepaire, E.; Aubriet, H.; Petersen, J.; Becker, C.; Ruch, D. *Appl. Phys. Lett.* **2009,** *95* (4), 043303. https://doi.org/10.1063/1.3192355.

172. Cucinotta, G.; Poggini, L.; Giaconi, N.; Cini, A.; Gonidec, M.; Atzori, M.; Berretti, E.; Lavacchi, A.; Fittipaldi, M.; Chumakov, A. I.; Rüffer, R.; Rosa, P.; Mannini, M. *ACS Appl. Mater. Interfaces* **2020,** *12* (28), 31696–31705. https://doi.org/10.1021/acsami.0c07445.
173. Lefter, C.; Rat, S.; Costa, J. S.; Manrique-Juárez, M. D.; Quintero, C. M.; Salmon, L.; Séguy, I.; Leichle, T.; Nicu, L.; Demont, P.; Rotaru, A.; Molnár, G.; Bousseksou, A. *Adv. Mater.* **2016,** *28* (34), 7508–7514. https://doi.org/10.1002/adma.201601420.
174. Schleicher, F.; Studniarek, M.; Kumar, K. S.; Urbain, E.; Katcko, K.; Chen, J.; Frauhammer, T.; Hervé, M.; Halisdemir, U.; Kandpal, L. M.; Lacour, D.; Riminucci, A.; Joly, L.; Scheurer, F.; Gobaut, B.; Choueikani, F.; Otero, E.; Ohresser, P.; Arabski, J.; Schmerber, G.; Wulfhekel, W.; Beaurepaire, E.; Weber, W.; Boukari, S.; Ruben, M.; Bowen, M. *ACS Appl. Mater. Interfaces* **2018,** *10* (37), 31580–31585. https://doi.org/10.1021/acsami.8b11495.
175. Hao, G.; Mosey, A.; Jiang, X.; Yost, A. J.; Sapkota, K. R.; Wang, G. T.; Zhang, X.; Zhang, J.; N'Diaye, A. T.; Cheng, R.; Xu, X.; Dowben, P. A. *Appl. Phys. Lett.* **2019,** *114* (3), 032901. https://doi.org/10.1063/1.5054909.
176. Shalabaeva, V.; Ridier, K.; Rat, S.; Manrique-Juarez, M. D.; Salmon, L.; Séguy, I.; Rotaru, A.; Molnár, G.; Bousseksou, A. *Appl. Phys. Lett.* **2018,** *112* (1), 013301. https://doi.org/10.1063/1.5017458.
177. Dugay, J.; Aarts, M.; Giménez-Marqués, M.; Kozlova, T.; Zandbergen, H. W.; Coronado, E.; van der Zant, H. S. J. *Nano Lett.* **2017,** *17* (1), 186–193. https://doi.org/10.1021/acs.nanolett.6b03780.
178. Geest, E. P.; Shakouri, K.; Fu, W.; Robert, V.; Tudor, V.; Bonnet, S.; Schneider, G. F. *Adv. Mater.* **2020,** *32* (10), 1903575. https://doi.org/10.1002/adma.201903575.
179. Djeghloul, F.; Gruber, M.; Urbain, E.; Xenioti, D.; Joly, L.; Boukari, S.; Arabski, J.; Bulou, H.; Scheurer, F.; Bertran, F.; Le Fèvre, P.; Taleb-Ibrahimi, A.; Wulfhekel, W.; Garreau, G.; Hajjar-Garreau, S.; Wetzel, P.; Alouani, M.; Beaurepaire, E.; Bowen, M.; Weber, W. *J. Phys. Chem. Lett.* **2016,** *7* (13), 2310–2315. https://doi.org/10.1021/acs.jpclett.6b01112.
180. Zhu, L.; Yao, K. L.; Liu, Z. L. *Appl. Phys. Lett.* **2010,** *96* (8), 082115. https://doi.org/10.1063/1.3319506.
181. Timm, C.; Elste, F. S. A. *Phys. Rev. B* **2006,** *73* (23). https://doi.org/10.1103/PhysRevB.73.235304.
182. Hueso, L. E.; Pruneda, J. M.; Ferrari, V.; Burnell, G.; Valdés-Herrera, J. P.; Simons, B. D.; Littlewood, P. B.; Artacho, E.; Fert, A.; Mathur, N. D. *Nature* **2007,** *445* (7126), 410–413. https://doi.org/10.1038/nature05507.
183. Monsma, D. J.; Lodder, J. C.; Popma, T. J. A.; Dieny, B. *Phys. Rev. Lett.* **1995,** *74* (26), 5260–5263. https://doi.org/10.1103/PhysRevLett.74.5260.
184. Urdampilleta, M.; Nguyen, N.-V.; Cleuziou, J.-P.; Klyatskaya, S.; Ruben, M.; Wernsdorfer, W. *Int. J. Mol. Sci.* **2011,** *12* (10), 6656–6667. https://doi.org/10.3390/ijms12106656.
185. Kyatskaya, S.; Galán Mascarós, J. R.; Bogani, L.; Hennrich, F.; Kappes, M.; Wernsdorfer, W.; Ruben, M. *J. Am. Chem. Soc.* **2009,** *131* (42), 15143–15151. https://doi.org/10.1021/ja906165e.
186. Urdampilleta, M.; Klyatskaya, S.; Ruben, M.; Wernsdorfer, W. *Phys. Rev. B* **2013,** *87* (19). https://doi.org/10.1103/PhysRevB.87.195412.
187. Krainov, I. V.; Klier, J.; Dmitriev, A. P.; Klyatskaya, S.; Ruben, M.; Wernsdorfer, W.; Gornyi, I. V. *ACS Nano* **2017,** *11* (7), 6868–6880. https://doi.org/10.1021/acsnano.7b02014.
188. Rostamzadeh Renani, F.; Kirczenow, G. *Phys. Rev. B* **2013,** *87* (12). https://doi.org/10.1103/PhysRevB.87.121403.
189. Hong, K.; Kim, W. Y. *Angew. Chem. Int. Ed.* **2013,** *52* (12), 3389–3393. https://doi.org/10.1002/anie.201208816.
190. Urdampilleta, M.; Klayatskaya, S.; Ruben, M.; Wernsdorfer, W. *ACS Nano* **2015,** *9* (4), 4458–4464. https://doi.org/10.1021/acsnano.5b01056.
191. Urdampilleta, M.; Klyatskaya, S.; Cleuziou, J.-P.; Ruben, M.; Wernsdorfer, W. *Nat. Mater.* **2011,** *10* (7), 502–506. https://doi.org/10.1038/nmat3050.
192. Lopes, M.; Candini, A.; Urdampilleta, M.; Reserbat-Plantey, A.; Bellini, V.; Klyatskaya, S.; Marty, L.; Ruben, M.; Affronte, M.; Wernsdorfer, W.; Bendiab, N. *ACS Nano* **2010,** *4* (12), 7531–7537. https://doi.org/10.1021/nn1018363.
193. Candini, A.; Klyatskaya, S.; Ruben, M.; Wernsdorfer, W.; Affronte, M. *Nano Lett.* **2011,** *11* (7), 2634–2639. https://doi.org/10.1021/nl2006142.
194. Candini, A.; Lumetti, S.; Godfrin, C.; Balestro, F.; Wernsdorfer, W.; Klyatskaya, S.; Ruben, M.; Affronte, M. In *Molecular Architectonics;* Ogawa, T., Ed.; *Advances in Atom and Single Molecule Machines*, Springer International Publishing: Cham, 2017; pp 165–184. https://doi.org/10.1007/978-3-319-57096-9_8.
195. Garanin, D. A.; Chudnovsky, E. M. *Phys. Rev. X* **2011,** *1* (1). https://doi.org/10.1103/PhysRevX.1.011005.
196. Kovalev, A. A.; Hayden, L. X.; Bauer, G. E. W.; Tserkovnyak, Y. *Phys. Rev. Lett.* **2011,** *106* (14). https://doi.org/10.1103/PhysRevLett.106.147203.
197. Lassagne, B.; Ugnati, D.; Respaud, M. *Phys. Rev. Lett.* **2011,** *107* (13). https://doi.org/10.1103/PhysRevLett.107.130801.
198. Ganzhorn, M.; Klyatskaya, S.; Ruben, M.; Wernsdorfer, W. *Nat. Nanotechnol.* **2013,** *8* (3), 165–169. https://doi.org/10.1038/nnano.2012.258.
199. Ganzhorn, M.; Klyatskaya, S.; Ruben, M.; Wernsdorfer, W. *ACS Nano* **2013,** *7* (7), 6225–6236. https://doi.org/10.1021/nn402968k.
200. Manrique-Juarez, M. D.; Mathieu, F.; Shalabaeva, V.; Cacheux, J.; Rat, S.; Nicu, L.; Leïchlé, T.; Salmon, L.; Molnár, G.; Bousseksou, A. *Angew. Chem. Int. Ed.* **2017,** *56* (28), 8074–8078. https://doi.org/10.1002/anie.201702739.
201. Vilan, A.; Aswal, D.; Cahen, D. *Chem. Rev.* **2017,** *117* (5), 4248–4286. https://doi.org/10.1021/acs.chemrev.6b00595.
202. Richter, S.; Mentovich, E.; Elnathan, R. *Adv. Mater.* **2018,** *30* (41), 1706941. https://doi.org/10.1002/adma.201706941.
203. Park, J.; Pasupathy, A. N.; Goldsmith, J. I.; Chang, C.; Yaish, Y.; Petta, J. R.; Rinkoski, M.; Sethna, J. P.; Abruña, H. D.; McEuen, P. L.; Ralph, D. C. *Nature* **2002,** *417* (6890), 722–725. https://doi.org/10.1038/nature00791.
204. Liang, W.; Shores, M. P.; Bockrath, M.; Long, J. R.; Park, H. *Nature* **2002,** *417* (6890), 725–729. https://doi.org/10.1038/nature00790.
205. Jo, M.-H.; Grose, J. E.; Baheti, K.; Deshmukh, M. M.; Sokol, J. J.; Rumberger, E. M.; Hendrickson, D. N.; Long, J. R.; Park, H.; Ralph, D. C. *Nano Lett.* **2006,** *6* (9), 2014–2020. https://doi.org/10.1021/nl061212i.
206. Heersche, H. B.; de Groot, Z.; Folk, J. A.; van der Zant, H. S. J.; Romeike, C.; Wegewijs, M. R.; Zobbi, L.; Barreca, D.; Tondello, E.; Cornia, A. *Phys. Rev. Lett.* **2006,** *96* (20). https://doi.org/10.1103/PhysRevLett.96.206801.
207. Zyazin, A. S.; van den Berg, J. W. G.; Osorio, E. A.; van der Zant, H. S. J.; Konstantinidis, N. P.; Leijnse, M.; Wegewijs, M. R.; May, F.; Hofstetter, W.; Danieli, C.; Cornia, A. *Nano Lett.* **2010,** *10* (9), 3307–3311. https://doi.org/10.1021/nl1009603.
208. Burzurí, E.; Zyazin, A. S.; Cornia, A.; van der Zant, H. S. J. *Phys. Rev. Lett.* **2012,** *109* (14). https://doi.org/10.1103/PhysRevLett.109.147203.
209. Burzurí, E.; Yamamoto, Y.; Warnock, M.; Zhong, X.; Park, K.; Cornia, A.; van der Zant, H. S. J. *Nano Lett.* **2014,** *14* (6), 3191–3196. https://doi.org/10.1021/nl500524w.
210. Haque, F.; Langhirt, M.; del Barco, E.; Taguchi, T.; Christou, G. *J. Appl. Phys.* **2011,** *109* (7), 07B112. https://doi.org/10.1063/1.3560891.
211. Osorio, E. A.; Ruben, M.; Seldenthuis, J. S.; Lehn, J. M.; van der Zant, H. S. J. *Small* **2010,** *6* (2), 174–178. https://doi.org/10.1002/smll.200901559.
212. Vincent, R.; Klyatskaya, S.; Ruben, M.; Wernsdorfer, W.; Balestro, F. *Nature* **2012,** *488* (7411), 357–360. https://doi.org/10.1038/nature11341.
213. Godfrin, C.; Thiele, S.; Ferhat, A.; Klyatskaya, S.; Ruben, M.; Wernsdorfer, W.; Balestro, F. *ACS Nano* **2017,** *11* (4), 3984–3989. https://doi.org/10.1021/acsnano.7b00451.
214. Thiele, S.; Vincent, R.; Holzmann, M.; Klyatskaya, S.; Ruben, M.; Balestro, F.; Wernsdorfer, W. *Phys. Rev. Lett.* **2013,** *111* (3). https://doi.org/10.1103/PhysRevLett.111.037203.
215. Leuenberger, M. N.; Loss, D. *Nature* **2001,** *410* (6830), 789–793. https://doi.org/10.1038/35071024.
216. Wernsdorfer, W.; Aliaga-Alcalde, N.; Hendrickson, D. N.; Christou, G. *Nature* **2002,** *416* (6879), 406–409. https://doi.org/10.1038/416406a.
217. Moreno-Pineda, E.; Godfrin, C.; Balestro, F.; Wernsdorfer, W.; Ruben, M. *Chem. Soc. Rev.* **2018,** *47* (2), 501–513. https://doi.org/10.1039/C5CS00933B.
218. Leuenberger, M. N.; Loss, D. *Phys. Rev. B* **2003,** *68* (16). https://doi.org/10.1103/PhysRevB.68.165317.
219. Lumetti, S.; Candini, A.; Godfrin, C.; Balestro, F.; Wernsdorfer, W.; Klyatskaya, S.; Ruben, M.; Affronte, M. *Dalton Trans.* **2016,** *45* (42), 16570–16574. https://doi.org/10.1039/C6DT02445A.
220. Tejada, J.; Zarzuela, R.; García-Santiago, A.; Imaz, I.; Espin, J.; Maspoch, D.; Chudnovsky, E. M. *J. Supercond. Nov. Magn.* **2016,** *29* (5), 1133–1137. https://doi.org/10.1007/s10948-016-3474-6.

221. Serrano, G.; Poggini, L.; Briganti, M.; Sorrentino, A. L.; Cucinotta, G.; Malavolti, L.; Cortigiani, B.; Otero, E.; Sainctavit, P.; Loth, S.; Parenti, F.; Barra, A.-L.; Vindigni, A.; Cornia, A.; Totti, F.; Mannini, M.; Sessoli, R. *Nat. Mater.* **2020,** *19* (5), 546–551. https://doi.org/10.1038/s41563-020-0608-9.
222. Ghirri, A.; Bonizzoni, C.; Righi, M.; Fedele, F.; Timco, G.; Winpenny, R.; Affronte, M. *Appl. Magn. Reson.* **2015,** *46* (7), 749–756. https://doi.org/10.1007/s00723-015-0672-5.
223. Wiemann, Y.; Simmendinger, J.; Clauss, C.; Bogani, L.; Bothner, D.; Koelle, D.; Kleiner, R.; Dressel, M.; Scheffler, M. *Appl. Phys. Lett.* **2015,** *106* (19), 193505. https://doi.org/10.1063/1.4921231.
224. Bonizzoni, C.; Ghirri, A.; Bader, K.; van Slageren, J.; Perfetti, M.; Sorace, L.; Lan, Y.; Fuhr, O.; Ruben, M.; Affronte, M. *Dalton Trans.* **2016,** *45* (42), 16596–16603. https://doi.org/10.1039/C6DT01953F.
225. Ghirri, A.; Bonizzoni, C.; Troiani, F.; Buccheri, N.; Beverina, L.; Cassinese, A.; Affronte, M. *Phys. Rev. A* **2016,** *93* (6). https://doi.org/10.1103/PhysRevA.93.063855.
226. Bonizzoni, C.; Ghirri, A.; Atzori, M.; Sorace, L.; Sessoli, R.; Affronte, M. *Sci. Rep.* **2017,** *7* (1). https://doi.org/10.1038/s41598-017-13271-w.
227. Bonizzoni, C.; Troiani, F.; Ghirri, A.; Affronte, M. *J. Appl. Phys.* **2018,** *124* (19), 194501. https://doi.org/10.1063/1.5050869.
228. Bonizzoni, C.; Ghirri, A.; Affronte, M. *Adv. Phys. X* **2018,** *3* (1), 1435305. https://doi.org/10.1080/23746149.2018.1435305.
229. Ghirri, A.; Troiani, F.; Affronte, M. In *Structure and Bonding;* Gao, S., Ed.; ; Springer Berlin Heidelberg: Berlin, Heidelberg, 2014; pp 383–430. https://doi.org/10.1007/430_2014_145.
230. Escalera-Moreno, L.; Baldoví, J. J.; Gaita-Ariño, A.; Coronado, E. *Chem. Sci.* **2018,** *9* (13), 3265–3275. https://doi.org/10.1039/C7SC05464E.
231. Studniarek, M.; Wäckerlin, C.; Singha, A.; Baltic, R.; Diller, K.; Donati, F.; Rusponi, S.; Brune, H.; Lan, Y.; Klyatskaya, S.; Ruben, M.; Seitsonen, A. P.; Dreiser, J. *Adv. Sci.* **2019,** *1901736.* https://doi.org/10.1002/advs.201901736.
232. van Slageren, J. *Nat. Mater.* **2019,** *18* (4), 300–301. https://doi.org/10.1038/s41563-019-0314-7.
233. Atzori, M.; Sessoli, R. *J. Am. Chem. Soc.* **2019,** *141* (29), 11339–11352. https://doi.org/10.1021/jacs.9b00984.
234. Wasielewski, M. R.; Forbes, M. D. E.; Frank, N. L.; Kowalski, K.; Scholes, G. D.; Yuen-Zhou, J.; Baldo, M. A.; Freedman, D. E.; Goldsmith, R. H.; Goodson, T.; Kirk, M. L.; McCusker, J. K.; Ogilvie, J. P.; Shultz, D. A.; Stoll, S.; Whaley, K. B. *Nat. Rev. Chem.* **2020,** *4* (9), 490–504. https://doi.org/10.1038/s41570-020-0200-5.
235. Urtizberea, A.; Natividad, E.; Alonso, P. J.; Andrés, M. A.; Gascón, I.; Goldmann, M.; Roubeau, O. *Adv. Funct. Mater.* **2018,** *28* (31), 1801695. https://doi.org/10.1002/adfm.201801695.
236. Morello, A.; Pla, J. J.; Zwanenburg, F. A.; Chan, K. W.; Tan, K. Y.; Huebl, H.; Möttönen, M.; Nugroho, C. D.; Yang, C.; van Donkelaar, J. A.; Alves, A. D. C.; Jamieson, D. N.; Escott, C. C.; Hollenberg, L. C. L.; Clark, R. G.; Dzurak, A. S. *Nature* **2010,** *467* (7316), 687–691. https://doi.org/10.1038/nature09392.
237. Staudacher, T.; Raatz, N.; Pezzagna, S.; Meijer, J.; Reinhard, F.; Meriles, C. A.; Wrachtrup, J. *Nat. Commun.* **2015,** *6* (1). https://doi.org/10.1038/ncomms9527.
238. Wrachtrup, J.; Finkler, A. *J. Magn. Reson.* **2016,** *269,* 225–236. https://doi.org/10.1016/j.jmr.2016.06.017.
239. Radtke, M.; Bernardi, E.; Slablab, A.; Nelz, R.; Neu, E. *Nano Futures* **2019,** *3* (4), 042004. https://doi.org/10.1088/2399-1984/ab5f9b.
240. Kolesov, R.; Xia, K.; Reuter, R.; Stöhr, R.; Zappe, A.; Meijer, J.; Hemmer, P. R.; Wrachtrup, J. *Nat. Commun.* **2012,** *3* (1). https://doi.org/10.1038/ncomms2034.
241. Bartholomew, J. G.; Ahlefeldt, R. L.; Sellars, M. J. *Phys. Rev. B* **2016,** *93* (1). https://doi.org/10.1103/PhysRevB.93.014401.
242. Raha, M.; Chen, S.; Phenicie, C. M.; Ourari, S.; Dibos, A. M.; Thompson, J. D. *Nat. Commun.* **2020,** *11* (1). https://doi.org/10.1038/s41467-020-15138-7.
243. Kindem, J. M.; Ruskuc, A.; Bartholomew, J. G.; Rochman, J.; Huan, Y. Q.; Faraon, A. *Nature* **2020,** *580* (7802), 201–204. https://doi.org/10.1038/s41586-020-2160-9.
244. Fataftah, M. S.; Freedman, D. E. *Chem. Commun.* **2018,** *54* (98), 13773–13781. https://doi.org/10.1039/C8CC07939K.
245. Wojnar, M. K.; Laorenza, D. W.; Schaller, R. D.; Freedman, D. E. *J. Am. Chem. Soc.* **2020,** *142* (35), 14826–14830. https://doi.org/10.1021/jacs.0c06909.
246. Bayliss, S. L.; Laorenza, D. W.; Mintun, P. J.; Diler, B.; Freedman, D. E.; Awschalom, D. D. *ArXiv200407998 Cond-Mat Physicsquant-Ph,* 2020.
247. Guo, F.-S.; Day, B. M.; Chen, Y.-C.; Tong, M.-L.; Mansikkamäki, A.; Layfield, R. A. *Science* **2018,** *362* (6421), 1400–1403. https://doi.org/10.1126/science.aav0652.
248. Wäckerlin, C.; Donati, F.; Singha, A.; Baltic, R.; Rusponi, S.; Diller, K.; Patthey, F.; Pivetta, M.; Lan, Y.; Klyatskaya, S.; Ruben, M.; Brune, H.; Dreiser, J. *Adv. Mater.* **2016,** *28* (26), 5195–5199. https://doi.org/10.1002/adma.201506305.